CZECH TECHNICAL UNIVERSITY IN PRAGUE

ČESKÉ VYSOKÉ UČENÍ TECHNICKÉ V PRAZE

Faculty of Electrical Engineering

Fakulta elektrotechnická

Department of Electromagnetic Field

Katedra elektromagnetického pole

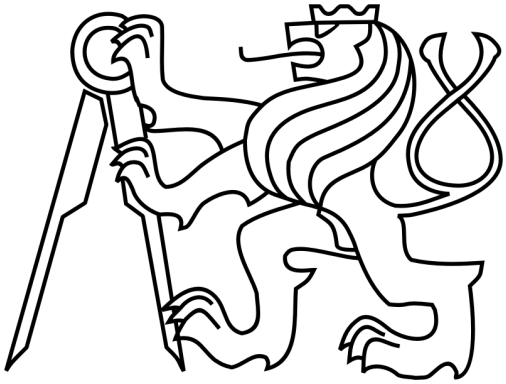

Doctoral Thesis

Disertační práce

Prague, August 2015

Praha, srpen 2015

Jan Kraček

CZECH TECHNICAL UNIVERSITY IN PRAGUE

ČESKÉ VYSOKÉ UČENÍ TECHNICKÉ V PRAZE

Faculty of Electrical Engineering

Fakulta elektrotechnická

Department of Electromagnetic Field

Katedra elektromagnetického pole

Wireless Power Transmission

Bezdrátové napájení

Doctoral Thesis

Disertační práce

Jan Kraček

Prague, August 2015

Praha, srpen 2015

Ph.D. Programme: Electrical Engineering and Information Technology

Doktorský studijní program: Elektrotechnika a informatika

Branch of Study: Radioelectronics

Studijní obor: Radioelektronika

Supervisor: Prof. Ing. Miloš Mazánek, CSc.

Školitel:

Supervisor-Specialist: Prof. Ing. Pavel Pechač, Ph.D.

Školitel specialista:

Content

Acknowledgement

I would like to express my deepest thanks to my supervisors Prof. Miloš Mazánek and Prof. Pavel Pechač for their useful advices and patience. I am also indebted to all colleges from Department of Electromagnetic Field of Czech Technical University in Prague who are always ready to help.

Abstract

This thesis deals with wireless power transmission (WPT). A concept with transmission by magnetic field (TMF) using induction coils and a concept with transmission by electromagnetic wave (TEW) using a dielectric slab waveguide are chosen for more detail study after review of different concepts of WPT.

A general circuit model of a transmission chain for TMF is developed. This model enables to define suitable characteristics of transmission, power transmission efficiency and normalized active powers, in a general way and to examine conditions of their optimum. The model demonstrates that efficiency and powers are functions of coupling coefficient and quality factors of coils used for transmission. The behaviour of coupling coefficient and quality factors is discussed subsequently. A complete parametrical analysis of three types of coils presented in the form of dimensionless parameters is performed in order to relate quality factor with geometrical and material properties describing the coils.

An analysis of magnetic field out of the winding of a multilayer coil whose turns of conductor are wound homogeneously close together around an air core of a shape of finite cylinder of arbitrary cross section is described. The magnetic flux density is found with the help of scalar magnetic potential. Due to this approach, one numerical integration is necessary for calculation of magnetic flux density only.

A basic principle of power extraction from a dielectric slab waveguide based on concept with TEW is studied. The suitable characteristics are found using power balance of the waveguide, in particular, the power reflection and transmission coefficients are used to quantify the efficiency of the process of power extraction and to formulate the optimal performance.

Abstrakt

Tato práce se zabývá bezdrátovým napájením. Na základě zhodnocení různých konceptů pro bezdrátové napájení jsou pro další studium zvoleny koncept přenosu magnetickým polem (PMP) s použitím indukčních cívek a koncept přenosu elektromagnetickou vlnou (PEV) s použitím dielektrického deskového vlnovodu.

Je vytvořen obecný obvodový model pro přenosový řetězec užívající PMP. Tento model umožňuje definovat vhodné charakteristiky přenosu, výkonovou účinnost přenosu a aktivní normalizované výkony, obecným způsobem a nalézt podmínky pro jejich optimum. Model demonstruje, že účinnost a výkony jsou funkcí vazebního činitele a činitelů jakosti cívek užitých pro přenos. Dále je diskutováno chování vazebního činitele a činitelů jakosti. Je provedena kompletní parametrická analýza činitele jakosti tří typů cívek prezentovaná ve formě bezrozměrných parametrů za účelem zjistit souvislost činitele jakosti s geometrickými a materiálovými vlastnostmi cívek.

Je popsána analýza magnetického pole vně vinutí vícevrstvé cívky, jejíž závity vodiče jsou navinuty homogenně závit vedle závitu okolo vzduchového jádra tvaru konečného válce libovolného průřezu. Magnetická indukce je nalezena s pomocí skalárního magnetického potenciálu. V důsledku použitého přístupu je při výpočtu magnetické indukce třeba pouze jedna numerická integrace.

Je studován základní princip vyvázání výkonu z dielektrického deskového vlnovodu založený na konceptu PEV. Pomocí výkonové bilance vlnovodu jsou nalezeny vhodné charakteristiky představované výkonovým činitelem odrazu a přenosu, které jsou použity k určení účinnosti procesu vyvázání výkonu a ke stanovení jeho optimálních podmínek.

Key Words

Wireless power transmission, magnetic field, electromagnetic field, induction coil, dielectric slab waveguide.

Klíčová slova

Bezdrátový přenos výkonu, magnetické pole, elektromagnetické pole, indukční cívka, dielektrický deskový vlnovod.

List of Figures

List of Tables

1. State of the Art

1.1. Introduction

The topic, which is dealing with this thesis, is known in literature namely as “wireless power supply” (WPS) or “contactless power supply”. The problem can be exactly expressed as power transmission between its source and its appliance where in a certain part of a transmission chain transmission is mediated without a connection of wires which are associated with the source and appliance. In addition, the appliance can be freely moved in certain bounds.

The WPS is motivated by simple and comfortable use of many small portable electric appliances with low power input in everyday life. WPS is being solved through reduction of power consumption of appliances on the one hand and through increase in efficiency in WPS concepts on the other hand. Nowadays, the conventional means for power supply is the interconnection of an appliance with a power grid socket, either for permanent power supply or only for accumulator charging. Both can be unsuitable or impractical in some cases. The cable connection restricts the movement of the appliance whereas the external charger, which differs for various appliances, is usually necessary for accumulator charging. The main idea of WPS is the deliverance of small electrical appliances with power input up to several W from such restrictions, the implementation of means for power supply as standard equipment of future buildings and the wireless power transmission (WPT) to appliances for distances up to several meters.

The concepts of WPT differ according to a distance between the source and appliance which is to overcome without the connection of wires, their mutual arrangement, degree of freedom of appliance movement with respect to the source, frequency and character of electromagnetic field, and power demand factor. The general block scheme of a WPT chain is depicted in Fig. 1.1. There is a “wireless” transmission medium between the side of source and the side of appliance. This medium is still separated from the source and appliance by adaptors, which ensure efficient transmission. The adaptors in part form the electromagnetic field with the help of suitable coupling elements, further contain matching networks and often include frequency converters because suitable frequencies for transmission through the medium differ from suitable frequencies for the source and appliance.

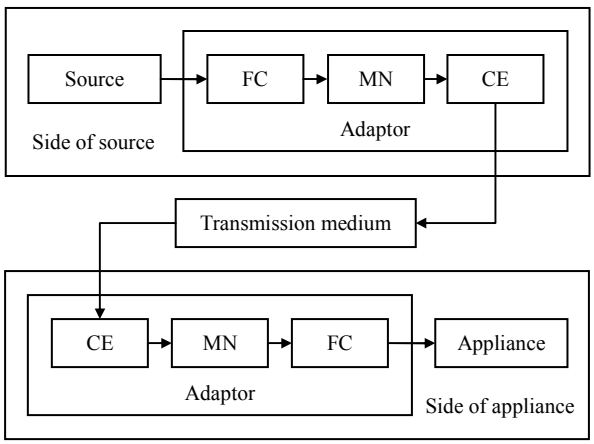

Fig. 1.1. General scheme of WPT chain (FC – Frequency Converter, MN – Matching Network, CE – Coupling Element).

The further text is aimed to the concepts of WPT suitable for power supply of the appliances with low power input (from microwatts up to watts) which are located in rooms of picocell size.

The concepts of WPT for power supply of appliances with low power input in picocells can be divided according to the two main criteria:

- Degree of freedom of the appliance movement.
- Character of electromagnetic field – type of power transmission.

According to the degree of freedom in which the appliance can be moved, the concepts can be divided in two dimensional (2D) and three dimensional (3D). In the case of 2D concept, the appliance is restricted to movement

along any determined surface which has different properties from the free space and serves for power transmission from the source to the appliance, see Fig. 1.2. a). The appliance can be translated along the x- and y-axis and rotated around the z'-axis by the angle γ. In the case of 3D concept, the appliance can be moved in the determined free space through which power is transmitted from the source to the appliance, see Fig. 1.2. b). The appliance can be translated along the x-, y- and z-axis and rotated around the x'-, y'-, and z'-axis by the angles α, β, γ.

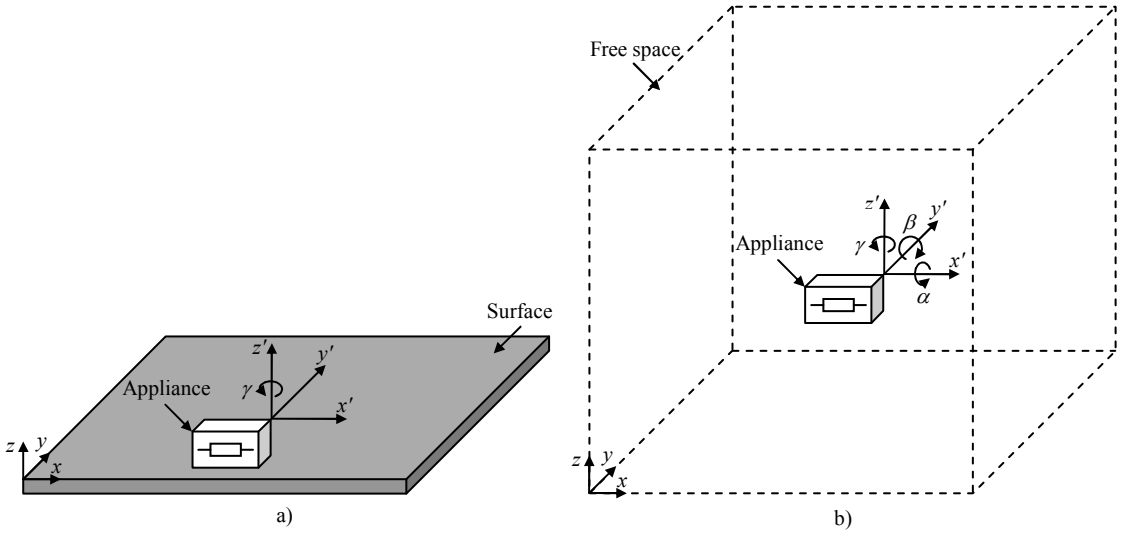

Fig. 1.2. a) Schemes of 2D concept and b) 3D concept.

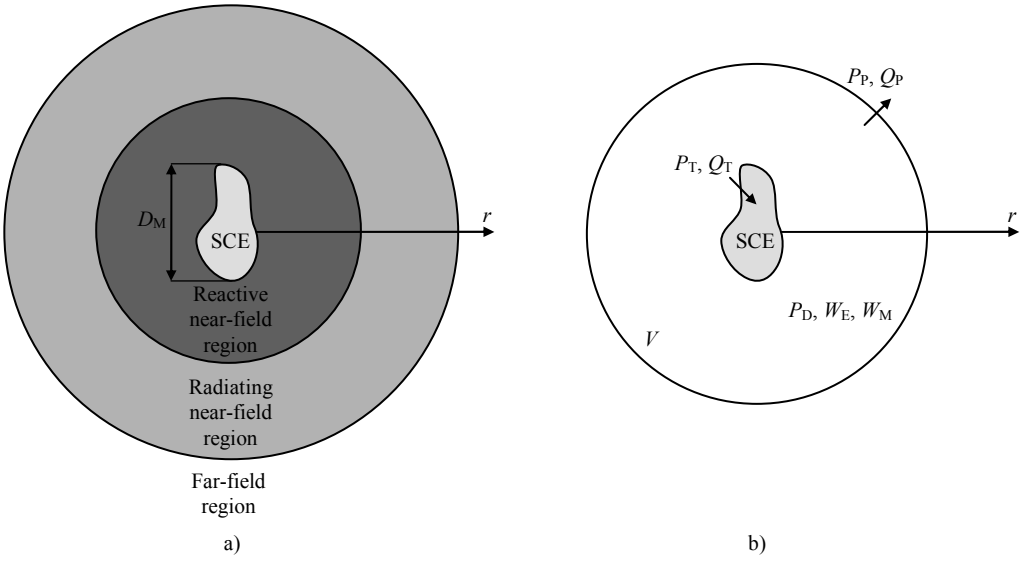

Fig. 1.3. a) Determination of electromagnetic field region with respect to source coupling element (SCE) and b) arrangement for description of its power balance.

With respect to electromagnetic field character (or power transmission type), the concepts can be classified in two groups. In the first group, there is formed wave for WPT whereas in the second group, there is not. In other words, the electromagnetic field has wave and non-wave character. Thus, there is used transmission by electromagnetic wave (TEW) for wave character and transmission by magnetic field (TMF) for non-wave character usually.

With the concepts classification according to the electromagnetic field character, determination of a region in which the appliance coupling element is placed with respect to the source coupling element is adherent. The space surrounding the source coupling element which emits electromagnetic field can be subdivided into three regions [1]: reactive near-field, radiating near-field, and far-field regions. These regions just differ in electromagnetic field character. The boundaries are given by distance r from the source coupling element and are related to wavelength λ in the transmission medium and the largest dimension D_M of the source coupling element, see Fig. 1.3. a) and Tab. 1.1. Although no abrupt changes in the field configurations are noted as the boundaries are crossed, there are

distinct differences among them. The boundaries separating these regions are not unique, although various criteria have been established and are commonly used to identify the regions.

The power balance [2] of harmonically time-varying electromagnetic field in a volume V represented by a sphere with arbitrary radius r and center in the source coupling element, see Fig. 1.3. b), can be written with the help of time average values of powers and energies as

$$P_{\mathrm{T}} = P_{\mathrm{D}} + P_{\mathrm{P}}\,, \tag{1.1}$$

$$Q_{\mathrm{T}} = 2\omega W_{\mathrm{E}} - 2\omega W_{\mathrm{M}} + Q_{\mathrm{P}} \tag{1.2}$$

where are

P_{T} total active power entering the source coupling element,

Q_{T} total reactive power entering the source coupling element,

P_{D} active power dissipated in the volume V,

P_{P} active power passing through the surface of volume V,

Q_{P} reactive power passing through the surface of volume V,

W_{E} electric energy,

W_{M} magnetic energy,

ω angular frequency.

The reactive near-field region is then an area where the reactive power Q_{P} is considerably dominant over the active power P_{P} for arbitrary r from this area. The angular field distribution is dependent on the distance r.

The radiating near-field region is an area where the active power P_{P} is becoming dominant over the reactive power Q_{P} with increasing r from this area. The angular field distribution is still dependent upon the distance r. For the source coupling element much smaller than wavelength ($\lambda >> D_{\mathrm{M}}$), this region may not exist.

The far-field region is an area where the reactive power Q_{P} vanishes and the active power P_{P} is dominant for arbitrary r from this area. The angular field distribution is essentially independent of the distance r. The electromagnetic field exists in a form of a wave here.

Region	Boundaries	Condition of validity
Reactive near-field	$r \in \left\langle 0,\ \frac{\lambda}{2\pi} \right\rangle$	$r << \lambda$
	$r \in \left\langle 0, 0.62\sqrt{\frac{D_{\mathrm{M}}^3}{\lambda}} \right\rangle$	$r \approx \lambda$
Radiating near-field	$r \in \left\langle \frac{\lambda}{2\pi},\ 2\lambda \right\rangle$	$r << \lambda$
	$r \in \left\langle 0.62\sqrt{\frac{D_{\mathrm{M}}^3}{\lambda}}, \frac{2D_{\mathrm{M}}^2}{\lambda} \right\rangle$	$r \approx \lambda$
Far-field	$r \in \left\langle 2\lambda, \infty \right)$	$r << \lambda$
	$r \in \left\langle \frac{2D_{\mathrm{M}}^2}{\lambda}, \infty \right\rangle$	$r \approx \lambda$

Tab. 1.1. Boundaries of electromagnetic field regions with respect to the source coupling element.

The concepts of WPT which use TEW have the appliance coupling element placed in the far-field region whereas the concepts which do not use TEW have the appliance coupling element placed in the reactive near-field region. However, there has to be fulfilled an additional condition for efficient transmission. The concepts based on TEW have to have active power P_{P} for r from far-field region comparable to the active power P_{T} entering the source coupling element whereas the concepts based on TMF have to have power P_{P} negligible in the far-field region. In other words, the radiation of the source coupling element is desirable in the former case whereas it is not in the latter one.

The power radiated by the source coupling element can be expressed as [3]

$$P_{\mathrm{R}} = \frac{\pi}{3}\left(\frac{L_{\mathrm{R}}}{\lambda}\right)^2 \sqrt{\frac{\mu}{\varepsilon}} \tag{1.3}$$

where are

L_{R} integral operator which is characteristic for radiation system (it takes into account the distribution of the radiation sources in the volume V),

ε permittivity of the medium,

μ permeability of the medium.

It is apparent that if $\lambda \to \infty$ (frequency $\to 0$) then $P_{\mathrm{R}} \to 0$. Thus, the radiated power is negligible for low frequencies. On the contrary, the radiated power increases with higher frequency.

According to the above mentioned behaviour of electromagnetic field, the dimension and working frequency of the coupling elements and the transmission distance are chosen in order to ensure efficient operation in the corresponding region of electromagnetic field for desired transmission type. Another criterion is the acceptable dimension for integration into the small appliances and overall acceptable size of the concept for WPT in the rooms.

1.2. Concepts

In this section, there are particularly described basic concepts of WPT for purposes of power supply as exemplification of the above mentioned categorization. For a brief overview with respect to the categorization, transmission distance, frequency, and transmission efficiency, see Tab. 1.2.

Concept	Dimension	Transm. type	Transm. distance	Frequency	Transm. efficiency
WSIC	2D	TMF	A few mm – a few cm	Tens of kHz – a few MHz	Tens of %
WSSW	2D	TEW	A few mm – a few cm	A few GHz	A few %
WISIC	3D	TMF	Tens of cm – a few m	Hundreds of kHz – a few MHz	A few % – tens of %
WISA	3D	TEW	Tens of cm – a few m	A few GHz	Hundredths of %

Tab. 1.2. Overview of properties of basic concepts of WPT for purposes of power supply.

1.2.1. WPT Surface with the Use of Induction Coils (WSIC)

This 2D concept [4] uses induction coils as the coupling elements, see Fig. 1.4. There is used TMF. On the side of source, a system of transceiving coils is arranged to create a surface. The purpose is to excite homogenous magnetic field in the proximity of the surface. On the side of appliance, which is placed on this surface, power is delivered to the load with the help of a receiving coil, which is coupled in this field. The transmission medium is a dielectric gap between the transceiving and receiving coils.

The transceiving and receiving coils mostly have flat shape. A wire is either coiled only in the peripheral line or filling the surface of the coil. For better homogeneity of magnetic field above the surface, the transceiving coils are arranged in several layers.

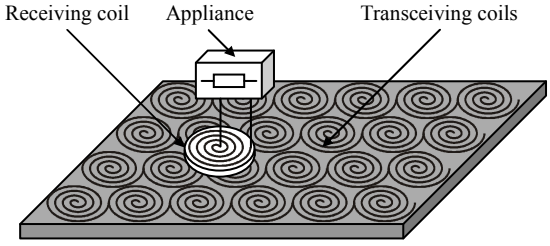

Fig. 1.4. Scheme of the concept of WPT surface with the use of induction coils.

1.2.2. WPT Surface with the Use of Slab Waveguide (WSSW)

This 2D concept [5] uses a waveguide with quasi-TEM wave as the transmission medium, see Fig. 1.5. The coupling elements are transitions between the waveguide with quasi-TEM wave and guides, which are associated with the sides of source and appliance. There is used TEW. The waveguide is created by a dielectric slab with an all-metal bottom wall and a top wall represented by a metal grid. On the side of source, power of electromagnetic wave is coupled by a transceiving transition through the metal grid to the waveguide. From the place of the transition, cylindrical wave propagates through the waveguide. On the side of appliance, which is placed on the surface, a part of wave power is extracted from the waveguide by a receiving transition and delivered to the load.

In a more complex configuration [6], the waveguide is excited on its edge by an array of sources as shown in Fig. 1.6. These sources independently adapt the phases of their harmonic signals in order to deliver maximal power to the appliance. It means the electromagnetic waves from the particular sources are summed under the receiving transition constructively.

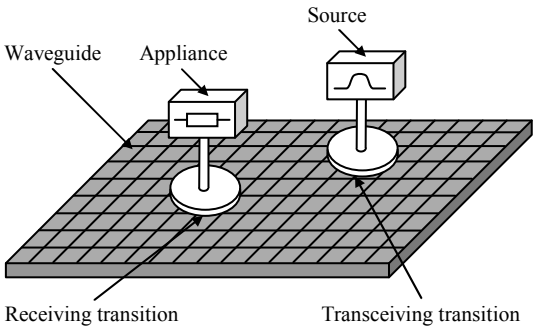

Fig. 1.5. Scheme of the concept of WPT surface with the use of slab waveguide.

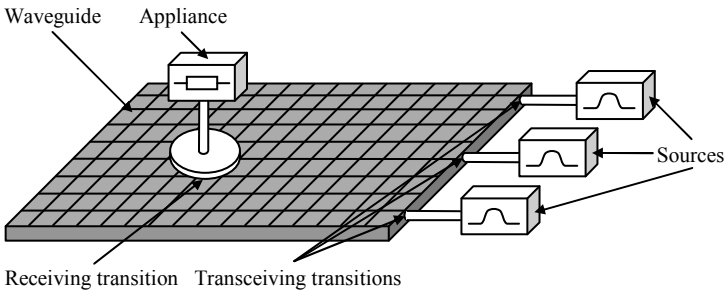

Fig. 1.6. Scheme of the more complex concept of WPT surface with the use of slab waveguide.

1.2.3. WPT in the Space with the Use of Induction Coils (WISIC)

This 3D concept [7] uses the free space as the transmission medium, see Fig. 1.7. The coupling elements are induction coils. There is used TMF. On the side of source, a transceiving coil excites magnetic field in the determined space. On the side of appliance, which is placed in this space, power is delivered to the load with the help of a receiving coil, which is coupled in this field.

In a more complex configuration [8], the transceiving coils are arranged as three orthogonal Helmholtz's coils, which enclose the determined space for better homogeneity of magnetic field inside, as shown in Fig. 1.8. The receiving coil is created from three orthogonal coils in order to decrease the dependence on arrangement with respect to the transceiving coils. It can have a core with high permeability for higher coupling. The concept is proposed as cellular. The space is dived into cubes and each cube is represented by a cell, as shown in Fig. 1.8.

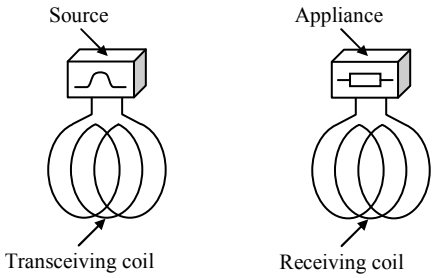

Fig. 1.7. Scheme of the concept of WPT in the space with the use of induction coils.

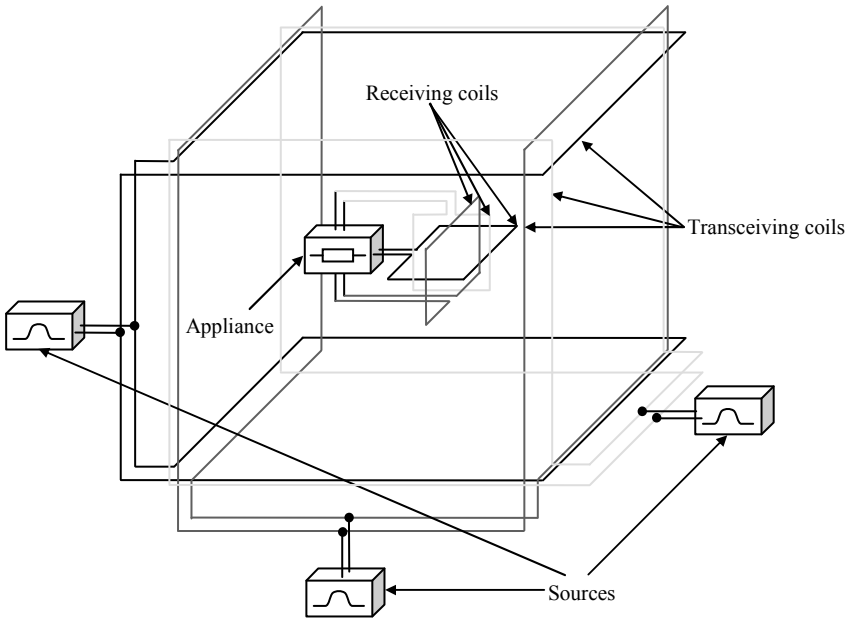

Fig. 1.8. Scheme of the more complex concept of WPT in the space with the use of induction coils.

1.2.4. WPT in the Space with the Use of Antennas (WISA)

This 3D concept [9] uses the free space as the transmission medium, see Fig. 1.9. The coupling elements are antennas. There is used TEW. On the side of source, a transceiving antenna radiates power of electromagnetic wave to the determined space. On the side of appliance, which is placed in this space, a part of wave power is received by a receiving antenna and delivered to the load.

The directive properties of the transceiving antenna are optimized for coverage of the determined space [10]. The receiving antenna is usually omnidirectional for easier receiving of incoming wave from different directions [11] or designed for circular polarization of wave to decrease the dependence on arrangement with respect to the transceiving antenna [12].

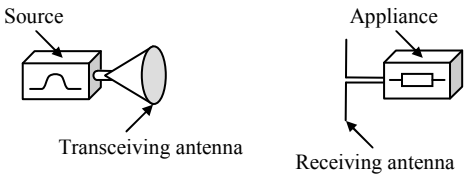

Fig. 1.9. Scheme of the concept of WPT in the space with the use of antennas.

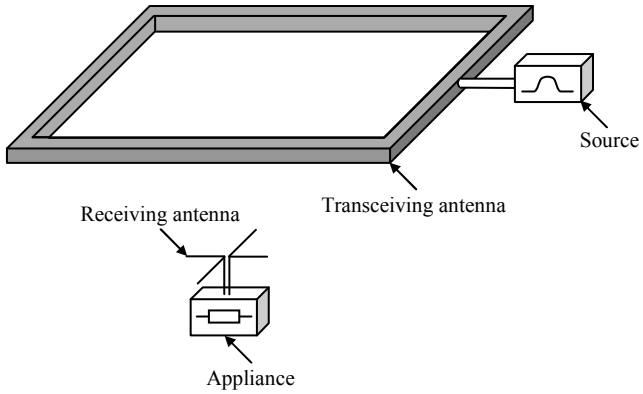

Fig. 1.10. Scheme of the more complex concept of WPT in the space with the use of antennas.

In a more complex configuration [13], the transceiving antenna is placed e.g. directly under the ceiling of the room. It is represented by a metal waveguide with many slots, as shown in Fig. 1.10. The slots are oriented to the determined space in order to ensure better homogeneity of power density there.

1.3. Milestones in WPT Development

The technology of WPT began to develop at the end of the 19th century. At that time, Nikola Tesla tried to transmit a significant amount of power with the help of the earth currents [14]. Its concept was aimed to transmission of power of hundreds of kW over a distance of a few kilometres. In the following decades, different concepts of WPT that differed in the distance of transmission, working frequency, and the amount of transmitted power were developed.

A more important progress was made in the 1960s: the concept of WPT by TMF at a frequency of several kHz for the powering of artificial heart was introduced [15]. It was aimed to transmission of power of tens of W over a distance of a few centimetres. This concept is conjoint with the advancement in high efficiency switched sources [16].

In the 1960s, the concept of WPT by TEW at a frequency of several GHz was proposed as well [17] and demonstrated by powering of a small pilotless helicopter from an earthbound base [18]. It was aimed to transmission of power of a few kW over a distance of a few meters. This concept was followed by the development of a special antenna with an integrated rectifier, which is called rectenna (rectifying antenna) [19].

In 1970s, 1980s, and 1990s, there was a wide discussion about particular elements of WPT. The efficiency, transmitted power, and transmission distance of concepts were considered. However, the intended applications were based only on transmission between the sides of source and appliance in the point-to-point mode. At the end of 1990s, the development of many small portable electric appliances with low power input began. The only thing which restricted their portability was the conventional means for power supply. There had to be an interconnection of an appliance with a power grid socket, either for permanent power supply or only for accumulator charging. On this basis, a need of adaptation of WPT concepts for this purpose arose. At the beginning of the 21st century, the different 2D and 3D concepts based on TMF and TEW were proposed for the powering of portable appliances in rooms [4], [5], [7], [9]. These ones represent concepts which perform transmission between the sides of source and appliance in the point-to-multipoint mode.

1.4. Comparison of Concepts

In this section, quantitative and qualitative comparison of the above mentioned basic concepts of WPT is made with respect to efficiency in section 1.4.1., reference levels in section 1.4.2., frequency in section 1.4.3., and influences on transmission in section 1.4.4. The comparison is concluded in section 1.4.5.

1.4.1. Efficiency

The assessment of the concepts from efficiency point of view is complex because it depends on distance and mutual arrangement of the source and appliance coupling elements, frequency and character of electromagnetic field (type of transmission), and extraneous objects in the transmission medium (namely for 3D concepts).

Here defined efficiency of power transmission is related to active power P_L delivered to the effective load represented by the appliance and to total active power P_T entering the source coupling element. This definition comprises the main causes of losses joint with a certain type of WPT and has formula

$$\eta = \frac{P_L}{P_T}. \tag{1.4}$$

In the case of TMF, the losses are predominately represented by ohmic resistance of the transceiving and receiving coils. In the case of TEW, the losses are predominately represented by decrease of power density on the wave-front with the increasing distance from the transceiving transition/antenna. In consequence of these phenomena, a portion of transmitted power reaches the appliance only.

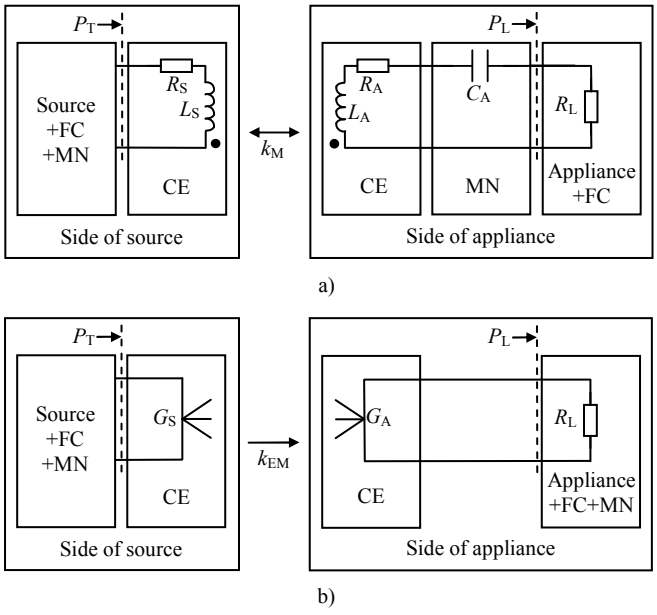

Fig. 1.11. Models for determination of power transmission efficiency of concepts with a) TMF and b) TEW (FC – Frequency Converter, MN – Matching Network, CE – Coupling Element).

In Fig. 1.11. a) and b) respectively, the simplified models for efficiency determination of the concepts with TMF and TEW are depicted. The symbols in Fig. 1.11. a) mean:

C_A matching capacitance,

L_A self inductance of receiving coil,

L_S self inductance of transceiving coil,

R_A ohmic resistance of receiving coil,

R_L effective resistance of appliance including frequency converter,

R_S ohmic resistance of transceiving coil,

k_M coupling coefficient of transceiving and receiving coils.

The symbols in Fig. 1.11. b) mean:

G_A gain of receiving transition (2D concept)/antenna (3D concept),

G_S gain of transceiving transition (2D concept)/antenna (3D concept),

R_L effective resistance of appliance including matching network and frequency converter,

k_{EM} transmission coefficient between transceiving and receiving transitions/antennas.

The efficiencies η_M and η_{EM} according to the models in Fig. 1.11. are given by formulas [20], [21]

$$\eta_M = \frac{(k_M Q)^2}{\left((k_M Q)^2 + \sqrt{1+(k_M Q)^2}\right)^2}, \tag{1.5}$$

$$\eta_{EM} = \left(\frac{k_{EM} G}{2^n \pi}\right)^2 \tag{1.6}$$

where are

$$Q_A = \frac{\omega L_A}{R_A},\ Q_S = \frac{\omega L_S}{R_S},\ Q = \sqrt{Q_A Q_S}, \tag{1.7}$$

$$G = \sqrt{G_A G_S}, \tag{1.8}$$

$$k_{EM} = \left(\frac{\lambda}{r}\right)^{\frac{n}{2}} \tag{1.9}$$

where Q_A and Q_S are quality factors of the receiving and transceiving coils, ω is angular frequency ($\omega = 2\pi f$, f is frequency), λ is wavelength in the transmission medium, r is distance between the transceiving and receiving transitions/antennas, $n = 1$ for 2D concept and $n = 2$ for 3D concept. In addition, the following conditions of optimal transmission for the model according to Fig. 1.11. a) are valid

$$R_L = \sqrt{R_A^2 + \omega^2 k_M^2 L_S L_A \frac{R_A}{R_S}} \wedge \omega L_A = \frac{1}{\omega C_A}. \tag{1.10}$$

In the case of the model according to Fig. 1.11. b), the impedance and polarization matching of the transitions/antennas are considered and multipath propagation and reflection in the transmission medium are not taken into account.

In Fig. 1.12., there are shown the curves of efficiencies η_M and η_{EM} based on equations (1.5) and (1.6). It is apparent that required efficiencies η_M or η_{EM} can be reached as a proper combination of k_M and Q for TMF or k_{EM} and G for TEW. It means decrease of transceiving and receiving coils coupling, which is respected by k_M, (increase of transceiving and receiving coils distance) can be compensated by increase of coils quality factors Q_A, Q_S (increase of angular frequency ω, increase of coils inductances L_A, L_S, decrease of coils resistances R_A, R_S). The resistances R_A, R_S depend on frequency roughly proportionally to $\omega^{1/2}$. Thus, the increase of frequency ω really increases factors Q_A, Q_S. Similarly, decrease of transmission, which is respected by k_{EM}, (decrease of wavelength λ, increase of distance r) can be compensated by increase of transitions/antennas gains G_A, G_S. The efficiencies η_M or η_{EM} tend to increase with increasing product $k_M Q$ or $k_{EM} G$, thus, with one increasing product component at least. The efficiency η_M limits with increasing product $k_M Q$ to 100 % whereas the efficiency η_{EM} seems to go over 100 % with increasing product $k_{EM} G$. This incorrectness is caused by invalidity of equation (1.6) for the near-field region of the transitions/antennas.

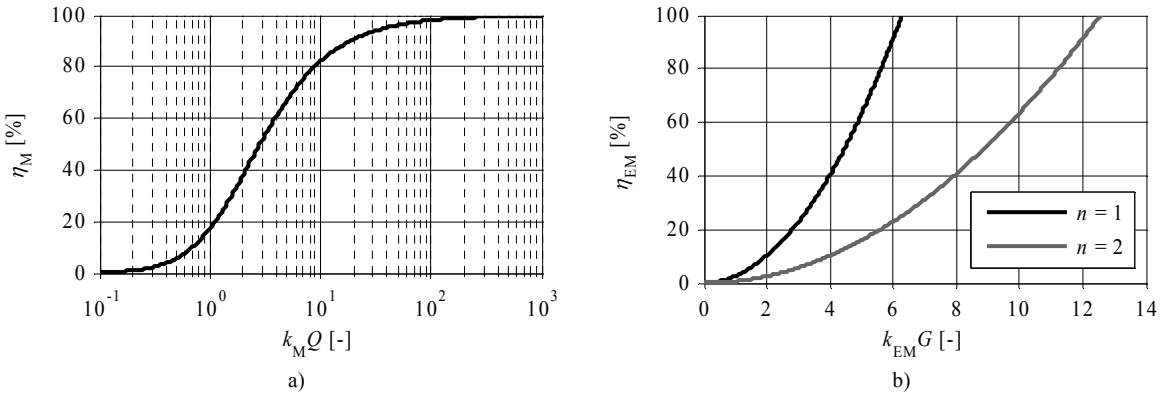

Fig. 1.12. Efficiencies a) η_M of concept with TMF and b) η_{EM} of concept with TEW ($n = 1$ for 2D concept, $n = 2$ for 3D concept).

Only weak dependence of efficiency on the direction in which the appliance coupling element is placed with respect to the source coupling element is desirable. With the increasing distance between the coupling elements the coefficients k_M and k_{EM} decrease. To maintain the efficiency by conservation of weak dependence on coupling elements mutual arrangement is better possible for TMF with increase of coils quality factors. Of course, for TEW the efficiency can be maintained by increase of transitions/antennas gains. However, it is in contradiction with weak dependence on mutual arrangement of the coupling elements. It can be said that the coupling elements represented by the coils can afford isotropic character even by higher quality factor, however, the coupling elements represented by the transitions/antennas become with higher gain directive.

1.4.2. Reference Levels

For using of WPS in areas where humans are presented, it is necessary to keep the reference levels for public exposure to electric and magnetic field [22], see Fig. 1.13. It is especially important for 3D concepts where transmission is accomplished through the free space. Further, with the help of certain simple examples of 3D concepts for TMF and TEW, the maximum achievable values of power, which can be delivered to the appliance by fulfilment of the reference levels, is calculated. For calculation, the models of the side of appliance according to Fig. 1.11. are used. It especially deals with characterization of the receiving couplings elements. It means determination of inductance L_A and resistance R_A of the receiving coil for TMF and gain G_A of the receiving antenna for TEW respectively. In the space, there is presumed existence of magnetic or electromagnetic field which is harmonically time-varying with angular frequency ω and has maximal acceptable rms value H_{max} of magnetic field strength or power density S_{max} with respect to the reference levels.

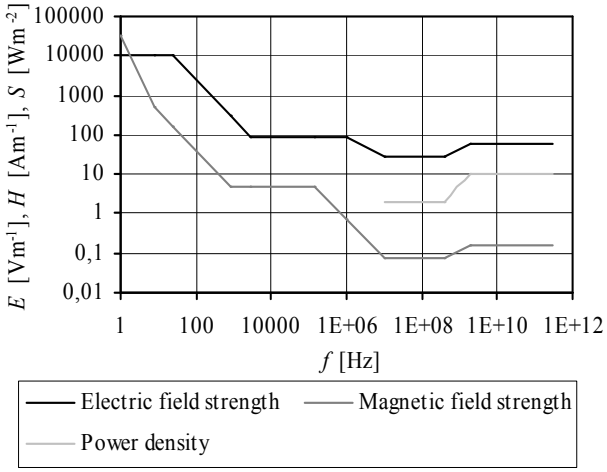

Fig. 1.13. Reference levels for general public exposure to time-varying electric and magnetic field (in rms scale).

In the case of TMF, a single layer cylindrical coil is considered as the coupling element (receiving coil). The coil has diameter D_C and it is created by N turns wound closely one by other by a copper wire with conductivity σ and diameter D_W. The power delivered to the appliance can be calculated with the help of the model in Fig. 1.14. a) and b). The voltage source u coresponds to voltage induced by magnetic inductive flux Φ which belongs to the receiving coil. For calculation of flux Φ, the homogenous magnetic field with strength H which direction is perpendicular to the turns area A_C of the receiving coil is assumed. The voltage u implies from induction law by equation [23]

$$u = -\frac{\partial \Phi}{\partial t} = -\frac{\partial}{\partial t}\left(\iint_{A_C} \mu_0 \boldsymbol{H} \cdot \mathrm{d}\boldsymbol{A} \right) = -\frac{\partial}{\partial t}\left(\mu_0 \sqrt{2} H_{\max} \cos(\omega t) \frac{\pi D_C^2 N}{4} \right) = \omega \mu_0 \sqrt{2} H_{\max} \sin(\omega t) \frac{\pi D_C^2 N}{4}. \quad (1.11)$$

The high frequency resistance R_A of the receiving coil is estimated by equation [21]

$$R_A = \frac{N D_C}{D_W} \sqrt{\frac{\omega \mu_0}{2\sigma}}. \quad (1.12)$$

For calculation on working frequency, it is not necessary to determine the inductance L_A of the receiving coil because its reactance ωL_A is compensated by reactance $-1/\omega C_A$ of the capacitor in the matching network according to (1.10). The power $P_{L,M}$ delivered to the appliance is determined with the help of the circuit model in Fig. 1.14. b) by equation

$$P_{L,M} = \left(\frac{\omega \mu_0 H_{max} \pi D_C^2 N}{4\left(R_A + R_L\right)} \right)^2 R_L . \tag{1.13}$$

In the case of TEW, a half-wave dipole is considered as the coupling element (receiving antenna) to which the electromagnetic plane wave with power density S is coming. For calculation, it is presumed that wave is coming in the maximum of antenna reception and it is polarization-matched (vector of electric field strength $\boldsymbol{E}$ is parallel to dipole axis), see Fig. 1.14. c). The power $P_{L,EM}$ delivered to the appliance is determined with the help of antenna effective aperture A_A by equation [21]

$$P_{L,EM} = SA_A = S_{max} \frac{\pi c^2 G_A}{\omega^2} \tag{1.14}$$

where c is speed of light.

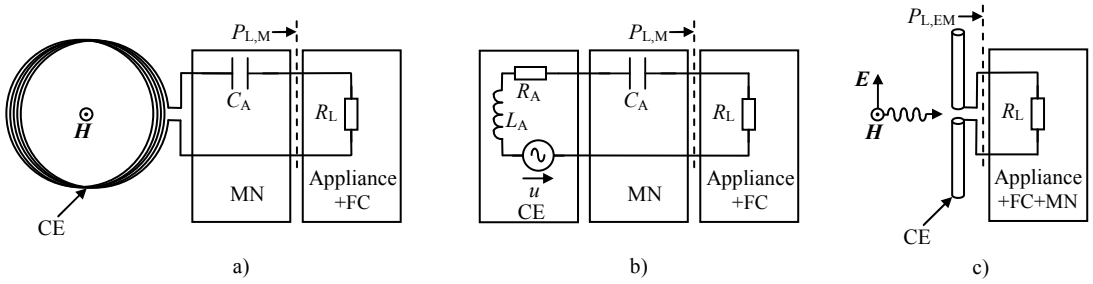

Fig. 1.14. Models for calculation of maximal possible delivered power to appliance with respect to reference levels for examples of 3D concepts with a), b) TMF and c) TEW (FC – Frequency Converter, MN – Matching Network, CE – Coupling Element).

TMF		TEW	
Chosen values			
D_C [m]	0.1	c [ms^{-1}]	$3 \cdot 10^8$
D_W [m]	0.001	G_A [-]	1,5
f [Hz]	$1 \cdot 10^6$	f [Hz]	$5 \cdot 10^9$
N [-]	100		
R_L [Ω]	50		
μ_0 [Hm^{-1}]	$4\pi \cdot 10^{-7}$		
σ [Sm^{-1}]	$5{,}96 \cdot 10^8$		
Reference levels			
H_{max} [Am^{-1}] @ f	0,73	S_{max} [Wm^{-2}] @ f	10
Evaluation			
$P_{L,M}$ [W]	0,37	$P_{L,EM}$ [W]	$4{,}3 \cdot 10^{-3}$

Tab. 1.3. Evaluation of calculation of maximal possible delivered power to appliance with respect to reference levels for examples of 3D concepts with TMF and TEW.

For evaluation of power calculation for chosen parameters of the side of appliance with the help of (1.13) and (1.14), see Tab. 1.3. From results, it is apparent that, in the case of TMF, power delivered to the appliance can be about orders higher than in the case of TEW. The calculated values are, of course, only estimation. In the nearer places to the transceiving coupling element, the values of electromagnetic field are usually higher than in the further places. However, the reference levels have to be fulfilled in all considered space. Thus, the values in the further places have to be necessarily lower than the reference levels allow.

Although these are only certain simple examples of the above mentioned concepts, the similar results can be generally expected for comparison of concepts with TMF and concepts with TEW by fulfillment of the reference levels.

1.4.3. Frequency

Frequency band and efficient WPT adheres to the conservation of electromagnetic field character in the desired field region of operation with respect to the dimensions of particular elements in the transmission chain. It means, for WPT by TMF/TEW, the wavelength has to be considerably bigger than/comparable with the elements of the transmission chain. In the case of TMF, efficiency decreases by too a low frequency or too a high frequency as a result of ohmic losses or losses by radiation. Thus as a compromise, a suitable frequency band corresponds to tens of kHz up to a few MHz [4], [8]. In the case of TEW, too a low frequency leads to an excessively big and impractical dimensions of elements in the transmission chain and low radiation efficiency of wave. On the other hand, too a high frequency leads to significantly small demanding production dimensions, the increase of losses by scattering of power, and problems with the implementation of power generator. Hence, as a compromise, a suitable frequency band coresponds to a few GHz [5], [11].

1.4.4. Influences on Transmission

The transmission can be impressed by objects which exist in the transmission medium. In the case of TMF, magnetic field distribution can be influenced by metal and ferromagnetic objects in which eddy currents are excited and which bend the magnetic field respectively. However, most objects in the room have a dielectric character. In the case of TEW, all objects in the path of wave propagation or in its proximity cause scattering, refraction, and multiple reflection of the wave. Thus, from the point of view of a shading transmission path between the source and appliance coupling element and the influence of extraneous objects on transmission, the concepts based on TMF are more resistant than the concepts based on TEW [7]. With respect to degree of freedom of the appliance movement, 2D concepts where the electromagnetic field is concentrated in the proximity of the surface are less influenced by extraneous object than 3D concepts. Generally, it can be said that the extraneous objects rather cause scattering and refraction of the electromagnetic field than its absorption because power reception in all concepts is based on the resonant principle.

1.4.5. Conclusion

According to the above discussed properties of the particular concepts, decision can be made about further research with respect to perspective of concepts improvements.

In the case of concept with TMF, the losses are predominately represented by ohmic resistance of the transceiving and receiving coils. It is result of finite conductivity of a real conductor and eddy currents. It means this phenomenon or its quantity are not necessary condition of excitation of magnetic field for transmission. The losses can be influenced by coupling elements (coils) construction.

In the case of concept with TEW, the looses are predominately represented by decrease of power density on the wave-front with the increasing distance from the transceiving transition/antenna. It is result of fundamental principle adherent to wave propagation, especially, when the wave is propagated isotropically (ideally) or omnidirectionally from the source coupling element, which is desirable for point source of wave and arbitrary appliance placing. In the case of 2D concept with TEW, there can be possibility to shape better the wave-front in order to avoid rapid decrease of its power density.

Further, the estimated power delivered to the appliance by fulfilment of the reference levels is higher for TMF than TEW in the case of 3D concept. Finally, the transmission is less influenced for TMF than TEW by extraneous object which can be in the transmission medium in the case of 3D concept.

Thus, the concept with TMF generally and 2D concept with TEW are chosen for further research. The previous research in these topics is based on experimental or circuital approach with low level of mathematization of the problem which leads to partial conclusions only.

2. Goals

The main aim of the thesis is to contribute to the theory of WPT. The goals and related problems are divided in two parts which correspond to concept with TMF, see section 2.1., and 2D concept with TEW, see section 2.2., respectively.

2.1. Concept with Transmission by Magnetic Field

The goal is: To use circuit approach to develop a general circuit model for the concept with TMF and, subsequently, to use electromagnetic field approach to link this circuit model with real structures of coupling elements represented by transceiving and receiving coils, see section 3.

With this goal, solving of following problems is adherent:

- A power balance of the concept has to be analysed using the circuit model in order to found suitable characteristics of the transmission chain and determine conditions of optimal performance, see section 3.1.
- The circuit model of the coupling elements represented by transceiving and receiving coils is given by their ability of cumulation of magnetic field energy, which is expressed by their self and mutual inductances, and ohmic losses in conductors of their windings, which correspond to their resistances. Additionally, the losses are dependent on frequency as a result of eddy currents. The integral parameters of inductances and resistances are determined by geometry and material of the coils. The analysis of these integral parameters based on electromagnetic field approach has to be used in order to link the circuit model of the concept with real structures of the coils (at least for certain types of coils), see section 3.4.
- The knowledge of the magnetic field of the coupling elements represented by the transceiving and receiving coils is useful for e.g. assessment of reference levels. Thus, the effective method for analysis of magnetic field which covers wide range of shapes of coils is desirable to develop, see sections 3.2., 3.3.

2.2. 2D Concept with Transmission by Electromagnetic Wave

The goal is: To developed analytical model of power extraction by the appliance based on 2D concept with TEW, see section 4.

With this goal, solving of following problems is adherent:

- A power balance of the concept has to be analysed in order to found suitable characteristics of the transmission chain and determine conditions of optimal performance, see sections 4.2., 4.3.3.
- A relevant solution of electromagnetic field in the transmission medium represented by a waveguide has to be constructed in order to take into account power extraction, see section 4.3.
- It is desirable to find an appropriate circuit representation of power extraction from the waveguide which can be used e.g. for design of a real structure of the appliance coupling element, see section 4.4.

3. Concept with Transmission by Magnetic Field

This section deals with concept with TMF. The section is structured as follows. In section 3.1., a circuit model of concept is presented. In sections 3.2. and 3.3., an analysis of magnetic field of induction coil, whose turns of conductor are wound homogeneously close together around air core of a shape of finite cylinder of arbitrary cross section, is performed. In section 3.4., maximal power transmission efficiency is discussed in relation to material and geometrical quantities describing induction coils.

3.1. Circuit Model

A circuit model for the concept with TMF is described in this section. The problem is formulated in section 3.1.1. Further, power transmission efficiency of the concept and conditions for its maximum given by (1.4), (1.10) and normalized active powers delivered to the appliance and lost in the coupling elements are derived with the help of this model in section 3.1.2. Finally, an impedance at the input of the source matching network is found in section 3.1.3.

3.1.1. Problem Formulation

A circuit model in Fig. 3.1. a) is very similar with the model in Fig. 1.11. a). For generality of derivation, there are only additionally collectively denoted the blocks of the appliance matching network and the appliance + the frequency converter as an equivalent load Z_L, which is connected to the appliance coupling element. On the contrary, the source matching network is detached as a separate block and it is represented by an unspecified serial reactance X_M. U_S is phasor (in rms scale) of voltage at the input of the source matching network and I_A, I_S are phasors (in rms scale) of currents in denoted loops. Other symbols are already known from description of the model in Fig. 1.12. a). The total active power P_T entering the source coupling element is considered to be the same as the power entering the source matching network since the matching is purely reactive.

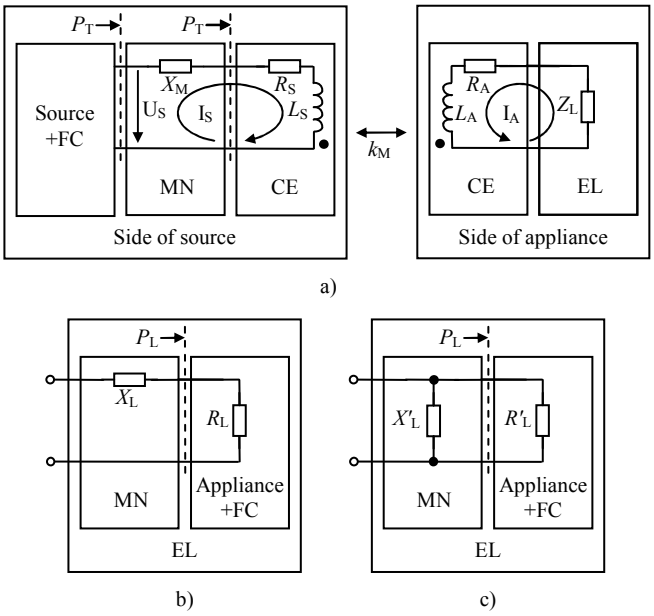

Fig. 3.1. Model for determination of power transmission efficiency of concept with TMF (FC – Frequency Converter, MN – Matching Network, CE – Coupling Element, EL – Equivalent Load).

The model can be described by circuit equations

$$\mathrm{U_S} = \left(R_\mathrm{S} + \mathrm{j}\left(X_\mathrm{M} + X_\mathrm{S}\right)\right)\mathrm{I_S} + \mathrm{j}X_\mathrm{K}\mathrm{I_A}\,, \tag{3.1}$$

$$0 = \mathrm{j}X_\mathrm{K}\mathrm{I_S} + \left(R_\mathrm{A} + \mathrm{j}X_\mathrm{A} + Z_\mathrm{L}\right)\mathrm{I_A} \tag{3.2}$$

where X_A, X_K, X_S are reactances, namely

$$X_\mathrm{A} = \omega L_\mathrm{A}\,,\ X_\mathrm{K} = \omega k_\mathrm{M}\sqrt{L_\mathrm{A}L_\mathrm{S}} = \omega M_\mathrm{AS}\,,\ X_\mathrm{S} = \omega L_\mathrm{S} \tag{3.3}$$

M_AS

and M_AS is mutual inductance of transceiving and receiving coils. The derivation is performed for equivalent load

$$Z_\mathrm{L} = R_\mathrm{L} + \mathrm{j}X_\mathrm{L} \tag{3.4}$$

which is represented by a serial combination of an effective appliance resistance (including frequency converter) R_L and an unspecified reactance X_L in the appliance matching network according to Fig. 3.1. b) (in comparison with Fig. 1.12. a), reactance X_L replaces capacitance C_A for generality). Solution of circuit equations (3.1) and (3.2) with respect to currents $\mathrm{I_A}$, $\mathrm{I_S}$ is

$$\mathrm{I_A} = \frac{-\mathrm{j}X_\mathrm{K}}{\left(R_\mathrm{A} + R_\mathrm{L} + \mathrm{j}\left(X_\mathrm{A} + X_\mathrm{L}\right)\right)\left(R_\mathrm{S} + \mathrm{j}\left(X_\mathrm{M} + X_\mathrm{S}\right)\right) + X_\mathrm{K}^2}\mathrm{U_S}\,, \tag{3.5}$$

$$\mathrm{I_S} = \frac{\left(R_\mathrm{A} + R_\mathrm{L} + \mathrm{j}\left(X_\mathrm{A} + X_\mathrm{L}\right)\right)}{\left(R_\mathrm{A} + R_\mathrm{L} + \mathrm{j}\left(X_\mathrm{A} + X_\mathrm{L}\right)\right)\left(R_\mathrm{S} + \mathrm{j}\left(X_\mathrm{M} + X_\mathrm{S}\right)\right) + X_\mathrm{K}^2}\mathrm{U_S}\,. \tag{3.6}$$

3.1.2. Power Balance

For determination of efficiency according to (1.4), it is necessary to find active power P_L which is delivered to the appliance represented by resistance R_L and rest of total active power P_T which is represented by active powers P_A and P_S lost in resistances R_A and R_S of the receiving and transceiving coils. These active powers are expressed by formulas

$$\begin{aligned} P_\mathrm{A} &= R_\mathrm{A}\left|\mathrm{I_A}\right|^2 \\ &= \frac{R_\mathrm{A}X_\mathrm{K}^2}{\left(\left(R_\mathrm{A} + R_\mathrm{L}\right)^2 + \left(X_\mathrm{A} + X_\mathrm{L}\right)^2\right)\left(R_\mathrm{S}^2 + \left(X_\mathrm{M} + X_\mathrm{S}\right)^2\right) + 2\left(\left(R_\mathrm{A} + R_\mathrm{L}\right)R_\mathrm{S} - \left(X_\mathrm{A} + X_\mathrm{L}\right)\left(X_\mathrm{M} + X_\mathrm{S}\right)\right)X_\mathrm{K}^2 + X_\mathrm{K}^4}\left|\mathrm{U_S}\right|^2\,, \end{aligned} \tag{3.7}$$

$$\begin{aligned} P_\mathrm{L} &= R_\mathrm{L}\left|\mathrm{I_A}\right|^2 \\ &= \frac{R_\mathrm{L}X_\mathrm{K}^2}{\left(\left(R_\mathrm{A} + R_\mathrm{L}\right)^2 + \left(X_\mathrm{A} + X_\mathrm{L}\right)^2\right)\left(R_\mathrm{S}^2 + \left(X_\mathrm{M} + X_\mathrm{S}\right)^2\right) + 2\left(\left(R_\mathrm{A} + R_\mathrm{L}\right)R_\mathrm{S} - \left(X_\mathrm{A} + X_\mathrm{L}\right)\left(X_\mathrm{M} + X_\mathrm{S}\right)\right)X_\mathrm{K}^2 + X_\mathrm{K}^4}\left|\mathrm{U_S}\right|^2\,, \end{aligned} \tag{3.8}$$

$$\begin{aligned} P_\mathrm{S} &= R_\mathrm{S}\left|\mathrm{I_S}\right|^2 \\ &= \frac{\left(\left(R_\mathrm{A} + R_\mathrm{L}\right)^2 + \left(X_\mathrm{A} + X_\mathrm{L}\right)^2\right)R_\mathrm{S}}{\left(\left(R_\mathrm{A} + R_\mathrm{L}\right)^2 + \left(X_\mathrm{A} + X_\mathrm{L}\right)^2\right)\left(R_\mathrm{S}^2 + \left(X_\mathrm{M} + X_\mathrm{S}\right)^2\right) + 2\left(\left(R_\mathrm{A} + R_\mathrm{L}\right)R_\mathrm{S} - \left(X_\mathrm{A} + X_\mathrm{L}\right)\left(X_\mathrm{M} + X_\mathrm{S}\right)\right)X_\mathrm{K}^2 + X_\mathrm{K}^4}\left|\mathrm{U_S}\right|^2\,. \end{aligned} \tag{3.9}$$

From (1.4), efficiency η_M is given by formula

$$\eta_\mathrm{M} = \frac{P_\mathrm{L}}{P_\mathrm{T}} = \frac{P_\mathrm{L}}{P_\mathrm{A} + P_\mathrm{L} + P_\mathrm{S}} = \frac{R_\mathrm{L}X_\mathrm{K}^2}{\left(\left(R_\mathrm{A} + R_\mathrm{L}\right)^2 + \left(X_\mathrm{A} + X_\mathrm{L}\right)^2\right)R_\mathrm{S} + \left(R_\mathrm{A} + R_\mathrm{L}\right)X_\mathrm{K}^2} \tag{3.10}$$

and can be rearranged as

$$\eta_{\mathrm{M}} = \frac{\dfrac{X_{\mathrm{K}}^2}{X_{\mathrm{A}}X_{\mathrm{S}}}\dfrac{X_{\mathrm{A}}}{R_{\mathrm{A}}}\dfrac{X_{\mathrm{S}}}{R_{\mathrm{S}}}\dfrac{X_{\mathrm{A}}}{R_{\mathrm{A}}}\dfrac{R_{\mathrm{L}}}{X_{\mathrm{A}}}}{\left(1+\dfrac{X_{\mathrm{A}}}{R_{\mathrm{A}}}\dfrac{R_{\mathrm{L}}}{X_{\mathrm{A}}}\right)^2+\left(\dfrac{X_{\mathrm{A}}}{R_{\mathrm{A}}}+\dfrac{X_{\mathrm{L}}}{R_{\mathrm{A}}}\right)^2+\dfrac{X_{\mathrm{K}}^2}{X_{\mathrm{A}}X_{\mathrm{S}}}\dfrac{X_{\mathrm{A}}}{R_{\mathrm{A}}}\dfrac{X_{\mathrm{S}}}{R_{\mathrm{S}}}\left(1+\dfrac{X_{\mathrm{A}}}{R_{\mathrm{A}}}\dfrac{R_{\mathrm{L}}}{X_{\mathrm{A}}}\right)}\,. \tag{3.11}$$

If it is denoted

$$\frac{X_{\mathrm{K}}}{\sqrt{X_{\mathrm{A}}X_{\mathrm{S}}}} = k_{\mathrm{M}}\,,\ \frac{X_{\mathrm{A}}}{R_{\mathrm{A}}} = Q_{\mathrm{A}}\,,\ \frac{X_{\mathrm{L}}}{R_{\mathrm{A}}} = -Q'_{\mathrm{A}}\,,\ \frac{X_{\mathrm{A}}}{R_{\mathrm{L}}} = Q_{\mathrm{L}}\,,\ \frac{X_{\mathrm{S}}}{R_{\mathrm{S}}} = Q_{\mathrm{S}} \tag{3.12}$$

efficiency η_{M} becomes

$$\eta_{\mathrm{M}} = \frac{k_{\mathrm{M}}^2 Q_{\mathrm{A}}Q_{\mathrm{S}}\dfrac{Q_{\mathrm{A}}}{Q_{\mathrm{L}}}}{\left(\left(1+\dfrac{Q_{\mathrm{A}}}{Q_{\mathrm{L}}}\right)^2+\left(Q_{\mathrm{A}}-Q'_{\mathrm{A}}\right)^2\right)+k_{\mathrm{M}}^2Q_{\mathrm{A}}Q_{\mathrm{S}}\left(1+\dfrac{Q_{\mathrm{A}}}{Q_{\mathrm{L}}}\right)} \tag{3.13}$$

Finding maximum of efficiency η_{M}, following parameters are defined

$$\kappa = k_{\mathrm{M}}\sqrt{Q_{\mathrm{A}}Q_{\mathrm{S}}}\,,\ \rho = \frac{Q_{\mathrm{A}}}{Q_{\mathrm{L}}}\,,\ \xi = Q_{\mathrm{A}} - Q'_{\mathrm{A}}\,. \tag{3.14}$$

Efficiency η_{M} can be then written as

$$\eta_{\mathrm{M}} = \frac{\kappa^2\rho}{\left(\left(1+\rho\right)^2+\xi^2\right)+\kappa^2\left(1+\rho\right)}\,. \tag{3.15}$$

By solving equation system

$$\frac{\partial\eta_{\mathrm{M}}}{\partial\rho} = 0\,, \tag{3.16}$$

$$\frac{\partial\eta_{\mathrm{M}}}{\partial\xi} = 0\,, \tag{3.17}$$

it is found that optimal values of parameters ρ and ξ for maximum of efficiency η_{M} are

$$\rho = \sqrt{1+\kappa^2}\,,\ \xi = 0\,. \tag{3.18}$$

Using (3.14), conditions for maximum of efficiency η_{M} are

$$k_{\mathrm{M}}^2Q_{\mathrm{A}}Q_{\mathrm{S}} = \frac{Q_{\mathrm{A}}^2}{Q_{\mathrm{L}}^2} - 1\,,\ Q_{\mathrm{A}} = Q'_{\mathrm{A}}\,. \tag{3.19}$$

Respecting (3.3) and (3.12), the conditions can be expressed as conditions for resistance R_{L} and reactance X_{L} in the form

$$R_{\mathrm{L}} = \sqrt{R_{\mathrm{A}}^2 + X_{\mathrm{K}}^2\frac{R_{\mathrm{A}}}{R_{\mathrm{S}}}} = \sqrt{R_{\mathrm{A}}^2 + \omega^2k_{\mathrm{M}}^2L_{\mathrm{S}}L_{\mathrm{A}}\frac{R_{\mathrm{A}}}{R_{\mathrm{S}}}}\,, \tag{3.20}$$

$$X_{\mathrm{L}} = -X_{\mathrm{A}} = -\omega L_{\mathrm{A}}\,. \tag{3.21}$$

Since the reactance X_{A} has inductive character the reactance X_{L} has to have capacitive character and it might be represented by capacitance C_{A}. The condition (3.21) becomes then

$$X_{\mathrm{L}} = -\frac{1}{\omega C_{\mathrm{A}}} = -X_{\mathrm{A}} = -\omega L_{\mathrm{A}}\,. \tag{3.22}$$

From (3.7)-(3.9), (3.13) through (3.12), (3.19)-(3.21), maximal efficiency η_{M} and corresponding power P_{L} delivered to the appliance and powers P_{A}, P_{S} lost in the coils resistances can be written as

$$\eta_{\mathrm{M}} = \frac{\left(k_{\mathrm{M}} Q\right)^2}{\left(1+\sqrt{1+\left(k_{\mathrm{M}} Q\right)^2}\right)^2}, \tag{3.23}$$

$$P_{\mathrm{A}} = \frac{R_{\mathrm{A}} X_{\mathrm{K}}^2}{\left(R_{\mathrm{A}} + \sqrt{R_{\mathrm{A}}^2 + X_{\mathrm{K}}^2 \frac{R_{\mathrm{A}}}{R_{\mathrm{S}}}}\right)^2 \left(R_{\mathrm{S}}^2 + \left(X_{\mathrm{M}} + X_{\mathrm{S}}\right)^2\right) + 2\left(R_{\mathrm{A}} + \sqrt{R_{\mathrm{A}}^2 + X_{\mathrm{K}}^2 \frac{R_{\mathrm{A}}}{R_{\mathrm{S}}}}\right) R_{\mathrm{S}} X_{\mathrm{K}}^2 + X_{\mathrm{K}}^4} \left|\mathrm{U}_{\mathrm{S}}\right|^2, \tag{3.24}$$

$$P_{\mathrm{L}} = \frac{\sqrt{R_{\mathrm{A}}^2 + X_{\mathrm{K}}^2 \frac{R_{\mathrm{A}}}{R_{\mathrm{S}}}}\, X_{\mathrm{K}}^2}{\left(R_{\mathrm{A}} + \sqrt{R_{\mathrm{A}}^2 + X_{\mathrm{K}}^2 \frac{R_{\mathrm{A}}}{R_{\mathrm{S}}}}\right)^2 \left(R_{\mathrm{S}}^2 + \left(X_{\mathrm{M}} + X_{\mathrm{S}}\right)^2\right) + 2\left(R_{\mathrm{A}} + \sqrt{R_{\mathrm{A}}^2 + X_{\mathrm{K}}^2 \frac{R_{\mathrm{A}}}{R_{\mathrm{S}}}}\right) R_{\mathrm{S}} X_{\mathrm{K}}^2 + X_{\mathrm{K}}^4} \left|\mathrm{U}_{\mathrm{S}}\right|^2, \tag{3.25}$$

$$P_{\mathrm{S}} = \frac{\left(R_{\mathrm{A}} + \sqrt{R_{\mathrm{A}}^2 + X_{\mathrm{K}}^2 \frac{R_{\mathrm{A}}}{R_{\mathrm{S}}}}\right)^2 R_{\mathrm{S}}}{\left(R_{\mathrm{A}} + \sqrt{R_{\mathrm{A}}^2 + X_{\mathrm{K}}^2 \frac{R_{\mathrm{A}}}{R_{\mathrm{S}}}}\right)^2 \left(R_{\mathrm{S}}^2 + \left(X_{\mathrm{M}} + X_{\mathrm{S}}\right)^2\right) + 2\left(R_{\mathrm{A}} + \sqrt{R_{\mathrm{A}}^2 + X_{\mathrm{K}}^2 \frac{R_{\mathrm{A}}}{R_{\mathrm{S}}}}\right) R_{\mathrm{S}} X_{\mathrm{K}}^2 + X_{\mathrm{K}}^4} \left|\mathrm{U}_{\mathrm{S}}\right|^2 \tag{3.26}$$

where is

$$Q = \sqrt{Q_{\mathrm{A}} Q_{\mathrm{S}}}\ . \tag{3.27}$$

It is apparent that (3.23) and (3.20), (3.22) are efficiency η_{M} of concept with TMF (1.4) and conditions (1.10) for its maximum mentioned in section 1.4.1. without derivation. Efficiency η_{M} is plotted in Fig. 1.12.

A dual case of equivalent load

$$Z_{\mathrm{L}} = \frac{R'_{\mathrm{L}} X'^2_{\mathrm{L}}}{R'^2_{\mathrm{L}} + X'^2_{\mathrm{L}}} + \mathrm{j}\frac{R'^2_{\mathrm{L}} X'_{\mathrm{L}}}{R'^2_{\mathrm{L}} + X'^2_{\mathrm{L}}}, \tag{3.28}$$

which is represented by a parallel combination of an appliance resistance R'_{L} and an unspecified reactance X'_{L} in the appliance matching network according to Fig. 3.1. c), can be converted into the case of equivalent load (3.4) with the help of equivalence principle setting equal right sides of (3.4) and (3.28)

$$R_{\mathrm{L}} + \mathrm{j}X_{\mathrm{L}} = \frac{R'_{\mathrm{L}} X'^2_{\mathrm{L}}}{R'^2_{\mathrm{L}} + X'^2_{\mathrm{L}}} + \mathrm{j}\frac{R'^2_{\mathrm{L}} X'_{\mathrm{L}}}{R'^2_{\mathrm{L}} + X'^2_{\mathrm{L}}}\ . \tag{3.29}$$

Hence, resistance R_{L} and reactance X_{L} can be expressed in terms of resistance R'_{L} and reactance X'_{L} as

$$R_{\mathrm{L}} = \frac{R'_{\mathrm{L}} X'^2_{\mathrm{L}}}{R'^2_{\mathrm{L}} + X'^2_{\mathrm{L}}},\ X_{\mathrm{L}} = \frac{R'^2_{\mathrm{L}} X'_{\mathrm{L}}}{R'^2_{\mathrm{L}} + X'^2_{\mathrm{L}}} \tag{3.30}$$

and substituted into equations of previous derivation. In this manner, optimal values of resistance R'_{L} and reactance X'_{L} for maximal efficiency η_{M} can be obtained from (3.20) and (3.21) as

$$R'_{\mathrm{L}} = \frac{X_{\mathrm{A}}^2}{\sqrt{R_{\mathrm{A}}^2 + X_{\mathrm{K}}^2 \frac{R_{\mathrm{A}}}{R_{\mathrm{S}}}}} + \sqrt{R_{\mathrm{A}}^2 + X_{\mathrm{K}}^2 \frac{R_{\mathrm{A}}}{R_{\mathrm{S}}}} = \frac{X_{\mathrm{A}}^2}{\sqrt{R_{\mathrm{A}}^2 + \omega^2 k_{\mathrm{M}}^2 L_{\mathrm{S}} L_{\mathrm{A}} \frac{R_{\mathrm{A}}}{R_{\mathrm{S}}}}} + \sqrt{R_{\mathrm{A}}^2 + \omega^2 k_{\mathrm{M}}^2 L_{\mathrm{S}} L_{\mathrm{A}} \frac{R_{\mathrm{A}}}{R_{\mathrm{S}}}}, \tag{3.31}$$

$$X'_{\mathrm{L}} = -X_{\mathrm{A}} - \frac{R_{\mathrm{A}}^2 + X_{\mathrm{K}}^2 \frac{R_{\mathrm{A}}}{R_{\mathrm{S}}}}{X_{\mathrm{A}}} = -\omega L_{\mathrm{A}} - \frac{R_{\mathrm{A}}^2 + \omega^2 k_{\mathrm{M}}^2 L_{\mathrm{S}} L_{\mathrm{A}} \frac{R_{\mathrm{A}}}{R_{\mathrm{S}}}}{\omega L_{\mathrm{A}}}\ . \tag{3.32}$$

From this, it is evident that reactance X'_{L} has to have capacitive character. Similarly, other arrangements of equivalent load can be converted.

For reactance X_{M}, any condition does not result from maximization of efficiency η_{M}. It is useful to determine it for maximal power P_{L} delivered to the appliance by maximal efficiency η_{M}. It means to solve the equation

$$\frac{\partial P_{\mathrm{L}}}{\partial X_{\mathrm{M}}} = 0\,. \tag{3.33}$$

Using (3.25), the condition for maximal power P_{L} by maximal efficiency η_{M} is

$$X_{\mathrm{M}} = -X_{\mathrm{S}} = -\omega L_{\mathrm{S}}\,. \tag{3.34}$$

Since the reactance X_{S} has inductive character the reactance X_{M} has to have capacitive character and it might be represented by capacitance. From (3.24)-(3.26) through (3.12), (3.27), (3.34) it can be written

$$P_{\mathrm{A}} = \frac{\left(k_{\mathrm{M}}Q\right)^2}{\left(1+\left(k_{\mathrm{M}}Q\right)^2+\sqrt{1+\left(k_{\mathrm{M}}Q\right)^2}\right)^2}\frac{\left|\mathrm{U_S}\right|^2}{R_{\mathrm{S}}}\,, \tag{3.35}$$

$$P_{\mathrm{L}} = \frac{\left(k_{\mathrm{M}}Q\right)^2\sqrt{1+\left(k_{\mathrm{M}}Q\right)^2}}{\left(1+\left(k_{\mathrm{M}}Q\right)^2+\sqrt{1+\left(k_{\mathrm{M}}Q\right)^2}\right)^2}\frac{\left|\mathrm{U_S}\right|^2}{R_{\mathrm{S}}}\,, \tag{3.36}$$

$$P_{\mathrm{S}} = \frac{\left(1+\sqrt{1+\left(k_{\mathrm{M}}Q\right)^2}\right)^2}{\left(1+\left(k_{\mathrm{M}}Q\right)^2+\sqrt{1+\left(k_{\mathrm{M}}Q\right)^2}\right)^2}\frac{\left|\mathrm{U_S}\right|^2}{R_{\mathrm{S}}}\,. \tag{3.37}$$

Further, it is suitable to define normalized active powers p_{A}, p_{L}, p_{S} by relations

$$p_{\mathrm{A}} = \frac{P_{\mathrm{A}}}{\frac{\left|\mathrm{U_S}\right|^2}{R_{\mathrm{S}}}} = \frac{\left(k_{\mathrm{M}}Q\right)^2}{\left(1+\left(k_{\mathrm{M}}Q\right)^2+\sqrt{1+\left(k_{\mathrm{M}}Q\right)^2}\right)^2}\,, \tag{3.38}$$

$$p_{\mathrm{L}} = \frac{P_{\mathrm{L}}}{\frac{\left|\mathrm{U_S}\right|^2}{R_{\mathrm{S}}}} = \frac{\left(k_{\mathrm{M}}Q\right)^2\sqrt{1+\left(k_{\mathrm{M}}Q\right)^2}}{\left(1+\left(k_{\mathrm{M}}Q\right)^2+\sqrt{1+\left(k_{\mathrm{M}}Q\right)^2}\right)^2}\,, \tag{3.39}$$

$$p_{\mathrm{S}} = \frac{P_{\mathrm{S}}}{\frac{\left|\mathrm{U_S}\right|^2}{R_{\mathrm{S}}}} = \frac{\left(1+\sqrt{1+\left(k_{\mathrm{M}}Q\right)^2}\right)^2}{\left(1+\left(k_{\mathrm{M}}Q\right)^2+\sqrt{1+\left(k_{\mathrm{M}}Q\right)^2}\right)^2}\,, \tag{3.40}$$

thus,

$$P_{\mathrm{A}} = p_{\mathrm{A}}\frac{\left|\mathrm{U_S}\right|^2}{R_{\mathrm{S}}}\,, \tag{3.41}$$

$$P_{\mathrm{L}} = p_{\mathrm{L}}\frac{\left|\mathrm{U_S}\right|^2}{R_{\mathrm{S}}}\,, \tag{3.42}$$

$$P_{\mathrm{S}} = p_{\mathrm{S}}\frac{\left|\mathrm{U_S}\right|^2}{R_{\mathrm{S}}}\,. \tag{3.43}$$

In Fig. 3.2., there are plotted normalized powers p_{A}, p_{L}, p_{S} based on (3.38)-(3.40). It is apparent that power p_{L} delivered to the appliance has a maximum for product $k_{\mathrm{M}}Q = 2$ approximately. However, powers p_{A}, p_{S} lost in resistances R_{A} and R_{S} of the receiving and transceiving coils are comparable with power p_{L} by that value. The powers p_{A}, p_{S} become about order lower from product $k_{\mathrm{M}}Q = 10$ approximately. This behaviour is in accordance with monotonic increase of efficiency η_{M} with increase of product $k_{\mathrm{M}}Q$ according to Fig. 1.12. a). It means there is compromise between efficiency η_{M} and normalized power p_{L} delivered to the appliance. Of course, the absolute power P_{L} delivered to the appliance can be adjusted by a value of fraction $|\mathrm{U_S}|^2/R_{\mathrm{S}}$ according to (3.42). The relation (3.42) can be interpreted as a demand on the value of $|\mathrm{U_S}|$ which the source should implement for given product $k_{\mathrm{M}}Q$ and resistance R_{S} since the product $k_{\mathrm{M}}Q$ is related with normalized power p_{L} through (3.39).

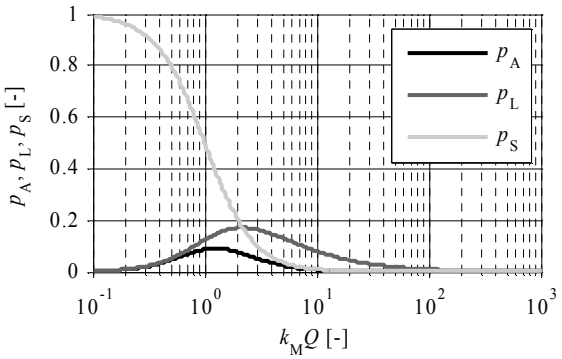

Fig. 3.2. Normalized active powers p_A, p_L, p_S by maximal power transmission efficiency η_M.

3.1.3. Input Impedance

Finally, it can be interesting to mention impedance Z_S at the input of the source matching network which is given by formula

$$Z_S = \frac{U_S}{I_S} = R_S + \frac{(R_A + R_L) X_K^2}{(R_A + R_L)^2 + (X_A + X_L)^2} + j\left(X_M + X_S - \frac{(X_A + X_L) X_K^2}{(R_A + R_L)^2 + (X_A + X_L)^2} \right). \tag{3.44}$$

If the conditions (3.20), (3.21), (3.34) are fulfilled impedance Z_S reduces to

$$Z_S = R_S + \frac{X_K^2}{R_A + \sqrt{R_A^2 + X_K^2 \frac{R_A}{R_S}}}. \tag{3.45}$$

It means impedance Z_S is then purely resistive.

3.2. Analysis of Magnetic Field of Thin-Wall Induction Coil with Air Core of Arbitrary Cross Section

This section describes analysis of magnetic field of a thin-wall induction coil with air core of a shape of finite cylinder of arbitrary cross section (arbitrary coil). The term thin-wall means that the coil is composed of turns which are wound homogeneously close together around the air core by a conductor with negligible cross section with respect to cross section of the air core. The turns create then so called wall of the coil, see Fig. 3.3. a). The single-layer coil is depicted in Fig. 3.3. a), however, the results of the analysis can be used for a multilayer coil which can be considered as thin-wall. It means the total thickness of the layers is negligible with respect to cross section of the air core.

Magnetic field of the arbitrary coil can be analyzed with the help of an elementary current loop which is placed as a probe in its magnetic field as it is shown in sections 3.2.1., 3.2.2. The arrangement of the arbitrary coil and loop is described in Fig. 3.4. a). The analysis of magnetic field is based on calculation of force with which the arbitrary coil acts on the loop and mutual inductance of the arbitrary coil and loop.

The result of the analysis is a method for finding of scalar magnetic potential of the arbitrary coil. The magnetic flux density of the arbitrary coil is found as gradient of scalar magnetic potential. A detail formula for calculation of magnetic flux density is given in section 3.2.3. The properties of scalar magnetic potential are described in section 3.2.4. The presented method is verified by two examples in section 3.2.5. The alternative approaches for analysis of magnetic field which are suitable for the mentioned type of the coil are discussed in [24]-[26].

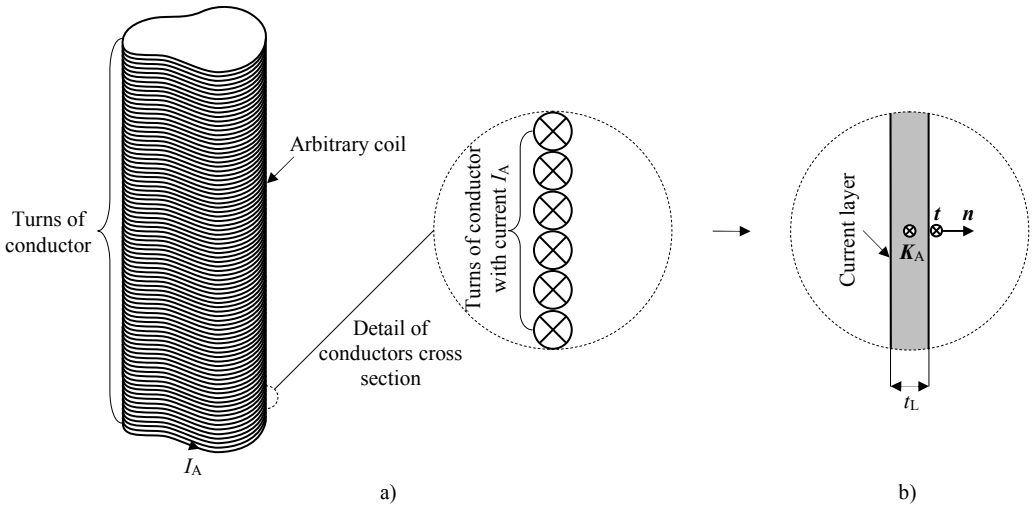

Fig. 3.3. a) Thin-wall coil with air core of arbitrary cross section, b) approximation of turns of conductor by current layer.

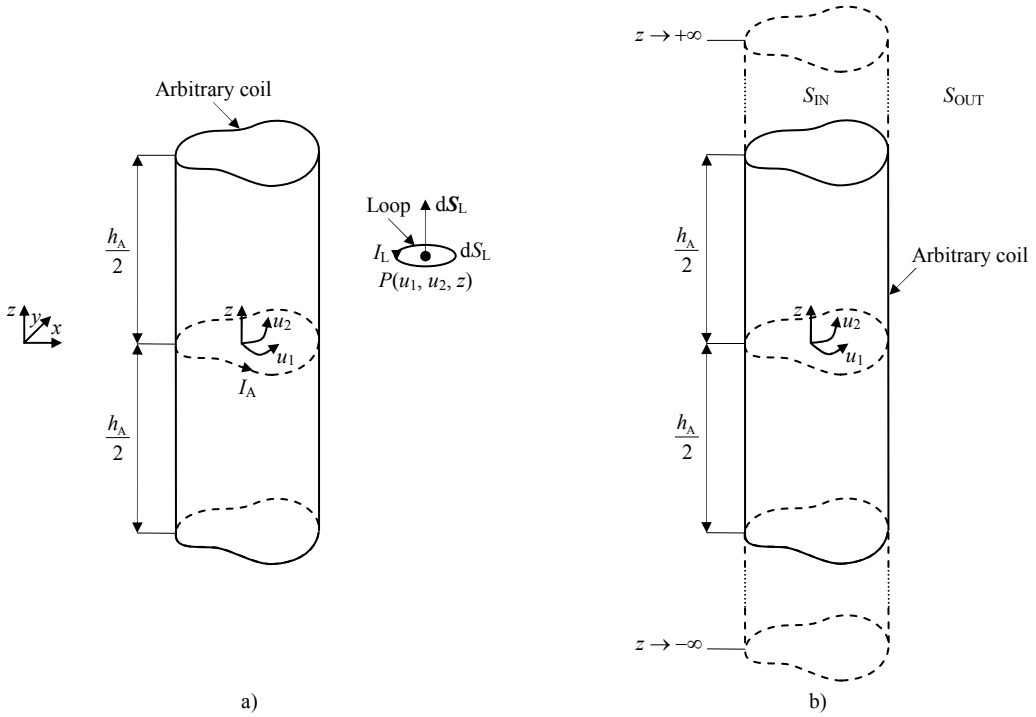

Fig. 3.4. a) Arrangement for analysis of magnetic field of arbitrary coil with the help of elementary loop, b) dividing of space around arbitrary coil.

3.2.1. Problem Formulation

The force $\boldsymbol{F}_L$ with which the arbitrary coil acts on the loop is given by expression [27]

$$\boldsymbol{F}_L = I_L \left(d\boldsymbol{S}_L \cdot \nabla \right) \boldsymbol{B}_A \tag{3.46}$$

where are

I_L current of loop,

$d\boldsymbol{S}_L$ oriented area of loop,

$$\nabla = \left(\frac{\partial}{\partial x}, \frac{\partial}{\partial y}, \frac{\partial}{\partial z} \right),$$

$\boldsymbol{B}_\mathrm{A}$ magnetic flux density excited by arbitrary coil in the point P where loop is placed.

If the loop is oriented as in Fig. 3.4. a), it means $\mathrm{d}\boldsymbol{S}_\mathrm{L} = \mathrm{d}S_\mathrm{L}\, \boldsymbol{z}_0$ where $\mathrm{d}S_\mathrm{L}$ is area of the loop, the equation (3.46) can be manipulated in the form

$$\boldsymbol{F}_\mathrm{L} = I_\mathrm{L}\, \mathrm{d}S_\mathrm{L}\, \frac{\partial \boldsymbol{B}_\mathrm{A}}{\partial z}\,. \tag{3.47}$$

However, the force $\boldsymbol{F}_\mathrm{L}$ can be expressed by other relation [28]

$$\boldsymbol{F}_\mathrm{L} = I_\mathrm{A} I_\mathrm{L} \nabla M_\mathrm{AL} \tag{3.48}$$

where are

I_A current of arbitrary coil,

M_AL mutual inductance of arbitrary coil and loop.

If the general curve-linear coordinates (u_1, u_2) are defined in the plane perpendicular to z-axis the meaning of the term ∇M_AL with respect to them is

$$\nabla M_\mathrm{AL} = \left(\frac{\partial M_\mathrm{AL}}{h_1 \partial u_1}, \frac{\partial M_\mathrm{AL}}{h_2 \partial u_2}, \frac{\partial M_\mathrm{AL}}{\partial z} \right) \tag{3.49}$$

where h_1, h_2 are scale coefficients of curve-linear coordinates (u_1, u_2) [29].

The position of the loop and place where magnetic flux density $\boldsymbol{B}_\mathrm{A}$ is calculated is determined by point $P(u_1, u_2, z)$, see Fig. 3.4. a). Mutual inductance M_AL is function of mutual position of the arbitrary coil and loop. The mutual position can be described in coordinates (u_1, u_2, z), thus, mutual inductance M_AL is function of the same. Comparison of (3.47) and (3.48) yields

$$\frac{\partial \boldsymbol{B}_\mathrm{A}}{\partial z} = \frac{I_\mathrm{A} \nabla M_\mathrm{AL}}{\mathrm{d}S_\mathrm{L}}\,. \tag{3.50}$$

Magnetic flux density $\boldsymbol{B}_\mathrm{A}$ is gained by integration of (3.50) with respect to coordinate z

$$\boldsymbol{B}_\mathrm{A} = I_\mathrm{A} \int \frac{\nabla M_\mathrm{AL}}{\mathrm{d}S_\mathrm{L}}\, \mathrm{d}z + \boldsymbol{C}_\mathrm{B} = I_\mathrm{A} \nabla \int \frac{M_\mathrm{AL}}{\mathrm{d}S_\mathrm{L}}\, \mathrm{d}z + \boldsymbol{C}_\mathrm{B} \tag{3.51}$$

where $\boldsymbol{C}_\mathrm{B}$ is vector of integration constants. Vector $\boldsymbol{C}_\mathrm{B}$ can be found with respect to the fact that $\boldsymbol{B}_\mathrm{A}(z \to \infty) = 0$

$$\boldsymbol{C}_\mathrm{B} = \lim_{z \to \infty} \left(\boldsymbol{B}_\mathrm{A} - I_\mathrm{A} \nabla \int \frac{M_\mathrm{AL}}{\mathrm{d}S_\mathrm{L}}\, \mathrm{d}z \right) = \lim_{z \to \infty} \left(-I_\mathrm{A} \nabla \int \frac{M_\mathrm{AL}}{\mathrm{d}S_\mathrm{L}}\, \mathrm{d}z \right). \tag{3.52}$$

3.2.2. Mutual Inductance of Arbitrary Coil and Elementary Loop

The mutual inductance M_AL of the arbitrary coil and loop can be found by an arbitrary method which leads to expression of mutual inductance M_AL as a function of mutual position of the arbitrary coil and loop. Additionally, the method should enable analytical integration of mutual inductance M_AL with respect to coordinate z in order to obtain simply calculable relation for magnetic flux density $\boldsymbol{B}_\mathrm{A}$. The method chosen here calculates mutual inductance M_AL as a special case of mutual inductance M_AC1 of the arbitrary coil and thin-wall coil with air core of a shape of finite cylinder of circular cross section (circular coil 1). The loop is then considered as the circular coil 1 with zero height, one turn, and zero radius. This method for calculation of mutual inductance of the thin-wall coil with air core of a shape of finite cylinder of arbitrary cross section and thin-wall coil with air core of a shape of finite cylinder of circular cross section is described in [30] and is proposed for different type of coil originally in [31]. The calculation of mutual inductance M_AC1 is based on well-known calculation of mutual inductance of two thin-wall air circular coils [32] and their magnetic flux linkage is modified according to a simple geometrical rule taking into account a cross section of the arbitrary coil.

Two cases can occur for calculation of mutual inductance M_AC1. The cases differ in position of axis ξ of the circular coil 1 with respect to the arbitrary coil. The space around the arbitrary coil is divided in two parts for

specification of position of the axis ξ. The boundary between these two parts of the space is represented by a surface of an imaginary infinite cylinder of the same cross section as the arbitrary coil. The inner space of the cylinder is called S_{IN} and the outer space S_{OUT}, see Fig. 3.4. b).

In the first case, the axis ξ of the circular coil 1 is in the outer space S_{OUT}, see Fig. 3.5. a). The calculation insists in description of the arbitrary coil by other thin-wall coil with air core of a shape of finite cylinder of circular cross section (circular coil 2). The circular coil 2 is circumscribed around the arbitrary coil by a specific manner, has the same height and number of turns, and is coaxial with respect to the circular coil 1. In the second case, the axis ξ of the circular coil 1 is in the inner space S_{IN}, see Fig. 3.5. b). The calculation insists in description of the arbitrary coil by other two thin-wall coils with air cores of a shape of finite cylinder of circular cross section (circular coil 2 and circular coil 3). The circular coil 2 has the same properties as in the first case. The circular coil 3 is inscribed to the arbitrary coil by a specific manner, has the same height and number of turns, and is coaxial with respect to the circular coil 1. The mutual position of the arbitrary coil and circular coil 1 is described in coordinates (u_1, u_2, z). The cylindrical coordinates (r, φ, z) are used for description of the circular coil 1.

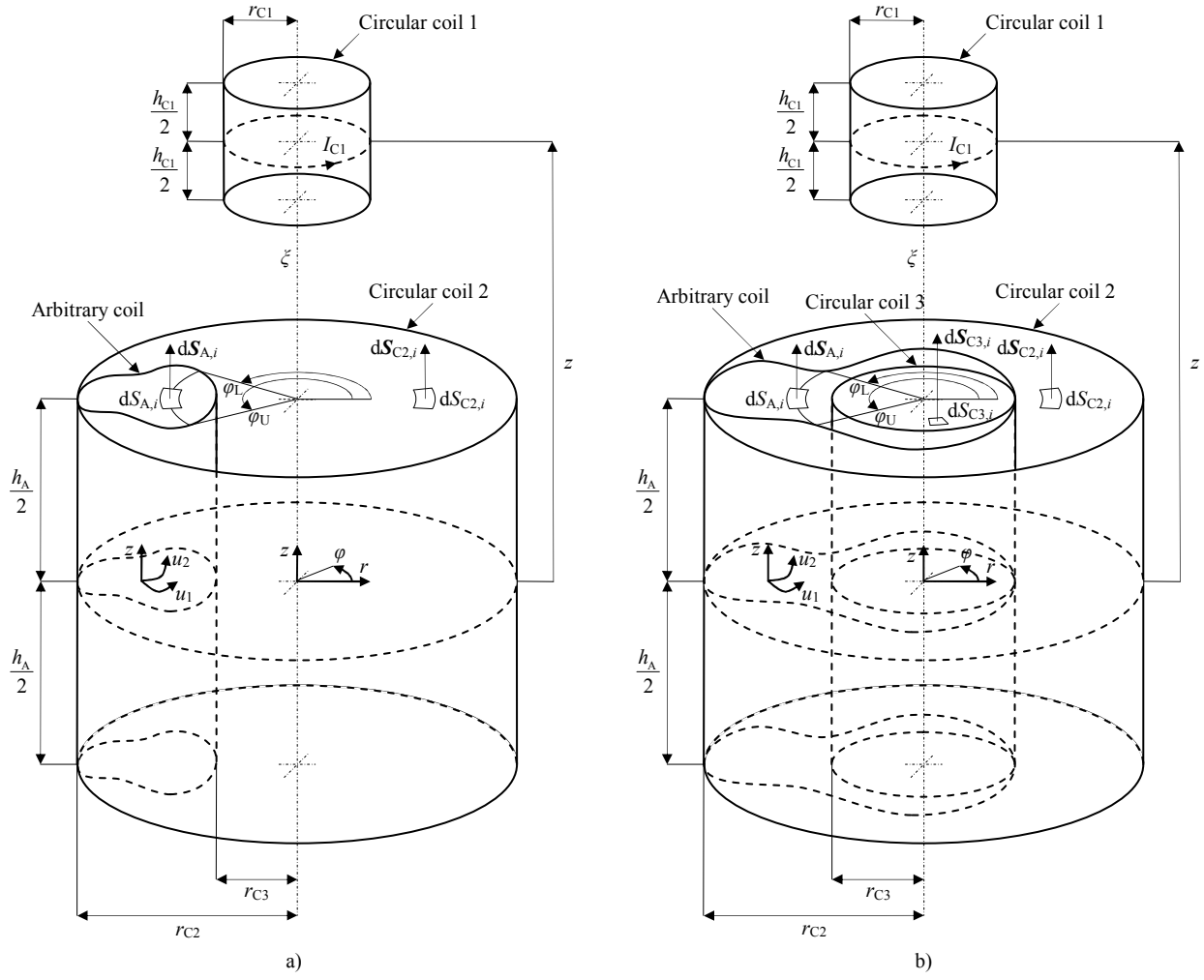

Fig. 3.5. Arrangement for calculation of mutual inductance of arbitrary coil and circular coil 1 for axis ξ in a) outer space S_{OUT}, b) inner space S_{IN}.

Mutual inductance M_{AC1} of the arbitrary coil and circular coil 1, mutual inductance M_{C1C2} of the circular coil 1 and 2 and mutual inductance M_{C1C3} of the circular coil 1 and 3 can be defined as [33]

$$M_{AC1} = \frac{\Phi_{AC1}}{I_{C1}}, \tag{3.53}$$

$$M_{C1C2} = \frac{\Phi_{C1C2}}{I_{C1}}, \tag{3.54}$$

$$M_{\mathrm{C1C3}} = \frac{\Phi_{\mathrm{C1C3}}}{I_{\mathrm{C1}}} \tag{3.55}$$

where are

I_{C1} current of circular coil 1,

Φ_{AC1} magnetic flux linkage of arbitrary coil due to current I_{C1},

Φ_{C1C2} magnetic flux linkage of circular coil 2 due to current I_{C1},

Φ_{C1C3} magnetic flux linkage of circular coil 3 due to current I_{C1}.

Magnetic flux linkages Φ_{AC1}, Φ_{C1C2}, Φ_{C1C3} are given by expressions [33]

$$\Phi_{\mathrm{AC1}} = \sum_{i=1}^{N_{\mathrm{A}}} \iint_{S_{\mathrm{A},i}} \boldsymbol{B}_{\mathrm{C1}} \mathrm{d}\boldsymbol{S}_{\mathrm{A},i} = \sum_{i=1}^{N_{\mathrm{A}}} \iint_{S_{\mathrm{A},i}} B_{\mathrm{C1Z}} \mathrm{d}S_{\mathrm{A},i} \,, \tag{3.56}$$

$$\Phi_{\mathrm{C1C2}} = \sum_{i=1}^{N_{\mathrm{C2}}} \iint_{S_{\mathrm{C2},i}} \boldsymbol{B}_{\mathrm{C1}} \mathrm{d}\boldsymbol{S}_{\mathrm{C2},i} = \sum_{i=1}^{N_{\mathrm{C2}}} \iint_{S_{\mathrm{C2},i}} B_{\mathrm{C1Z}} \mathrm{d}S_{\mathrm{C2},i} \,, \tag{3.57}$$

$$\Phi_{\mathrm{C1C3}} = \sum_{i=1}^{N_{\mathrm{C3}}} \iint_{S_{\mathrm{C3},i}} \boldsymbol{B}_{\mathrm{C1}} \mathrm{d}\boldsymbol{S}_{\mathrm{C3},i} = \sum_{i=1}^{N_{\mathrm{C3}}} \iint_{S_{\mathrm{C3},i}} B_{\mathrm{C1Z}} \mathrm{d}S_{\mathrm{C3},i} \tag{3.58}$$

where are

$\boldsymbol{B}_{\mathrm{C1}}$ magnetic flux density excited by circular coil 1,

B_{C1Z} z-component of $\boldsymbol{B}_{\mathrm{C1}}$,

N_{A} number of turns of conductor of arbitrary coil,

N_{C2} number of turns of conductor of circular coil 2 (it is equal to N_{A}),

N_{C3} number of turns of conductor of circular coil 3 (it is equal to N_{A}),

$S_{\mathrm{A},i}$ area of i^{th} turn of arbitrary coil,

$\mathrm{d}\boldsymbol{S}_{\mathrm{A},i}$ oriented element of $S_{\mathrm{A},i}$, see Fig. 3.5.,

$S_{\mathrm{C2},i}$ area of i^{th} turn of circular coil 2,

$\mathrm{d}\boldsymbol{S}_{\mathrm{C2},i}$ oriented element of $S_{\mathrm{C2},i}$, see Fig. 3.5.,

$S_{\mathrm{C3},i}$ area of i^{th} turn of circular coil 3,

$\mathrm{d}\boldsymbol{S}_{\mathrm{C3},i}$ oriented element of $S_{\mathrm{C3},i}$, see Fig. 3.5. b).

If integrations in (3.56)-(3.58) are performed in cylindrical coordinates (r, φ, z) and it is considered that magnetic field of circular coil 1 is rotationally symmetrical with respect to the axis ξ (it is constant for given coordinates r, z and all coordinates φ) it can be written

$$\mathrm{d}S_{\mathrm{A},i} = \mathrm{d}S_{\mathrm{C2},i} = \mathrm{d}S_{\mathrm{C3},i} = r\mathrm{d}\varphi\mathrm{d}r \,, \tag{3.59}$$

$$\Phi_{\mathrm{AC1}} = \int_{r_{\mathrm{C3}}}^{r_{\mathrm{C2}}} \sum_{i=1}^{N_{\mathrm{A}}} \int_{\varphi_{\mathrm{L}}}^{\varphi_{\mathrm{U}}} B_{\mathrm{C1Z}} r\mathrm{d}\varphi\mathrm{d}r + \Phi_{\mathrm{C}} = \int_{r_{\mathrm{C3}}}^{r_{\mathrm{C2}}} \alpha \underbrace{\sum_{i=1}^{N_{\mathrm{A}}} B_{\mathrm{C1Z}} r\mathrm{d}r}_{\mathrm{d}\Phi_{\mathrm{AC1}}} + \Phi_{\mathrm{C}} \,, \tag{3.60}$$

$$\Phi_{\mathrm{C1C2}} = \int_{0}^{r_{\mathrm{C2}}} \sum_{i=1}^{N_{\mathrm{A}}} \int_{0}^{2\pi} B_{\mathrm{C1Z}} r\mathrm{d}\varphi\mathrm{d}r = \int_{0}^{r_{\mathrm{C2}}} 2\pi \underbrace{\sum_{i=1}^{N_{\mathrm{A}}} B_{\mathrm{C1Z}} r\mathrm{d}r}_{\mathrm{d}\Phi_{\mathrm{C1C2}}} \,, \tag{3.61}$$

$$\Phi_{\mathrm{C1C3}} = \int_{0}^{r_{\mathrm{C3}}} \sum_{i=1}^{N_{\mathrm{A}}} \int_{0}^{2\pi} B_{\mathrm{C1Z}} r\mathrm{d}\varphi\mathrm{d}r = \int_{0}^{r_{\mathrm{C3}}} 2\pi \sum_{i=1}^{N_{\mathrm{A}}} B_{\mathrm{C1Z}} r\mathrm{d}r \tag{3.62}$$

where are

α shape function

$$\alpha = \varphi_{\mathrm{U}} - \varphi_{\mathrm{L}} \,, \tag{3.63}$$

φ_{L} lower angle which defines cross section of arbitrary coil for given radius r, see Fig. 3.5.,

φ_{U} upper angle which defines cross section of arbitrary coil for given radius r, see Fig. 3.5.,

r_{C2} radius of circular coil 2, see Fig. 3.5.,

r_{C3} radius determining arbitrary coil, see Fig. 3.5. a), or radius of circular coil 3, see Fig. 3.5. b),

Φ_{C} part of magnetic flux linkage Φ_{AC1}

$$\Phi_{\mathrm{C}} = \begin{cases} 0, \ \xi \in S_{\mathrm{OUT}}, \\ \Phi_{\mathrm{C1C3}}, \ \xi \in S_{\mathrm{IN}}. \end{cases} \tag{3.64}$$

The shape function α describes the cross section of the arbitrary coil. Its value represents the total angle of arcs which define cross section of the arbitrary coil for given radius r. Fig. 3.5. shows the case where total angle consists of only one part (one arc) for given radius r for simplicity. However, the total angle can consist of more parts (more arcs) for given radius r generally, see Fig. 3.6. Thus, the shape function α (3.63) can be generalized in the form

$$\alpha = \sum_{i} \left(\varphi_{\mathrm{U},i} - \varphi_{\mathrm{L},i} \right) \tag{3.65}$$

where are

$\varphi_{\mathrm{L},i}$ i^{th} lower angle which defines cross section of arbitrary coil for given radius r,

$\varphi_{\mathrm{U},i}$ i^{th} upper angle which defines cross section of arbitrary coil for given radius r.

The analytical formulation of shape function α is possible when the points $P_{\mathrm{L},i}$ and $P_{\mathrm{U},i}$ (corresponding to angles $\varphi_{\mathrm{L},i}$ and $\varphi_{\mathrm{U},i}$ respectively) of intersections of the curve which describes cross section of the arbitrary coil and circle with given radius r and center $P_{\mathrm{C}}(u_1, u_2)$ can be found analytically. This two-dimensional problem is described in the plane of coordinates (u_1, u_2) where the auxiliary coordinate axis r lies as well. The shape function α is then function of coordinates u_1, u_2, r and dimensions which describe the cross section of the arbitrary coil.

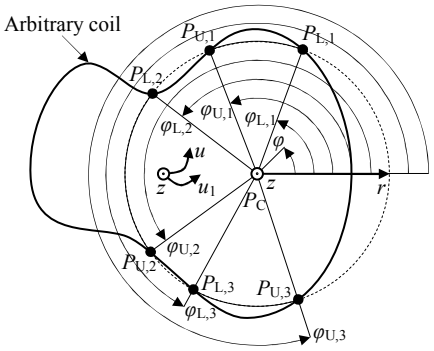

Fig. 3.6. Definition of shape function α.

Comparison of differentials $\mathrm{d}\Phi_{\mathrm{AC1}}$ and $\mathrm{d}\Phi_{\mathrm{C1C2}}$ in (3.60), (3.61) yields

$$\mathrm{d}\Phi_{\mathrm{AC1}} = \frac{\alpha}{2\pi} \mathrm{d}\Phi_{\mathrm{C1C2}}. \tag{3.66}$$

The differential $\mathrm{d}\Phi_{\mathrm{C1C2}}$ can be formally found with the help of derivative of Φ_{C1C2} with respect to the upper bound r_{C2} of the integral in (3.61)

$$\mathrm{d}\Phi_{\mathrm{C1C2}} = \left. \frac{\partial \Phi_{\mathrm{C1C2}}}{\partial r_{\mathrm{C2}}} \right|_{r_{\mathrm{C2}}=r} \mathrm{d}r. \tag{3.67}$$

The equation (3.53) for mutual inductance M_{AC1} can be manipulated using (3.54), (3.55), (3.60), (3.64), (3.66), (3.67) in the form

$$M_{\mathrm{AC1}} = \frac{\int_{r_{\mathrm{C3}}}^{r_{\mathrm{C2}}} \left. \frac{\partial \Phi_{\mathrm{C1C2}}}{\partial r_{\mathrm{C2}}} \right|_{r_{\mathrm{C2}}=r} \frac{\alpha}{2\pi} \mathrm{d}r}{I_{\mathrm{C1}}} + \frac{\Phi_{\mathrm{C}}}{I_{\mathrm{C1}}} = \int_{r_{\mathrm{C3}}}^{r_{\mathrm{C2}}} \left. \frac{\partial M_{\mathrm{C1C2}}}{\partial r_{\mathrm{C2}}} \right|_{r_{\mathrm{C2}}=r} \frac{\alpha}{2\pi} \mathrm{d}r + M_{\mathrm{C}} \tag{3.68}$$

where is

$$M_{\mathrm{C}} = \begin{cases} 0, \ \xi \in S_{\mathrm{OUT}}, \\ M_{\mathrm{C1C3}}, \ \xi \in S_{\mathrm{IN}}. \end{cases} \tag{3.69}$$

The mutual inductances M_{C1C2}, M_{C1C3} are given by relations [30]

$$M_{\mathrm{C1C2}} = \frac{\mu_0}{2} \frac{r_{\mathrm{C1}} N_{\mathrm{C1}}}{h_{\mathrm{C1}}} \frac{r_{\mathrm{C2}} N_{\mathrm{C2}}}{h_{\mathrm{C2}}} \int_{z-\frac{h_{\mathrm{C1}}}{2}}^{z+\frac{h_{\mathrm{C1}}}{2}} \int_{-\frac{h_{\mathrm{C2}}}{2}}^{\frac{h_{\mathrm{C2}}}{2}} \int_{0}^{2\pi} \frac{\cos(\varphi)}{\sqrt{r_{\mathrm{C1}}^2 + r_{\mathrm{C2}}^2 - 2 r_{\mathrm{C1}} r_{\mathrm{C2}} \cos(\varphi) + (z' - z'')^2}} \mathrm{d}\varphi \mathrm{d}z' \mathrm{d}z'', \tag{3.70}$$

$$M_{\mathrm{C1C3}} = \frac{\mu_0}{2} \frac{r_{\mathrm{C1}} N_{\mathrm{C1}}}{h_{\mathrm{C1}}} \frac{r_{\mathrm{C3}} N_{\mathrm{C3}}}{h_{\mathrm{C3}}} \int_{z-\frac{h_{\mathrm{C1}}}{2}}^{z+\frac{h_{\mathrm{C1}}}{2}} \int_{-\frac{h_{\mathrm{C3}}}{2}}^{\frac{h_{\mathrm{C3}}}{2}} \int_{0}^{2\pi} \frac{\cos(\varphi)}{\sqrt{r_{\mathrm{C1}}^2 + r_{\mathrm{C3}}^2 - 2 r_{\mathrm{C1}} r_{\mathrm{C3}} \cos(\varphi) + (z' - z'')^2}} \mathrm{d}\varphi \mathrm{d}z' \mathrm{d}z'' \tag{3.71}$$

where are

h_{C1} height of circular coil 1,

h_{C2} height of circular coil 2 (it is equal to h_{A} where h_{A} is height of arbitrary coil),

h_{C3} height of circular coil 3 (it is equal to h_{A} where h_{A} is height of arbitrary coil),

N_{C1} number of turns of circular coil 1,

N_{C2} number of turns of circular coil 2 (it is equal to N_{A} where N_{A} is number of turns of arbitrary coil),

N_{C3} number of turns of circular coil 3 (it is equal to N_{A} where N_{A} is number of turns of arbitrary coil),

r_{C1} radius of circular coil 1,

r_{C2} radius of circular coil 2,

r_{C3} radius of circular coil 3,

μ_0 permeability of vacuum.

Mutual inductance M_{AL} of the arbitrary coil and loop is found as a limit case of mutual inductance M_{AC1} since the loop can be considered as the circular coil 1 with zero height, one turn, and zero radius

$$M_{\mathrm{AL}} = \lim_{(h_{\mathrm{C1}}, N_{\mathrm{C1}}, r_{\mathrm{C1}}) \to (0,1,0)} M_{\mathrm{AC1}}. \tag{3.72}$$

The area $\mathrm{d}S_{\mathrm{L}}$ of the loop is then expressed as

$$\mathrm{d}S_{\mathrm{L}} = \lim_{r_{\mathrm{C1}} \to 0} \left(\pi r_{\mathrm{C1}}^2 \right). \tag{3.73}$$

Mutual inductance M_{AL} and, thus, magnetic flux density $\boldsymbol{B}_{\mathrm{A}}$ are then not dependant on height h_{C1}, number of turns N_{C1}, and radius r_{C1}.

3.2.3. Final Formula for Magnetic Flux Density

The equation (3.51) for magnetic flux density $\boldsymbol{B}_{\mathrm{A}}$ can be manipulated using (3.52), (3.68)-(3.73) in the form

$$\begin{aligned} \boldsymbol{B}_{\mathrm{A}} &= I_{\mathrm{A}} \nabla \int \frac{1}{\lim\limits_{r_{\mathrm{C1}} \to 0} \left(\pi r_{\mathrm{C1}}^2 \right)} \lim_{(h_{\mathrm{C1}}, N_{\mathrm{C1}}, r_{\mathrm{C1}}) \to (0,1,0)} \left(\int_{r_{\mathrm{C3}}}^{r_{\mathrm{C2}}} \left. \frac{\partial M_{\mathrm{C1C2}}}{\partial r_{\mathrm{C2}}} \right|_{r_{\mathrm{C2}} = r} \frac{\alpha}{2\pi} \mathrm{d}r + M_{\mathrm{C}} \right) \mathrm{d}z + \lim_{(h_{\mathrm{C1}}, N_{\mathrm{C1}}, r_{\mathrm{C1}}) \to (0,1,0)} \boldsymbol{C}_{\mathrm{B}} \\ &= -\mu_0 \nabla \left(-I_{\mathrm{A}} N_{\mathrm{A}} \left(\int_{r_{\mathrm{C3}}}^{r_{\mathrm{C2}}} \frac{\alpha}{2\pi} \psi \mathrm{d}r + \Psi \right) \right) \\ &\qquad\qquad \varphi_{\mathrm{M}} \end{aligned} \tag{3.74}$$

where are

$$\begin{aligned}\psi &= \frac{1}{\mu_0 N_\mathrm{A}} \frac{\partial}{\partial r_{\mathrm{C2}}} \left(\int \lim_{(h_{\mathrm{C1}}, N_{\mathrm{C1}}, r_{\mathrm{C1}}) \to (0,1,0)} \left(\frac{M_{\mathrm{C1C2}}}{\pi r_{\mathrm{C1}}^2} \right) \mathrm{d}z \right) \Bigg|_{r_{\mathrm{C2}} = r} \\ &= \frac{1}{\mu_0 N_\mathrm{A}} \frac{\partial}{\partial r_{\mathrm{C2}}} \left(\int \frac{\mu_0 N_{\mathrm{C2}}}{2 h_{\mathrm{C2}}} \left(\frac{h_{\mathrm{C2}} + 2z}{\sqrt{\left(h_{\mathrm{C2}} + 2z\right)^2 + 4 r_{\mathrm{C2}}^2}} + \frac{h_{\mathrm{C2}} - 2z}{\sqrt{\left(h_{\mathrm{C2}} - 2z\right)^2 + 4 r_{\mathrm{C2}}^2}} \right) \mathrm{d}z \right) \Bigg|_{r_{\mathrm{C2}} = r} \\ &= \frac{r}{h_\mathrm{A}} \left(\frac{1}{\sqrt{\left(h_\mathrm{A} + 2z\right)^2 + 4r^2}} - \frac{1}{\sqrt{\left(h_\mathrm{A} - 2z\right)^2 + 4r^2}} \right),\end{aligned} \tag{3.75}$$

$$\Psi = \begin{cases} 0, \ \xi \in S_{\mathrm{OUT}}, \\ \dfrac{1}{\mu_0 N_\mathrm{A}} \displaystyle\int \lim_{(h_{\mathrm{C1}}, N_{\mathrm{C1}}, r_{\mathrm{C1}}) \to (0,1,0)} \left(\frac{M_{\mathrm{C1C3}}}{\pi r_{\mathrm{C1}}^2} \right) \mathrm{d}z = \frac{1}{\mu_0 N_\mathrm{A}} \int \frac{\mu_0 N_{\mathrm{C3}}}{2 h_{\mathrm{C3}}} \left(\frac{h_{\mathrm{C3}} + 2z}{\sqrt{\left(h_{\mathrm{C3}} + 2z\right)^2 + 4 r_{\mathrm{C3}}^2}} + \frac{h_{\mathrm{C3}} - 2z}{\sqrt{\left(h_{\mathrm{C3}} - 2z\right)^2 + 4 r_{\mathrm{C3}}^2}} \right) \mathrm{d}z \\ = \dfrac{1}{4 h_\mathrm{A}} \left(\sqrt{\left(h_\mathrm{A} + 2z\right)^2 + 4 r_{\mathrm{C3}}^2} - \sqrt{\left(h_\mathrm{A} - 2z\right)^2 + 4 r_{\mathrm{C3}}^2} \right), \ \xi \in S_{\mathrm{IN}}. \end{cases} \tag{3.76}$$

Vector of integration constants $\boldsymbol{C}_\mathrm{B}$ becomes through manipulation zero. The final relation (3.74) for magnetic flux density $\boldsymbol{B}_\mathrm{A}$ (with functions ψ (3.75) and Ψ (3.76)) is rewritten lower more in detail and with highlighting of dependence of its parts on input parameters of the analysis

$$\begin{aligned}&\boldsymbol{B}_\mathrm{A}\left(u_1, u_2, z, h_\mathrm{A}, \boldsymbol{d}, N_\mathrm{A}, I_\mathrm{A}\right) = \left(B_{\mathrm{U1}}, B_{\mathrm{U2}}, B_\mathrm{Z}\right) \\ &= -\mu_0 \left(\frac{\partial}{h_1 \partial u_1}, \frac{\partial}{h_2 \partial u_2}, \frac{\partial}{\partial z} \right) \left(-I_\mathrm{A} N_\mathrm{A} \left(\int_{r_{\mathrm{C3}}(u_1, u_2, \boldsymbol{d})}^{r_{\mathrm{C2}}(u_1, u_2, \boldsymbol{d})} \frac{\alpha\left(u_1, u_2, r, \boldsymbol{d}\right)}{2\pi} \psi\left(z, r, h_\mathrm{A}\right) \mathrm{d}r + \Psi\left(z, r_{\mathrm{C3}}\left(u_1, u_2, \boldsymbol{d}\right), h_\mathrm{A}\right) \right) \right),\end{aligned} \tag{3.77}$$

$$\psi\left(z, r, h_\mathrm{A}\right) = \frac{r}{h_\mathrm{A}} \left(\frac{1}{\sqrt{\left(h_\mathrm{A} + 2z\right)^2 + 4r^2}} - \frac{1}{\sqrt{\left(h_\mathrm{A} - 2z\right)^2 + 4r^2}} \right), \tag{3.78}$$

$$\Psi\left(z, r_{\mathrm{C3}}\left(u_1, u_2, \boldsymbol{d}\right), h_\mathrm{A}\right) = \begin{cases} 0, \ \xi \in S_{\mathrm{OUT}}, \\ \dfrac{1}{4 h_\mathrm{A}} \left(\sqrt{\left(h_\mathrm{A} + 2z\right)^2 + 4 r_{\mathrm{C3}}^2\left(u_1, u_2, \boldsymbol{d}\right)} - \sqrt{\left(h_\mathrm{A} - 2z\right)^2 + 4 r_{\mathrm{C3}}^2\left(u_1, u_2, \boldsymbol{d}\right)} \right), \ \xi \in S_{\mathrm{IN}} \end{cases} \tag{3.79}$$

where $\boldsymbol{d}$ is vector of dimensions which describe certain cross section of the air core. The choice of transversal coordinates u_1, u_2 and, thus, the decomposition of vector of magnetic flux density $\boldsymbol{B}_\mathrm{A}$ in components B_{U1}, B_{U2} depends on a certain cross section of the arbitrary coil. The expressions for shape function α and radii r_{C2}, r_{C3} are given by the cross section as well. The functions ψ and Ψ are the same for arbitrary cross section of the coil, however, the function Ψ depends on radius r_{C3}.

It is usually necessary to perform integration in (3.77) with respect to r numerically since it is not possible to find primitive function for product of functions α and ψ generally. The order of integration with respect to r and derivation with respect to coordinates u_1, u_2, z in (3.77) can be interchanged and derivatives can be performed analytically. However, derivatives with respect to coordinates u_1, u_2 can be quite complex because it is necessary to derive shape function α and integral bounds r_{C2}, r_{C3} as well and both can be defined with respect to coordinates u_1, u_2 piece-wise. Thus, it is easier to perform derivatives with respect to coordinates u_1, u_2 numerically after numerical integration and summation with function Ψ which depends on coordinates u_1, u_2 through radius r_{C3} as well. Only in the case of derivative with respect to coordinate z, it can be useful to perform the derivative analytically since it is necessary to derive only functions ψ and Ψ which are simple functions of coordinate z.

3.2.4. Scalar Magnetic Potential

The expression in (3.74) which is denoted φ_{M}

$$\varphi_{\mathrm{M}} = -I_{\mathrm{A}} N_{\mathrm{A}} \left(\int_{r_{\mathrm{C3}}}^{r_{\mathrm{C2}}} \frac{\alpha}{2\pi} \psi \mathrm{d}r + \Psi \right) \tag{3.80}$$

is scalar function and its gradient multiplied by $-\mu_0$ yields desired vector of magnetic flux density $\boldsymbol{B}_{\mathrm{A}}$. The function φ_{M} can be called scalar magnetic potential because it corresponds to its definition [33]

$$\boldsymbol{B}_{\mathrm{A}} = -\mu_0 \boldsymbol{\nabla} \varphi_{\mathrm{M}} \,. \tag{3.81}$$

Thus, the result of the analysis is method for finding of scalar magnetic potential φ_{M} of the arbitrary coil with the help of mutual inductance of the arbitrary coil and elementary loop. The potential φ_{M} can be defined inside the space where the condition

$$\boldsymbol{\nabla} \times \boldsymbol{B}_{\mathrm{A}} = 0 \tag{3.82}$$

is valid and potential φ_{M} is continuous then there [33].

The following approximation is used for thin-wall coil here. The individual turns of conductor with current I_{A}, see Fig. 3.3. a), are replaced by a continuous current layer thickness t_{L} of which is considered as zero, see Fig. 3.3. b). Thus, the current of the layer is surface current and the current layer is contained in the boundary between spaces S_{IN} and S_{OUT}. Surface current density $\boldsymbol{K}_{\mathrm{A}}$ of the layer is given then by relation

$$\boldsymbol{K}_{\mathrm{A}} = \frac{N_{\mathrm{A}}}{h_{\mathrm{A}}} I_{\mathrm{A}} \boldsymbol{t} \tag{3.83}$$

where are

h_{A} height of arbitrary coil,

N_{A} number of turns of conductor of arbitrary coil,

$\boldsymbol{t}$ unit tangent vector to curve which turn tracks.

If the surface current is considered, the condition (3.82) becomes

$$\boldsymbol{n} \times \left(\boldsymbol{B}_{\mathrm{A},1} - \boldsymbol{B}_{\mathrm{A},2} \right) = 0 \tag{3.84}$$

for an arbitrary imaginary boundary inside the space with defined potential φ_{M} where

$\boldsymbol{n}$ is normal vector to boundary,

indices 1 and 2 denote one and other sides of boundary.

In the space, where the arbitrary coil represented by the current layer with surface current density $\boldsymbol{K}_{\mathrm{A}}$ is present, the condition (3.84) is not fulfilled generally since a boundary can be found (part of the boundary between spaces S_{IN} and S_{OUT}) where

$$\boldsymbol{n} \times \left(\boldsymbol{B}_{\mathrm{A},1} - \boldsymbol{B}_{\mathrm{A},2} \right) = \mu_0 \boldsymbol{K}_{\mathrm{A}} \tag{3.85}$$

as follows from boundary condition [33]. However, this space can be divided in parts inside which the condition (3.84) is valid. Potential φ_{M} can be discontinuous at the boundary between these parts of space.

The previous analysis gives the answer how to divide the space in order to define potential φ_{M}. The term $\int_{r_{\mathrm{C3}}}^{r_{\mathrm{C2}}} \frac{\alpha}{2\pi} \psi \mathrm{d}r$ in (3.80) is continuous function of coordinates (u_1, u_2, z) in the whole space. The function Ψ is continuous function of coordinates (u_1, u_2, z) in the inner space S_{IN} and outer space S_{OUT} with a discontinuity between them. Thus, potential φ_{M} given by (3.80) is continuous function of coordinates (u_1, u_2, z) in the inner space S_{IN} and outer space S_{OUT} with a discontinuity at the boundary between them. This leads to assumption that space has to be divided in two parts which correspond to inner space S_{IN} and outer space S_{OUT} in order to define potential φ_{M}. This assumption is confirmed since no surface current density exists inside these parts of space and condition (3.84) is fulfilled inside them.

Potential φ_M determines magnetic flux density $\boldsymbol{B}_A$ inside the spaces S_{IN} and S_{OUT}. However, potential φ_M is not defined at the boundary between these spaces where it is discontinuous and cannot determine magnetic flux density $\boldsymbol{B}_A$ there. It is evident from boundary conditions [33] that it is valid at the boundary between the spaces

$$\left.\begin{aligned}\boldsymbol{n}\times\left(\boldsymbol{B}_{A,OUT}-\boldsymbol{B}_{A,IN}\right)&=0,\\ \boldsymbol{n}\cdot\left(\boldsymbol{B}_{A,OUT}-\boldsymbol{B}_{A,IN}\right)&=0,\end{aligned}\right\}\ z\in\left(-\infty,-\frac{h_A}{2}\right)\cup\left(\frac{h_A}{2},\infty\right), \tag{3.86}$$

$$\left.\begin{aligned}\boldsymbol{n}\times\left(\boldsymbol{B}_{A,OUT}-\boldsymbol{B}_{A,IN}\right)&=\mu_0\boldsymbol{K}_A,\\ \boldsymbol{n}\cdot\left(\boldsymbol{B}_{A,OUT}-\boldsymbol{B}_{A,IN}\right)&=0,\end{aligned}\right\}\ z\in\left\langle-\frac{h_A}{2},\frac{h_A}{2}\right\rangle \tag{3.87}$$

where

$\boldsymbol{n}$ is normal vector to this boundary, see Fig. 3.3. b),

indices IN and OUT denote sides of boundary corresponding to inner space S_{IN} and outer space S_{OUT}.

For components B_{U1}, B_{U2}, B_Z of vector of magnetic flux density $\boldsymbol{B}_A$ at the boundary, it can be then written using (3.81), (3.83), (3.86), (3.87)

$$\left.\begin{aligned}B_{U1}=B_{U1,IN}=B_{U1,OUT}&=-\mu_0\frac{\partial\varphi_{M,IN}}{h_1\partial u_1}=-\mu_0\frac{\partial\varphi_{M,OUT}}{h_1\partial u_1},\\ B_{U2}=B_{U2,IN}=B_{U2,OUT}&=-\mu_0\frac{\partial\varphi_{M,IN}}{h_2\partial u_2}=-\mu_0\frac{\partial\varphi_{M,OUT}}{h_2\partial u_2},\end{aligned}\right\}\ z\in\left(-\infty,\infty\right), \tag{3.88}$$

$$B_Z=B_{Z,IN}=B_{Z,OUT}=-\mu_0\frac{\partial\varphi_{M,IN}}{\partial z}=-\mu_0\frac{\partial\varphi_{M,OUT}}{\partial z},\ z\in\left(-\infty,-\frac{h_A}{2}\right)\cup\left(\frac{h_A}{2},\infty\right), \tag{3.89}$$

$$\mu_0K_A=B_{Z,IN}-B_{Z,OUT}=-\mu_0\frac{\partial\varphi_{M,IN}}{\partial z}+\mu_0\frac{\partial\varphi_{M,OUT}}{\partial z},\ z\in\left\langle-\frac{h_A}{2},\frac{h_A}{2}\right\rangle. \tag{3.90}$$

It means that the determination of components B_{U1}, B_{U2} from potential φ_M can be extended for the whole boundary and component B_Z out of the current layer since partial derivatives of potential φ_M have to be equal at the both sides of the boundary for corresponding regions as the conditions (3.86), (3.87) show. Component B_Z is not defined at the current layer and it is discontinuous there since partial derivatives of potential φ_M with respect to coordinate z differ at its sides due to surface current density $\boldsymbol{K}_A$.

It is important to avoid inaccuracy in calculation of potential φ_M which can be critical for calculation of magnetic flux density $\boldsymbol{B}_A$ through gradient in (3.81) using numerical derivatives. Thus, the interval $\langle r_{C3}, r_{C2}\rangle$ for numerical integration with respect to r in (3.80) has to be divided into subintervals where shape function α is continuous and has continuous derivative with respect to r.

The presented method can be used as a basic element for analysis of magnetic field of complex configurations of multiple coils, especially, when magnetic flux density is calculated in the whole given space. The advantage of the presented method with respect to methods which calculate components of magnetic flux density separately insists in calculation of scalar magnetic potentials of individual coils and their successive superposition with respect to one coordinate system. The resultant magnetic flux density can be then obtained by gradient of scalar magnetic potential which avoids vector superposition of magnetic flux densities of individual coils. When the magnetic flux density is calculated in the whole given space the scalar magnetic potential can be evaluated in an orthogonal spatial grid. The resultant magnetic flux density can be then calculated by numerical gradient between neighbouring points of the grid in given direction which reduces the number of numerical integrations which are necessary for evaluation of every component of magnetic flux density in the other case.

3.2.5. Examples

The above described analysis of magnetic field of the arbitrary coil is verified using two examples of the arbitrary coil. Magnetic flux density $\boldsymbol{B}_A$ calculated by presented method is compared with other approaches for both examples.

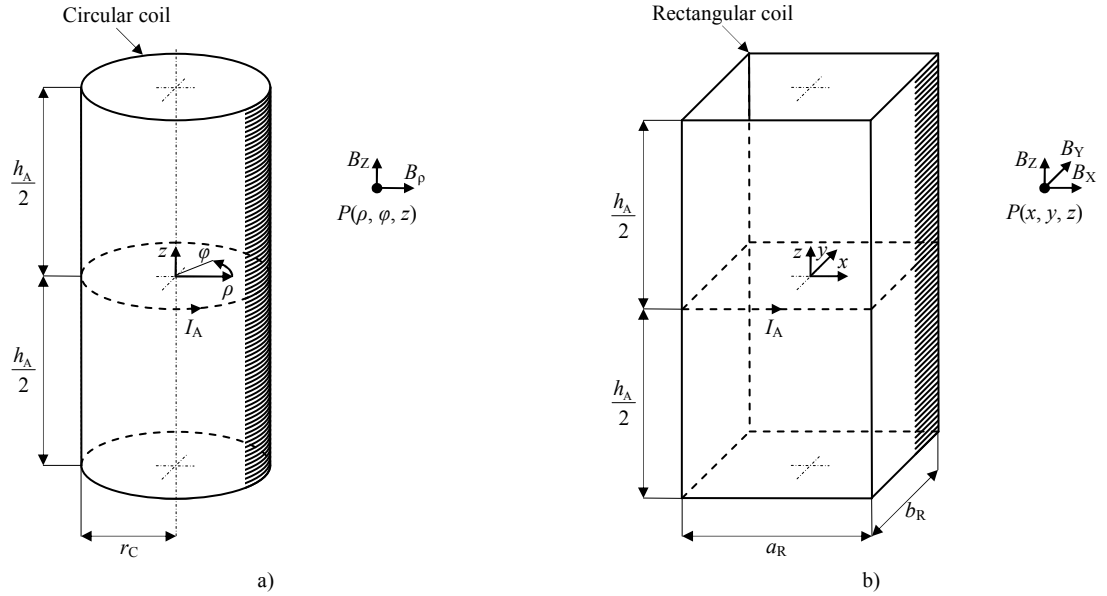

Fig. 3.7. Arrangement for analysis of magnetic field of a) circular coil, b) rectangular coil.

The first example is a thin-wall coil with air core of a shape of finite cylinder of circular cross section (circular coil). The circular coil has height h_A, number of turns N_A, radius r_C of the air core and current I_A, see Fig. 3.7. a). Its magnetic field is described in cylindrical coordinates (ρ, φ, z). Magnetic flux density $\boldsymbol{B}_A$ calculated by the presented method is compared with four other methods.

The first method uses general complete elliptic integral for expression of components B_ρ, B_Z of magnetic flux density $\boldsymbol{B}_A$ by relations

$$B_\rho = \frac{\mu_0 I_A}{2\pi}\frac{N_A}{h_A}\left(-\beta_\rho\left(\rho, z, r_C, \frac{h_A}{2}\right)+\beta_\rho\left(\rho, z, r_C, -\frac{h_A}{2}\right)\right), \tag{3.91}$$

$$B_Z = \frac{\mu_0 I_A}{2\pi}\frac{N_A}{h_A}\left(\beta_Z\left(\rho, z, r_C, \frac{h_A}{2}\right)-\beta_Z\left(\rho, z, r_C, -\frac{h_A}{2}\right)\right) \tag{3.92}$$

where are

$$\beta_\rho\left(\rho, z, r_C, z'\right) = \begin{cases} \sqrt{\frac{r_C}{\rho}\left(1-p_C^2\right)}\,\mathrm{cel}\left(p_C, 1, 1, -1\right), & \rho > 0, \\ 0, & \rho = 0, \end{cases} \tag{3.93}$$

$$\beta_Z\left(\rho, z, r_C, z'\right) = \begin{cases} -\sqrt{\frac{r_C}{\rho}\left(1-p_C^2\right)}\,\frac{\left(z-z'\right)}{r_C+\rho}\,\mathrm{cel}\left(p_C, \left(\frac{r_C-\rho}{r_C+\rho}\right)^2, 1, \frac{r_C-\rho}{r_C+\rho}\right), & \rho > 0, \\ -\frac{\pi\left(z-z'\right)}{\sqrt{r_C^2+\left(z-z'\right)^2}}, & \rho = 0, \end{cases} \tag{3.94}$$

$$\mathrm{cel}\left(p_C, q_1, q_2, q_3\right) = \int_0^{\frac{\pi}{2}} \frac{q_2\cos^2\left(\theta\right)+q_3\sin^2\left(\theta\right)}{\left(\cos^2\left(\theta\right)+q_1\sin^2\left(\theta\right)\right)\sqrt{\cos^2\left(\theta\right)+p_C^2\sin^2\left(\theta\right)}}\mathrm{d}\theta, \tag{3.95}$$

$$p_C = \sqrt{\frac{\left(r_C-\rho\right)^2+\left(z-z'\right)^2}{\left(r_C+\rho\right)^2+\left(z-z'\right)^2}}. \tag{3.96}$$

The expression $\mathrm{cel}(p_C, q_1, q_2, q_3)$ represents general complete elliptic integral and can be evaluated effectively by numerical method described in [34]. The component B_φ is zero for circular coil. The relations (3.91)-(3.96) can be found using [33]

$$\boldsymbol{B}_{\mathrm{A}} = \nabla \times \boldsymbol{A}_{\mathrm{C}} \tag{3.97}$$

where $\boldsymbol{A}_{\mathrm{C}}$ is vector magnetic potential of circular coil given by expression [32]

$$\mathbf{A}_{\mathrm{C}} = \left(0, A_{\mathrm{C}\varphi}, 0\right) = \left(0, \frac{\mu_0 I_{\mathrm{A}}}{4\pi} \frac{r_{\mathrm{C}} N_{\mathrm{A}}}{h_{\mathrm{A}}} \int_{-\frac{h_{\mathrm{A}}}{2}}^{\frac{h_{\mathrm{A}}}{2}} \int_{0}^{2\pi} \frac{\cos(\theta)}{\sqrt{r_{\mathrm{C}}^2 + \rho^2 - 2 r_{\mathrm{C}} \rho \cos(\theta) + (z - z')^2}} \mathrm{d}\theta \mathrm{d}z', 0 \right). \tag{3.98}$$

The second method uses direct integration of surface current density $\boldsymbol{K}_{\mathrm{A}}$ according to the Biot-Savart law [33]

$$\boldsymbol{B}_{\mathrm{A}} = \frac{\mu_0}{4\pi} \iint_{S_{\mathrm{T}}} \frac{\boldsymbol{K}_{\mathrm{A}} \mathrm{d}S_{\mathrm{T}} \times \boldsymbol{r}_{\mathrm{T}}}{\left|\boldsymbol{r}_{\mathrm{T}}\right|^3} \tag{3.99}$$

where are

S_{T} surface of thin-wall of arbitrary coil,

$\mathrm{d}S_{\mathrm{T}}$ element of S_{T},

$\boldsymbol{r}_{\mathrm{T}}$ position vector from point on surface S_{T} to point where magnetic flux density $\boldsymbol{B}_{\mathrm{A}}$ is calculated.

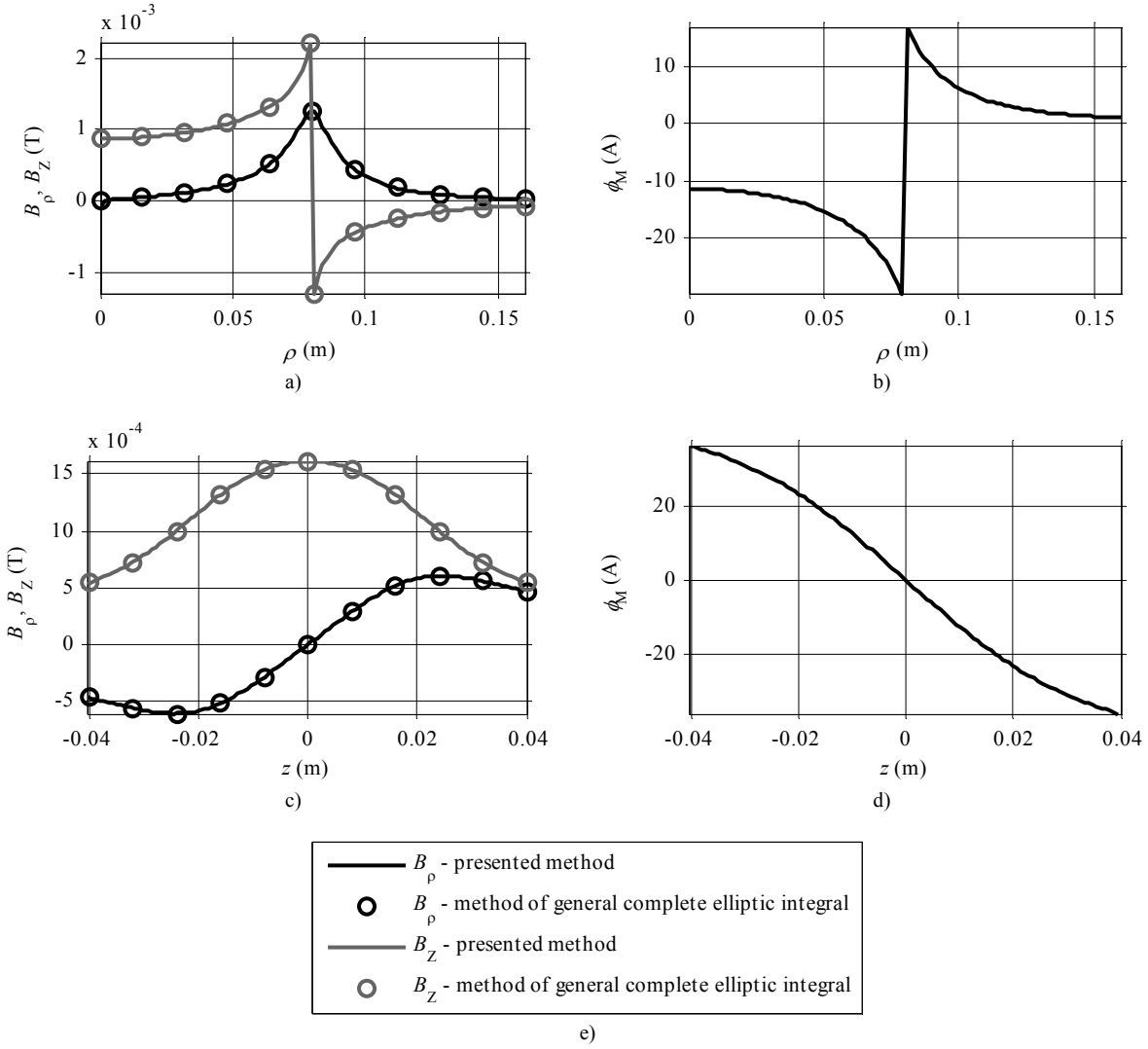

Fig. 3.8. Components B_{ρ}, B_Z of vector of magnetic flux density $\boldsymbol{B}_{\mathrm{A}}$ (comparison of presented method and method of general complete elliptic integral) and scalar magnetic potential φ_{M} of circular coil along chosen lines a), b) ρ, $z = 0.4h_{\mathrm{A}}$, c), d) $\rho = 0.8r_{\mathrm{C}}$, z, e) legend for graphs of components of magnetic flux density.

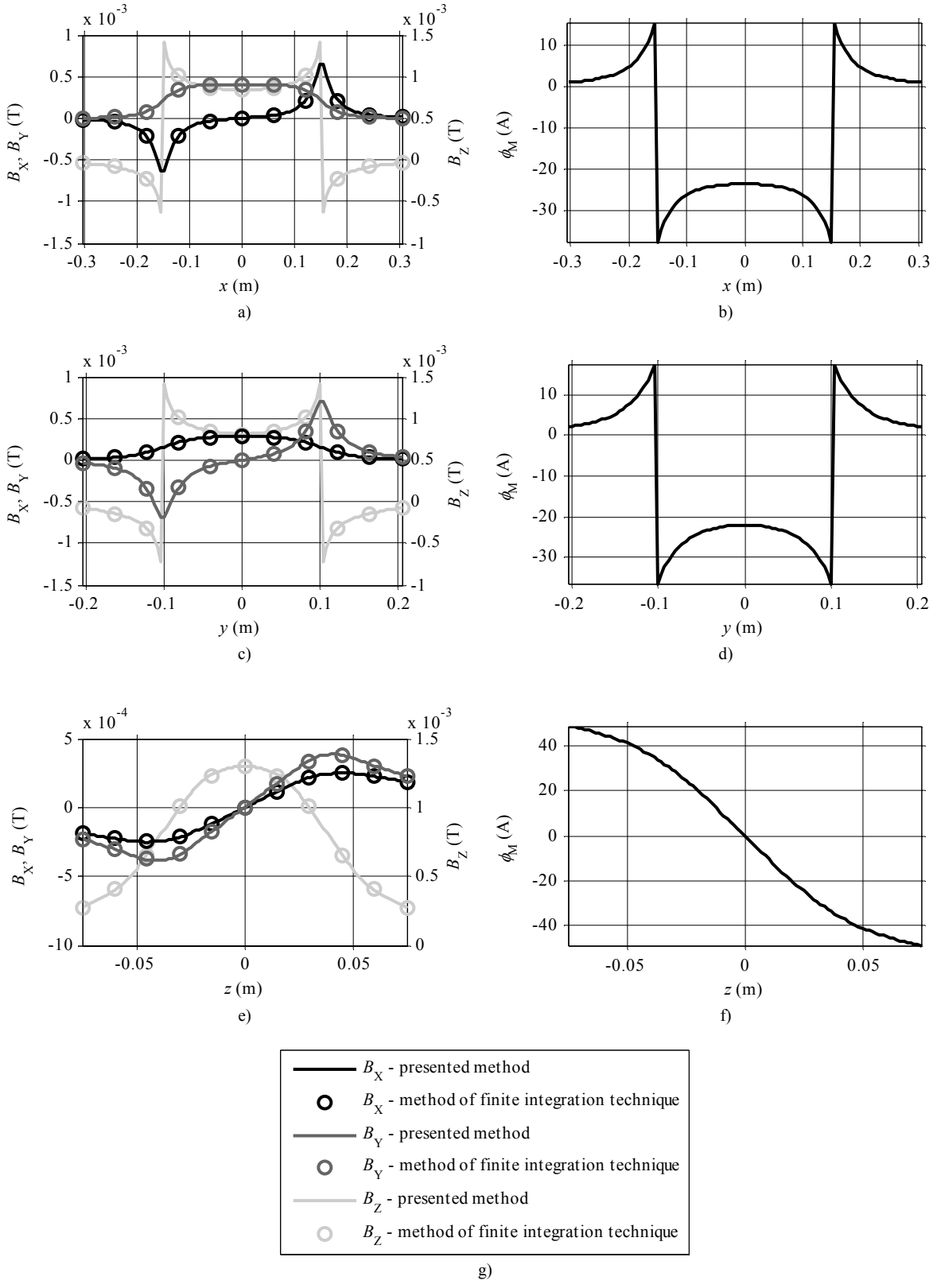

Fig. 3.9. Components B_X, B_Y, B_Z of vector of magnetic flux density $\boldsymbol{B}_A$ (comparison of presented method and method of finite integration technique) and scalar magnetic potential φ_M of rectangular coil along chosen lines a), b) x, $y = 0.4b_R$, $z = 0.4h_A$, c), d) $x = 0.4a_R$, y, $z = 0.4h_A$, e), f) $x = 0.4a_R$, $y = 0.4b_R$, z, g) legend for graphs of components of magnetic flux density.

Name	Circular coil	Rectangular coil
u_1	ρ	x
u_2	φ	y
h_1	1	1
h_2	ρ	1
$\boldsymbol{d}$	r_C	(a_R, b_R)
Inner parameters of analysis	$p_1 = \rho - r_C\ ,\ p_2 = \rho + r_C$	$p_1 = \lvert x\rvert - \frac{a_R}{2}\ ,\ p_2 = \lvert x\rvert + \frac{a_R}{2}\ ,\ p_3 = \lvert y\rvert - \frac{b_R}{2}\ ,\ p_4 = \lvert y\rvert + \frac{b_R}{2}$
$\alpha'(x, r, a_R, y')$		$p_{\alpha 1} = \sqrt{p_1^2 + \left(\frac{y'}{2}\right)^2}\ ,\ p_{\alpha 2} = \sqrt{p_2^2 + \left(\frac{y'}{2}\right)^2}$ $\alpha' = \begin{cases} 0, & (r=0) \vee (r < \lvert p_1\rvert \wedge p_1 > 0) \vee (r \geq p_{\alpha 2}), \\ 2\pi, & r < \lvert p_1\rvert \wedge p_1 < 0, \\ 2\arccos\left(\frac{p_1}{r}\right), & \lvert p_1\rvert \leq r < p_{\alpha 1}, \\ 2\arcsin\left(\frac{y'}{2r}\right), & p_{\alpha 1} \leq r < p_{\alpha 2} \end{cases}$ if $(p_2 \leq r < p_{\alpha 2})$ then $\alpha' \leftarrow \alpha' - 2\arccos\left(\frac{p_2}{r}\right)$ if $\left(\frac{y'}{2} < r < p_{\alpha 1}\right) \wedge (p_1 < 0)$ then $\alpha' \leftarrow \alpha' - 4\arccos\left(\frac{y'}{2r}\right)$
r_{C2}	p_2	$\sqrt{p_2^2 + p_4^2}$
r_{C3}	$\lvert p_1\rvert$	$\begin{cases} \sqrt{p_1^2 + p_3^2}, & p_1 > 0 \wedge p_3 > 0, \\ p_1, & p_1 > 0 \wedge p_3 \leq 0, \\ p_3, & p_1 \leq 0 \wedge p_3 > 0, \\ \lvert p_1\rvert, & p_1 \leq 0 \wedge p_3 \leq 0 \wedge \lvert p_1\rvert < \lvert p_3\rvert, \\ \lvert p_3\rvert, & p_1 \leq 0 \wedge p_3 \leq 0 \wedge \lvert p_1\rvert \geq \lvert p_3\rvert \end{cases}$
α	$\begin{cases} 2\pi, & 0 < r \leq \lvert p_1\rvert \wedge p_1 < 0, \\ 2\arccos\left(\frac{r^2 + \rho^2 - r_C^2}{2r\rho}\right), & \lvert p_1\rvert < r < p_2, \\ 0, & \text{otherwise} \end{cases}$	$\begin{cases} \alpha'(x, r, a_R, b_R), & y = 0, \\ \frac{\alpha'(x, r, a_R, 2\lvert y\rvert + b_R) + \alpha'(x, r, a_R, \lvert 2\lvert y\rvert - b_R\rvert)}{2}, & \lvert y\rvert < \frac{b_R}{2}, \\ \frac{\alpha'(x, r, a_R, 2\lvert y\rvert + b_R) - \alpha'(x, r, a_R, \lvert 2\lvert y\rvert - b_R\rvert)}{2}, & \lvert y\rvert \geq \frac{b_R}{2} \end{cases}$
ξ	$\xi \in \begin{cases} S_{IN}, p_1 < 0, \\ S_{OUT}, \text{otherwise} \end{cases}$	$\xi \in \begin{cases} S_{IN}, p_1 < 0 \wedge p_3 < 0, \\ S_{OUT}, \text{otherwise} \end{cases}$

Tab. 3.1. Specification of parts of relations (3.77), (3.79) which depend on cross section of air core.

Name	Circular coil	Rectangular coil
h_A [m]	0.04	0.075
N_A [-]	120	140
r_C [m]	0.08	-
a_R [m]	-	0.305
b_R [m]	-	0.205
I_A [A]	1	1

Tab. 3.2. Input parameters of analysis of magnetic field of circular and rectangular coils.

Method	Line			
	ρ, $z = 0.4h_A$ Fig. 3.8. a)		$\rho = 0.8r_C$, z Fig. 3.8. c)	
	B_ρ	B_Z	B_ρ	B_Z
Presented in section 3.2.	0.016	0.016	0.016	0.016
Presented in section 3.3.	0.034	0.026	0.016	0.014
General complete elliptic integral	0.001	0.001	0.001	0.001
Direct integration of Biot-Savart law	0.640	0.609	0.359	0.327
Method in [36]	0.046	0.032	0.031	0.031

The CPU time is in seconds.

Tab. 3.3. CPU time required for evaluation of magnetic flux density $\boldsymbol{B}_A$ using different methods for circular coil.

Method	Line								
	$x, y = 0.4b_R, z = 0.4h_A$ Fig. 3.9. a)			$x = 0.4a_R, y, z = 0.4h_A$ Fig. 3.9. c)			$x = 0.4a_R, y = 0.4b_R, z$ Fig. 3.9. e)		
	B_X	B_Y	B_Z	B_X	B_Y	B_Z	B_X	B_Y	B_Z
Presented in section 3.2.	0.156	0.156	0.156	0.156	0.156	0.156	0.172	0.172	0.172
Presented in section 3.3.	0.171	0.154	0.154	0.160	0.160	0.164	0.127	0.125	0.126
Finite integration technique	257	257	257	257	257	257	257	257	257
Direct integration of Biot-Savart law	0.249	0.359	0.592	0.140	0.359	0.484	0.156	0.359	0.499
Method in [36]	0.062	0.031	0.032	0.063	0.032	0.047	0.078	0.046	0.047

The CPU time is in seconds.

Tab. 3.4. CPU time required for evaluation of magnetic flux density $\boldsymbol{B}_A$ using different methods for rectangular coil.

The third and fourth methods are methods described in section 3.3. and in [36] respectively.

The second example is a thin-wall coil with air core of a shape of finite cylinder of rectangular cross section (rectangular coil). The rectangular coil has height h_A, number of turns N_A, dimensions a_R, b_R of the air core and current I_A, see Fig. 3.7. b). Its magnetic field is described in Cartesian coordinates (x, y, z). Magnetic flux density $\boldsymbol{B}_A$ calculated by the presented method is compared with four other methods.

The first method calculates magnetic flux density with the help of finite integration technique [35]. The second method uses direct integration of surface current density $\boldsymbol{K}_A$ according to the Biot-Savart law (3.99). The third and fourth methods are methods described in section 3.3. and in [36] respectively.

The parts of relations (3.77), (3.79) which differ for circular and rectangular coil are specified for both examples in Tab. 3.1. The expressions for shape function α and radii r_{C2}, r_{C3} are taken from [30]. Fig. 3.8. and Fig. 3.9. show comparison of magnetic flux density $\boldsymbol{B}_A$ calculated by the presented method with the method of general complete elliptic integral and method of finite integration technique for the circular and rectangular coils respectively. The magnetic flux density $\boldsymbol{B}_A$ is evaluated along chosen lines for input analysis parameters given in Tab. 3.2. The evaluation is performed for 100 equidistant points (all points are not plotted for clarity) along every line for every component of magnetic flux density $\boldsymbol{B}_A$ by every method. The same evaluation is performed for other mentioned methods. The results of other methods are not plotted in Fig. 3.8. and Fig. 3.9. for clarity since they are very similar. The required CPU time of evaluation for every method is summarized in Tab. 3.3. and Tab. 3.4. for the circular and rectangular coil respectively. The CPU time of the presented method is equal for all components evaluated along the given line since the character of evaluation through scalar magnetic potential φ_M is identical for all components. In the case of the method of finite integration technique, the CPU time is equal for all components due to simultaneous evaluation of all components along all lines. The CPU time of other methods can differ for different components since components are evaluated according to different relations. The maximal deviation of the results of the presented method with respect to the results of other methods is 0.4 %.

Numerical integrations in the presented method, method of direct integration of Biot-Savart law and method described in [36] are evaluated using the adaptive quadrature method implemented in Mathcad [38]. All derivatives contained in gradient in (3.81) are evaluated numerically using central difference approximation.

3.3. Analysis of Magnetic Field of Multilayer Induction Coil with Air Core of Arbitrary Cross Section

The method of calculation of mutual inductance M_{AL} discussed in section 3.2.2. needs shape function α for characterization of cross section of the air core. This method is effective when shape function α is known for a given cross section, however, it can be time-consuming when the shape function α has to be found firstly. For this reason, other method for characterization of cross section is treated in this section. This method generalizes use of scalar magnetic potential φ_M for description of magnetic field out of the winding of a multilayer coil whose turns of conductor are wound homogeneously close together around air core of a shape of finite cylinder of arbitrary cross section, see Fig. 3.10. a) This method needs only parametrical expression of the curve which determines circumference of cross section of the air core. The problem is formulated in section 3.3.1. Formulas for calculation of magnetic flux density and scalar magnetic potential are derived in section 3.3.2. The presented method is verified by four examples in section 3.3.3.

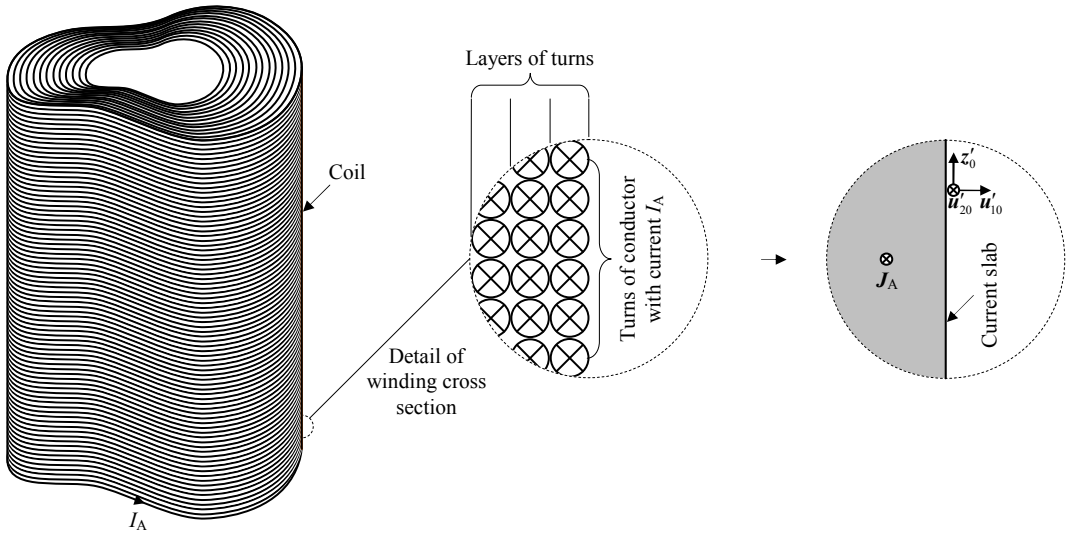

Fig. 3.10. a) Multilayer coil with air core of arbitrary cross section, b) approximation of turns of conductor by current slab.

3.3.1. Problem Formulation

Magnetic field of the coil and the coil are described in coordinates (u_1, u_2, z) and (u'_1, u'_2, z') respectively where (u_1, u_2) and (u'_1, u'_2) are general orthogonal curvilinear coordinates defined in the plane perpendicular to z- and z'-axis respectively, see Fig. 3.11. The corresponding Cartesian coordinates are (x, y, z) and (x', y', z') respectively. The coordinates (x, y) and (x', y') are expected to be functions of coordinates (u_1, u_2) and (u'_1, u'_2) respectively

$$(x, y) = (x(u_1, u_2), y(u_1, u_2)), \tag{3.100}$$

$$(x', y') = (x'(u'_1, u'_2), y'(u'_1, u'_2)). \tag{3.101}$$

The position vectors of these coordinates are $\boldsymbol{r}$ and $\boldsymbol{r}'$ respectively.

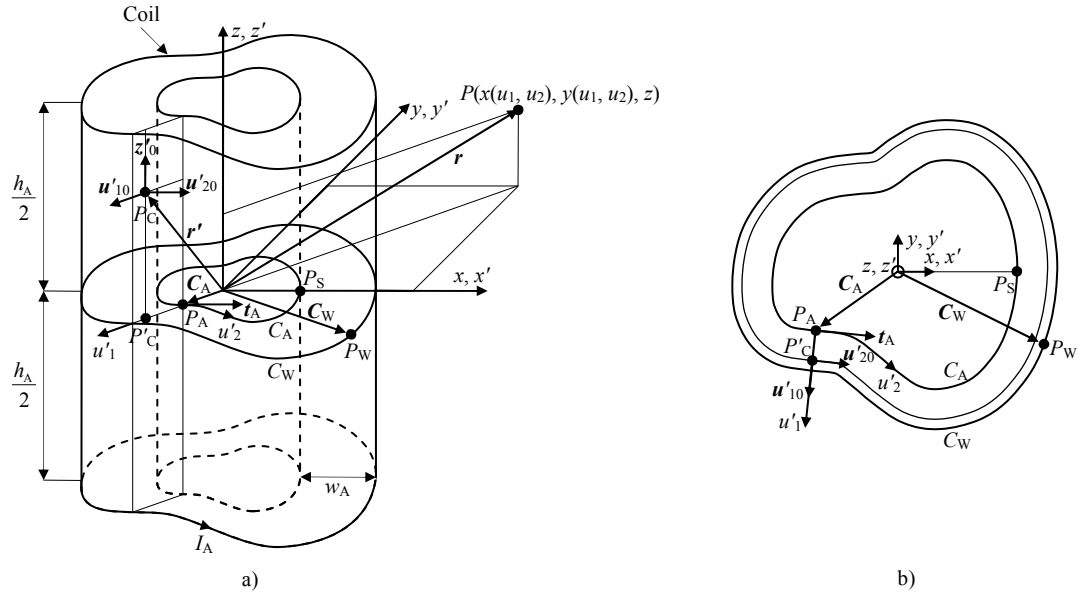

Fig. 3.11. a) Arrangement for analysis of magnetic field of multilayer coil, b) description of cross section of multilayer coil.

The choice of coordinates (u_1, u_2) and, thus, the decomposition of vector of magnetic flux density $\boldsymbol{B}_\mathrm{A}$ in components B_U1, B_U2 depends on a certain cross section of the air core. Coordinates (u_1, u_2) can differ from coordinates (u'_1, u'_2) generally. Position vector $\boldsymbol{r}$ of coordinates (u_1, u_2, z) can be generally written in the sense of (3.100) as

$$\boldsymbol{r} = x(u_1,u_2)\boldsymbol{x}_0 + y(u_1,u_2)\boldsymbol{y}_0 + z\boldsymbol{z}_0 \tag{3.102}$$

where $\boldsymbol{x}_0$, $\boldsymbol{y}_0$, $\boldsymbol{z}_0$ are orthonornal basis vectors of coordinates (x, y, z). Orthonormal basis vectors of coordinates (u_1, u_2, z) are $\boldsymbol{u}_{10}$, $\boldsymbol{u}_{20}$, $\boldsymbol{z}_0$. The directions of vectors $\boldsymbol{u}_{10}$, $\boldsymbol{u}_{20}$ are changing with changing vector $\boldsymbol{r}$ since the coordinates (u_1, u_2) are curvilinear and they are defined by relations [29]

$$\boldsymbol{u}_{10} = \frac{1}{h_1}\frac{\partial \boldsymbol{r}}{\partial u_1}, \tag{3.103}$$

$$\boldsymbol{u}_{20} = \frac{1}{h_2}\frac{\partial \boldsymbol{r}}{\partial u_2} \tag{3.104}$$

where h_1, h_2 are scale coefficients

$$h_1 = \left|\frac{\partial \boldsymbol{r}}{\partial u_1}\right|, \tag{3.105}$$

$$h_2 = \left|\frac{\partial \boldsymbol{r}}{\partial u_2}\right|. \tag{3.106}$$

The cross section of the air core is characterized by a closed curve C_A in the plane perpendicular to z-axis and parameterized by a position vector $\boldsymbol{C}_\mathrm{A}$ which is assumed to be function of coordinate u'_2 and is in the plane perpendicular to z-axis as well, see Fig. 3.11. Vector $\boldsymbol{C}_\mathrm{A}$ can be generally written in the sense of (3.101) as

$$\boldsymbol{C}_\mathrm{A} = C_{\mathrm{AX'}}(u'_2)\boldsymbol{x}'_0 + C_{\mathrm{AY'}}(u'_2)\boldsymbol{y}'_0, u'_2 \in \langle u'_{2\mathrm{S}}, u'_{2\mathrm{E}} \rangle \tag{3.107}$$

where are

$C_{\mathrm{AX'}}(u'_2)$ function indicating x' coordinate of curve C_A for given coordinate u'_2,

$C_{\mathrm{AY'}}(u'_2)$ function indicating y' coordinate of curve C_A for given coordinate u'_2,

$u'_{2\mathrm{S}}$ coordinate u'_2 for starting point P_S of the curve C_A,

$u'_{2\mathrm{E}}$ coordinate u'_2 for ending point of curve C_A which is identical with point P_S since curve C_A is closed

and $\boldsymbol{x}'_0$, $\boldsymbol{y}'_0$, $\boldsymbol{z}'_0$ are orthonornal basis vectors of coordinates (x', y', z'). The curve C_A is considered to have the same counterclockwise orientation, in which it is traversed by increasing coordinate u'_2, as current I_A flowing in the conductor of the winding of the coil, see Fig. 3.10. and Fig. 3.11.

Coordinates (u'_1, u'_2, z') and its position vector $\boldsymbol{r}'$ are constructed in the following way, see Fig. 3.11.,

$$\boldsymbol{r}' = \boldsymbol{C}_\mathrm{A}(u'_2) + \left(\frac{\boldsymbol{t}_\mathrm{A}(u'_2)}{|\boldsymbol{t}_\mathrm{A}(u'_2)|} \times \boldsymbol{z}'_0\right)u'_1 + z'\boldsymbol{z}'_0, \quad u'_1 \in \langle 0, w_\mathrm{A} \rangle, u'_2 \in \langle u'_{2\mathrm{S}}, u'_{2\mathrm{E}} \rangle, z' \in \left\langle -\frac{h_\mathrm{A}}{2}, \frac{h_\mathrm{A}}{2} \right\rangle \tag{3.108}$$

where are

w_A width of winding,

h_A height of coil,

$\boldsymbol{t}_\mathrm{A}$ tangential vector of the curve C_A

$$\boldsymbol{t}_\mathrm{A} = \frac{\partial \boldsymbol{C}_\mathrm{A}(u'_2)}{\partial u'_2}. \tag{3.109}$$

Tangential vector $\boldsymbol{t}_\mathrm{A}$ lies in the plane perpendicular to z'-axis since vector $\boldsymbol{C}_\mathrm{A}$ and coordinate u'_2 belong to this plane as well. Coordinates (u'_1, u'_2, z') are orthogonal as it is mentioned before. Their orthonormal basis vectors are $\boldsymbol{u}'_{10}$, $\boldsymbol{u}'_{20}$, $\boldsymbol{z}'_0$. The directions of vectors $\boldsymbol{u}'_{10}$, $\boldsymbol{u}'_{20}$ are changing with changing vector $\boldsymbol{r}'$ since coordinates (u'_1, u'_2) are curvilinear and they are defined by relations [29]

$$\boldsymbol{u}'_{10} = \frac{1}{h'_1}\frac{\partial \boldsymbol{r}'}{\partial u'_1}, \tag{3.110}$$

$$\boldsymbol{u}'_{20} = \frac{1}{h'_2}\frac{\partial \boldsymbol{r}'}{\partial u'_2} \tag{3.111}$$

where h'_1, h'_2 are scale coefficients

$$h'_1 = \left|\frac{\partial \boldsymbol{r}'}{\partial u'_1}\right|, \tag{3.112}$$

$$h'_2 = \left|\frac{\partial \boldsymbol{r}'}{\partial u'_2}\right|. \tag{3.113}$$

The relations (3.110)-(3.113) become using (3.108)

$$\boldsymbol{u}'_{10} = \frac{\boldsymbol{t}_\mathrm{A}}{|\boldsymbol{t}_\mathrm{A}|}\times \boldsymbol{z}'_0, \tag{3.114}$$

$$\boldsymbol{u}'_{20} = \frac{1}{h'_2}\left(\boldsymbol{t}_\mathrm{A} + \left(\frac{\partial}{\partial u'_2}\left(\frac{\boldsymbol{t}_\mathrm{A}}{|\boldsymbol{t}_\mathrm{A}|}\right)\times \boldsymbol{z}'_0\right)u'_1\right), \tag{3.115}$$

$$h'_1 = 1, \tag{3.116}$$

$$h'_2 = \left|\boldsymbol{t}_\mathrm{A} + \left(\frac{\partial}{\partial u'_2}\left(\frac{\boldsymbol{t}_\mathrm{A}}{|\boldsymbol{t}_\mathrm{A}|}\right)\times \boldsymbol{z}'_0\right)u'_1\right|. \tag{3.117}$$

The orthogonality of coordinates (u'_1, u'_2, z') can be verified by investigation of dot products $\boldsymbol{u}'_{10}\cdot\boldsymbol{u}'_{20}$, $\boldsymbol{u}'_{10}\cdot\boldsymbol{z}'_0$, $\boldsymbol{u}'_{20}\cdot\boldsymbol{z}'_0$ which are expected to be zero for orthogonal coordinates in all points of described space. The results of dot products are using (3.114), (3.115)

$$\begin{aligned}\boldsymbol{u}'_{10}\cdot\boldsymbol{u}'_{20} &= \frac{1}{h'_2}\left(\left(\frac{\boldsymbol{t}_\mathrm{A}}{|\boldsymbol{t}_\mathrm{A}|}\times \boldsymbol{z}'_0\right)\cdot\boldsymbol{t}_\mathrm{A} + \left(\frac{\boldsymbol{t}_\mathrm{A}}{|\boldsymbol{t}_\mathrm{A}|}\times \boldsymbol{z}'_0\right)\cdot\left(\frac{\partial}{\partial u'_2}\left(\frac{\boldsymbol{t}_\mathrm{A}}{|\boldsymbol{t}_\mathrm{A}|}\right)\times \boldsymbol{z}'_0\right)u'_1\right)\\ &= \frac{1}{h'_2}\left(\underbrace{|\boldsymbol{t}_\mathrm{A}|\boldsymbol{z}'_0\cdot\left(\frac{\boldsymbol{t}_\mathrm{A}}{|\boldsymbol{t}_\mathrm{A}|}\times\frac{\boldsymbol{t}_\mathrm{A}}{|\boldsymbol{t}_\mathrm{A}|}\right)}_{\mathbf{0}} + \underbrace{\left(\frac{\boldsymbol{t}_\mathrm{A}}{|\boldsymbol{t}_\mathrm{A}|}\times \boldsymbol{z}'_0\right)\cdot\frac{\partial}{\partial u'_2}\left(\frac{\boldsymbol{t}_\mathrm{A}}{|\boldsymbol{t}_\mathrm{A}|}\times \boldsymbol{z}'_0\right)u'_1}_{\boldsymbol{u}'_{10}\qquad\qquad\boldsymbol{u}'_{10}}\right) = 0,\end{aligned} \tag{3.118}$$

(unit vector $\boldsymbol{u}'_{10}$ and its derivative are perpendicular [37])

$$\boldsymbol{u}'_{10}\cdot\boldsymbol{z}'_0 = \left(\frac{\boldsymbol{t}_\mathrm{A}}{|\boldsymbol{t}_\mathrm{A}|}\times \boldsymbol{z}'_0\right)\cdot\boldsymbol{z}'_0 = \frac{\boldsymbol{t}_\mathrm{A}}{|\boldsymbol{t}_\mathrm{A}|}\cdot\underbrace{\left(\boldsymbol{z}'_0\times\boldsymbol{z}'_0\right)}_{\mathbf{0}} = 0, \tag{3.119}$$

$$\boldsymbol{u}'_{20}\cdot\boldsymbol{z}'_0 = \frac{1}{h'_2}\left(\underbrace{\boldsymbol{t}_\mathrm{A}\cdot\boldsymbol{z}'_0}_{0} + \left(\frac{\partial}{\partial u'_2}\left(\frac{\boldsymbol{t}_\mathrm{A}}{|\boldsymbol{t}_\mathrm{A}|}\right)\times \boldsymbol{z}'_0\right)u'_1\cdot\boldsymbol{z}'_0\right) = \frac{1}{h'_2}\left(\frac{\partial}{\partial u'_2}\left(\frac{\boldsymbol{t}_\mathrm{A}}{|\boldsymbol{t}_\mathrm{A}|}\right)\cdot\underbrace{\left(\boldsymbol{z}'_0\times\boldsymbol{z}'_0\right)}_{\mathbf{0}}u'_1\right) = 0, \tag{3.120}$$

as it is expected.

Additionally, vectors $\boldsymbol{u}'_{20}$ and $\boldsymbol{t}_\mathrm{A}$ are collinear for fixed coordinate u'_2 and all coordinates u'_1, z' which can be proven as follows. The relation (3.115) for $\boldsymbol{u}'_{20}$ contains sum of vectors $\boldsymbol{t}_\mathrm{A}$ and $\left(\frac{\partial}{\partial u'_2}\left(\frac{\boldsymbol{t}_\mathrm{A}}{|\boldsymbol{t}_\mathrm{A}|}\right)\times \boldsymbol{z}'_0\right)u'_1$. Derivative of unit vector is perpendicular to this vector, thus, derivative $\frac{\partial}{\partial u'_2}\left(\frac{\boldsymbol{t}_\mathrm{A}}{|\boldsymbol{t}_\mathrm{A}|}\right)$ is perpendicular to vector $\boldsymbol{t}_\mathrm{A}$ and lies in the

plane perpendicular to z'-axis since coordinate u'_2 belong to this plane as well. Vector $\frac{\partial}{\partial u'_2}\left(\frac{\boldsymbol{t}_\mathrm{A}}{|\boldsymbol{t}_\mathrm{A}|}\right)\times \boldsymbol{z}'_0$ (multiplied by coordinate u'_1) and vector $\boldsymbol{t}_\mathrm{A}$ are then collinear and this proofs collinearity of vectors $\boldsymbol{u}'_{20}$ and $\boldsymbol{t}_\mathrm{A}$. It means as well that vectors $\boldsymbol{u}'_{10}$ and $\boldsymbol{t}_\mathrm{A}$ are perpendicular for fixed coordinate u'_2 and all coordinates u'_1, z' since vectors $\boldsymbol{u}'_{10}$ and $\boldsymbol{u}'_{20}$ are perpendicular, thus, ending point of vector $\boldsymbol{r}'$ is moving with changing coordinate u'_1 along a straight line through the winding in direction perpendicular to curve C_A, see Fig. 3.11. The vectors $\boldsymbol{u}'_{20}$ and $\boldsymbol{t}_\mathrm{A}$ are collinear, however, their directions can be either the same or opposite which can be shown in the following way. It is useful to consider for further derivation that the parameterization of curve C_A is natural [37]. It means that coordinate u'_2 is expected to be length of arc of the curve C_A from the starting point P_S to the point of interest P_A, see Fig. 3.11. The parameterization by vector $\boldsymbol{C}_\mathrm{A}$ has then following properties:

$$\left|\boldsymbol{t}_\mathrm{A}\right| = \left|\frac{\partial \boldsymbol{C}_\mathrm{A}\left(u'_2\right)}{\partial u'_2}\right| = 1\,, \tag{3.121}$$

$$\left|\frac{\partial \boldsymbol{t}_\mathrm{A}\left(u'_2\right)}{\partial u'_2}\right| = \frac{1}{r_\mathrm{A}\left(u'_2\right)} \tag{3.122}$$

where r_A is called radius of curvature of the curve C_A in the point P_A [37]. The relation (3.115) can be then written as

$$\boldsymbol{u}'_{20} = \frac{1}{h'_2}\left(\boldsymbol{t}_\mathrm{A} + \left(\frac{\partial \boldsymbol{t}_\mathrm{A}}{\partial u'_2}\times \boldsymbol{z}'_0\right)u'_1\right). \tag{3.123}$$

The relation (3.123) contains sum of vectors $\boldsymbol{t}_\mathrm{A}$ and $\left(\frac{\partial \boldsymbol{t}_\mathrm{A}}{\partial u'_2}\times \boldsymbol{z}'_0\right)u'_1$. The size of vector $\boldsymbol{t}_\mathrm{A}$ is 1 and size of vector $\left(\frac{\partial \boldsymbol{t}_\mathrm{A}}{\partial u'_2}\times \boldsymbol{z}'_0\right)u'_1$ is using (3.122)

$$\left|\left(\frac{\partial \boldsymbol{t}_\mathrm{A}}{\partial u'_2}\times \boldsymbol{z}'_0\right)u'_1\right| = \frac{u'_1}{r_\mathrm{A}}\,. \tag{3.124}$$

If the curve C_A is convex then directions of vectors $\boldsymbol{t}_\mathrm{A}$ and $\left(\frac{\partial \boldsymbol{t}_\mathrm{A}}{\partial u'_2}\times \boldsymbol{z}'_0\right)u'_1$ are the same, thus, directions of vectors $\boldsymbol{u}'_{20}$ and $\boldsymbol{t}_\mathrm{A}$ are the same as well, see Fig. 3.12. a). If the curve C_A is not convex then directions of vectors $\boldsymbol{t}_\mathrm{A}$ and $\left(\frac{\partial \boldsymbol{t}_\mathrm{A}}{\partial u'_2}\times \boldsymbol{z}'_0\right)u'_1$ can be opposite for any u'_2, thus, directions of vectors $\boldsymbol{u}'_{20}$ and $\boldsymbol{t}_\mathrm{A}$ are the same only if

$$u'_1 < r_\mathrm{A} \tag{3.125}$$

as follows from (3.121), (3.123), (3.124), see Fig. 3.12. b). If directions of vectors $\boldsymbol{u}'_{20}$ and $\boldsymbol{t}_\mathrm{A}$ should be the same for all coordinates $u'_2 \in \langle u'_{2\mathrm{S}}, u'_{2\mathrm{E}}\rangle$ of non-convex curve C_A and all coordinates $u'_1 \in \langle 0, w_\mathrm{A}\rangle$ then condition (3.125) becomes

$$w_\mathrm{A} < r_\mathrm{A}\left(u'_2\right), \quad u'_2 \in \left\langle u'_{2\mathrm{S}}, u'_{2\mathrm{E}}\right\rangle. \tag{3.126}$$

Coordinates (u'_1, u'_2, z') are suitable for all constructible coils of the kind depicted in Fig. 3.10. Constructability of the coil depends on air core cross section in conjunction with width w_A of the winding. It means it depends on a curve C_W which characterizes outer perimeter of winding cross section in the plane perpendicular to z-axis, see Fig. 3.11. The curve C_W must not to intersect itself for constructability. The curve C_W can be parameterized by position vector $\boldsymbol{C}_\mathrm{W}$ which can be expressed using (3.108) as

$$\boldsymbol{C}_\mathrm{W} = \boldsymbol{r}'\left(u'_1 = w_\mathrm{A}, u'_2, z' = 0\right) = \boldsymbol{C}_\mathrm{A}\left(u'_2\right) + \left(\frac{\boldsymbol{t}_\mathrm{A}\left(u'_2\right)}{\left|\boldsymbol{t}_\mathrm{A}\left(u'_2\right)\right|}\times \boldsymbol{z}'_0\right)w_\mathrm{A}, \quad u'_2 \in \left\langle u'_{2\mathrm{S}}, u'_{2\mathrm{E}}\right\rangle. \tag{3.127}$$

In the sense of (3.127), the curve does not intersect itself if

$$\boldsymbol{C}_\mathrm{W}\left(u'_2 = u'_{2,1}\right) \neq \boldsymbol{C}_\mathrm{W}\left(u'_2 = u'_{2,2}\right), \quad u'_{2,1} \neq u'_{2,2}\,. \tag{3.128}$$

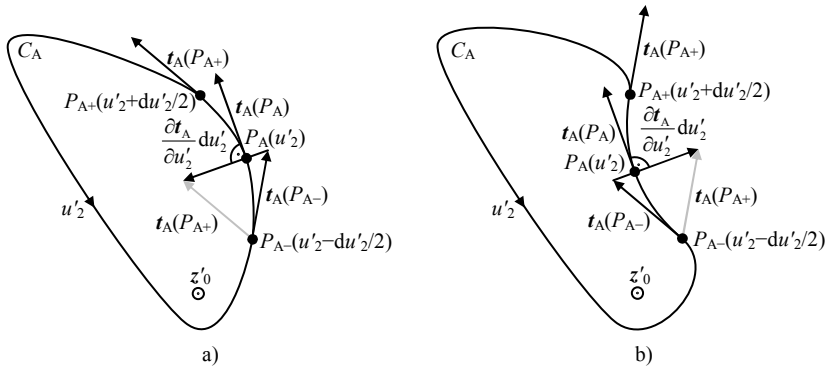

Fig. 3.12. a) Convex curve C_A, b) non-convex curve C_A.

The curves which the turns of conductor trace are assumed to be perpendicular to vector $\boldsymbol{u}'_{10}$ and collinear with vector $\boldsymbol{u}'_{20}$. The pitch of the winding is neglected. The following approximation is used for the winding. The individual turns of conductor are replaced by a slab with homogenous current density $\boldsymbol{J}_A$, see Fig. 3.10., given by relation

$$\boldsymbol{J}_A = \frac{M_A N_A I_A}{h_A w_A}\boldsymbol{u}'_{20} \tag{3.129}$$

where are

N_A number of turns of conductor in one layer of winding,

M_A number of layers.

The directions of current density $\boldsymbol{J}_A$ and vector $\boldsymbol{u}'_{20}$ are the same for all constructible coils which can be shown as follows. The vectors $\boldsymbol{u}'_{20}$, $\boldsymbol{t}_A$, and $\boldsymbol{J}_A$ are collinear. Additionally, the directions of vectors $\boldsymbol{t}_A$ and $\boldsymbol{J}_A$ are the same since orientation in which the curve C_A is traversed by increasing coordinate u'_2 is the same as orientation of current I_A. The directions of vectors $\boldsymbol{u}'_{20}$ and $\boldsymbol{t}_A$ are the same for all convex curves C_A and for non-convex curves C_A if the condition (3.126) holds true. This condition holds true since the condition (3.128) holds true. It means if the curve C_W does not intersect itself then radius of curvature r_A of the curve C_A is smaller than width w_A of the winding (perpendicular distance of curves C_A and C_W) for all coordinates $u'_2 \in \langle u'_{2S}, u'_{2E}\rangle$.

3.3.2. Magnetic Flux Density and Scalar Magnetic Potential

The Biot-Savart law [33] is used in further derivation. It is given by relation

$$\boldsymbol{B}_A = \frac{\mu_0}{4\pi}\iiint_{V_A}\boldsymbol{J}_A \times \frac{\boldsymbol{r}-\boldsymbol{r}'}{|\boldsymbol{r}-\boldsymbol{r}'|^3}\mathrm{d}V_A \tag{3.130}$$

where are

V_A volume of winding,

$\mathrm{d}V_A$ element of V_A

$$\mathrm{d}V_A = h'_1 h'_2 \mathrm{d}u'_1 \mathrm{d}u'_2 \mathrm{d}z' . \tag{3.131}$$

Potential φ_M can be defined inside the space where the condition (3.82) holds true [33]. It means potential φ_M can be defined outside the winding where current density is zero as it is necessary for zero on right side of the condition (3.82). This space corresponds to union of spaces S_{IN+}, S_{W+}, S_{OUT+}, S_{IN-}, S_{W-}, S_{OUT-}, see Fig. 3.13., which are characterized as

$$S_{IN+} = \left\{\sqrt{x^2+y^2} \le |\boldsymbol{C}_A|, 0 \le z < \infty\right\}, \tag{3.132}$$

$$S_{W+} = \left\{|\boldsymbol{C}_A| \le \sqrt{x^2+y^2} \le |\boldsymbol{C}_W|, \frac{h_A}{2} \le z < \infty\right\}, \tag{3.133}$$

$$S_{\mathrm{OUT+}} = \left\{ \left| \boldsymbol{C}_{\mathrm{W}} \right| \le \sqrt{x^2 + y^2} < \infty, 0 \le z < \infty \right\}, \tag{3.134}$$

$$S_{\mathrm{IN-}} = \left\{ \sqrt{x^2 + y^2} \le \left| \boldsymbol{C}_{\mathrm{A}} \right|, -\infty < z \le 0 \right\}, \tag{3.135}$$

$$S_{\mathrm{W-}} = \left\{ \left| \boldsymbol{C}_{\mathrm{A}} \right| \le \sqrt{x^2 + y^2} \le \left| \boldsymbol{C}_{\mathrm{W}} \right|, -\infty < z \le -\frac{h_{\mathrm{A}}}{2} \right\}, \tag{3.136}$$

$$S_{\mathrm{OUT-}} = \left\{ \left| \boldsymbol{C}_{\mathrm{W}} \right| \le \sqrt{x^2 + y^2} < \infty, -\infty < z \le 0 \right\}. \tag{3.137}$$

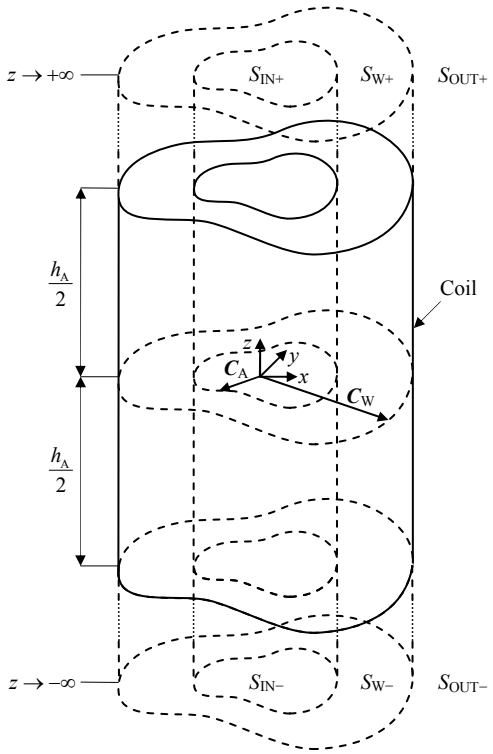

Fig. 3.13. Dividing of space around multilayer coil for calculation of scalar magnetic potential.

The expression for potential φ_{M} can be found by the following manipulation using (3.130):

$$\begin{aligned}
\boldsymbol{B}_{\mathrm{A}} &= \frac{\partial}{\partial z}\int \boldsymbol{B}_{\mathrm{A}}\,\mathrm{d}z = (z_0 \cdot \nabla)\int \boldsymbol{B}_{\mathrm{A}}\,\mathrm{d}z = (z_0 \cdot \nabla)\int \boldsymbol{B}_{\mathrm{A}}\,\mathrm{d}z + \Big(\int \boldsymbol{B}_{\mathrm{A}}\,\mathrm{d}z \cdot \nabla\Big)z_0 + z_0 \times \int_0 \nabla \times \boldsymbol{B}_{\mathrm{A}}\,\mathrm{d}z + \int_0 \boldsymbol{B}_{\mathrm{A}}\,\mathrm{d}z \times (\nabla \times z_0) \\
&= (z_0 \cdot \nabla)\int \boldsymbol{B}_{\mathrm{A}}\,\mathrm{d}z + \Big(\int_0 \boldsymbol{B}_{\mathrm{A}}\,\mathrm{d}z \cdot \nabla\Big)z_0 + z_0 \times \Big(\underbrace{\nabla \times \int \boldsymbol{B}_{\mathrm{A}}\,\mathrm{d}z}_{z_0 \times \int \nabla \times \boldsymbol{B}_{\mathrm{A}}\mathrm{d}z = 0} + \boldsymbol{C}_{\mathrm{B1}}\Big) + \int_0 \boldsymbol{B}_{\mathrm{A}}\,\mathrm{d}z \times (\nabla \times z_0) \\
&= -\mu_0 \nabla\left(-\frac{z_0}{\mu_0} \cdot \int \boldsymbol{B}_{\mathrm{A}}\,\mathrm{d}z \right) + z_0 \times \boldsymbol{C}_{\mathrm{B1}} = -\mu_0 \nabla\left(-\frac{z_0}{\mu_0} \cdot \int \frac{\mu_0}{4\pi} \underbrace{\iiint_{V_{\mathrm{A}}} \boldsymbol{J}_{\mathrm{A}} \times \frac{\boldsymbol{r} - \boldsymbol{r}'}{|\boldsymbol{r} - \boldsymbol{r}'|^3}\,\mathrm{d}V_{\mathrm{A}}}_{\boldsymbol{B}_{\mathrm{A}}}\,\mathrm{d}z \right) + z_0 \times \boldsymbol{C}_{\mathrm{B1}} \\
&= -\mu_0 \nabla\left(-\frac{z_0}{4\pi} \cdot \left(\iiint_{V_{\mathrm{A}}} \boldsymbol{J}_{\mathrm{A}} \times \frac{\boldsymbol{r} - \boldsymbol{r}'}{|\boldsymbol{r} - \boldsymbol{r}'|^3}\,\mathrm{d}z\mathrm{d}V_{\mathrm{A}} + \boldsymbol{C}_{\mathrm{B2}} \right) \right) + z_0 \times \boldsymbol{C}_{\mathrm{B1}} \\
&= -\mu_0 \nabla\left(-\frac{z_0}{4\pi} \cdot \underbrace{\iiint_{V_{\mathrm{A}}} \boldsymbol{J}_{\mathrm{A}} \times \frac{\boldsymbol{r} - \boldsymbol{r}'}{|\boldsymbol{r} - \boldsymbol{r}'|^3}\,\mathrm{d}z\mathrm{d}V_{\mathrm{A}}}_{\varphi_{\mathrm{R}}} \right) + z_0 \times \boldsymbol{C}_{\mathrm{B1}} + \underbrace{\frac{\mu_0}{4\pi} \nabla(z_0 \cdot \boldsymbol{C}_{\mathrm{B2}})}_{\boldsymbol{C}_{\mathrm{B}} = (C_{\mathrm{U1}}, C_{\mathrm{U2}}, C_{\mathrm{Z}} = 0)}.
\end{aligned} \tag{3.138}$$

The terms $\left(\int \boldsymbol{B}_{\mathrm{A}}\mathrm{d}z\cdot\nabla\right)z_0$ and $\nabla\times z_0$ in (3.138) are zero since the operator ∇ is applied on vector z_0 of unit size and constant direction. The term $\nabla\times\boldsymbol{B}_{\mathrm{A}}$ is zero since the condition (3.82) holds true outside the winding where the potential φ_{M} should be calculated. The interchange of operator of curl $\nabla\times$ and integration with respect to coordinate z or the interchange of integration with respect to volume V_{A} and integration with respect to coordinate z in (3.138) is taken into account by vectors of integration constants $\boldsymbol{C}_{\mathrm{B1}}$ and $\boldsymbol{C}_{\mathrm{B2}}$ which are merged into vectors of integration constants $\boldsymbol{C}_{\mathrm{B}}$. Vector $\boldsymbol{C}_{\mathrm{B}}$ has component C_{Z} equal to zero since vector $z_0\times\boldsymbol{C}_{\mathrm{B1}}$ is perpendicular to vector z_0 and operator of gradient ∇ is applied on scalar $z_0\cdot\boldsymbol{C}_{\mathrm{B2}}$ which is constant with respect to coordinate z. The expression in (3.138) which is denoted φ_{R}

$$\varphi_{\mathrm{R}}=-\frac{z_0}{4\pi}\cdot\iiint_{V_{\mathrm{A}}}\boldsymbol{J}_{\mathrm{A}}\times\frac{\boldsymbol{r}-\boldsymbol{r}'}{\left|\boldsymbol{r}-\boldsymbol{r}'\right|^3}\mathrm{d}z\mathrm{d}V_{\mathrm{A}} \tag{3.139}$$

can be considered as regular part of potential φ_{M}, however, there is other part φ_{C} of potential φ_{M} hidden in vector $\boldsymbol{C}_{\mathrm{B}}$ which has to be found. From (3.138), vector $\boldsymbol{C}_{\mathrm{B}}$ can be obtained with respect to the fact that $\boldsymbol{B}_{\mathrm{A}}(z\to\infty)=0$ for spaces $S_{\mathrm{IN+}}$, $S_{\mathrm{W+}}$, $S_{\mathrm{OUT+}}$ or $\boldsymbol{B}_{\mathrm{A}}(z\to-\infty)=0$ for spaces $S_{\mathrm{IN-}}$, $S_{\mathrm{W-}}$, $S_{\mathrm{OUT-}}$

$$\boldsymbol{C}_{\mathrm{B}}=\left(C_{\mathrm{U1}},C_{\mathrm{U2}},C_{\mathrm{Z}}=0\right)=\lim_{z\to\pm\infty}\left(\boldsymbol{B}_{\mathrm{A}}-\left(-\mu_0\nabla\varphi_{\mathrm{R}}\right)\right)=\mu_0\nabla\left(\lim_{z\to\pm\infty}\varphi_{\mathrm{R}}\right) \tag{3.140}$$

The relation (3.138) can be manipulate using (3.140) in the form

$$\boldsymbol{B}_{\mathrm{A}}=-\mu_0\nabla\Big(\underbrace{\varphi_{\mathrm{R}}-\lim_{z\to\pm\infty}\left(\varphi_{\mathrm{R}}\right)}_{\varphi_{\mathrm{M}}}\Big)=-\mu_0\nabla\left(\underbrace{-\frac{z_0}{4\pi}\cdot\iiint_{V_{\mathrm{A}}}\boldsymbol{J}_{\mathrm{A}}\times\frac{\boldsymbol{r}-\boldsymbol{r}'}{\left|\boldsymbol{r}-\boldsymbol{r}'\right|^3}\mathrm{d}z\mathrm{d}V_{\mathrm{A}}+\lim_{z\to\pm\infty}\left(\frac{z_0}{4\pi}\cdot\iiint_{V_{\mathrm{A}}}\boldsymbol{J}_{\mathrm{A}}\times\frac{\boldsymbol{r}-\boldsymbol{r}'}{\left|\boldsymbol{r}-\boldsymbol{r}'\right|^3}\mathrm{d}z\mathrm{d}V_{\mathrm{A}}\right)}_{\varphi_{\mathrm{M}}}\right). \tag{3.141}$$

The expression in (3.141) which is denoted φ_{M}

$$\varphi_{\mathrm{M}}=\varphi_{\mathrm{R}}-\underbrace{\lim_{z\to\pm\infty}\left(\varphi_{\mathrm{R}}\right)}_{\varphi_{\mathrm{C}}}=-\frac{z_0}{4\pi}\cdot\iiint_{V_{\mathrm{A}}}\boldsymbol{J}_{\mathrm{A}}\times\frac{\boldsymbol{r}-\boldsymbol{r}'}{\left|\boldsymbol{r}-\boldsymbol{r}'\right|^3}\mathrm{d}z\mathrm{d}V_{\mathrm{A}}+\underbrace{\lim_{z\to\pm\infty}\left(\frac{z_0}{4\pi}\cdot\iiint_{V_{\mathrm{A}}}\boldsymbol{J}_{\mathrm{A}}\times\frac{\boldsymbol{r}-\boldsymbol{r}'}{\left|\boldsymbol{r}-\boldsymbol{r}'\right|^3}\mathrm{d}z\mathrm{d}V_{\mathrm{A}}\right)}_{\varphi_{\mathrm{C}}} \tag{3.142}$$

is scalar magnetic potential corresponding to its definition [33]

$$\boldsymbol{B}_{\mathrm{A}}=\left(B_{\mathrm{U1}},B_{\mathrm{U2}},B_{\mathrm{Z}}\right)=\mu_0\boldsymbol{H}_{\mathrm{A}}=\mu_0\left(H_{\mathrm{U1}},H_{\mathrm{U2}},H_{\mathrm{Z}}\right)=-\mu_0\nabla\varphi_{\mathrm{M}}=-\mu_0\left(\frac{\partial}{h_1\partial u_1},\frac{\partial}{h_2\partial u_2},\frac{\partial}{\partial z}\right)\left(\varphi_{\mathrm{R}}+\varphi_{\mathrm{C}}\right) \tag{3.143}$$

where $\boldsymbol{H}_{\mathrm{A}}$ is magnetic field strength of the coil. The relation (3.139) becomes using (3.111), (3.116), (3.129), (3.131)

$$\varphi_{\mathrm{R}}=-\frac{M_{\mathrm{A}}N_{\mathrm{A}}I_{\mathrm{A}}}{4\pi h_{\mathrm{A}}w_{\mathrm{A}}}\oint_{C_{\mathrm{A}}}\int_{0}^{w_{\mathrm{A}}}\int_{-\frac{h_{\mathrm{A}}}{2}}^{\frac{h_{\mathrm{A}}}{2}}\int z_0\cdot\left(\frac{\boldsymbol{r}-\boldsymbol{r}'}{\left|\boldsymbol{r}-\boldsymbol{r}'\right|^3}\times\frac{\partial\left(\boldsymbol{r}-\boldsymbol{r}'\right)}{\partial u_2'}\right)\mathrm{d}z\mathrm{d}z'\mathrm{d}u_1'\mathrm{d}u_2'. \tag{3.144}$$

The relation (3.144) can be manipulated using (3.102), (3.107), (3.108), (3.109) to the form

$$\varphi_{\mathrm{R}}=-\frac{M_{\mathrm{A}}N_{\mathrm{A}}I_{\mathrm{A}}}{4\pi h_{\mathrm{A}}w_{\mathrm{A}}}\oint_{C_{\mathrm{A}}}\int_{0}^{w_{\mathrm{A}}}\int_{-\frac{h_{\mathrm{A}}}{2}}^{\frac{h_{\mathrm{A}}}{2}}\int\underbrace{\frac{p_{\mathrm{N2}}u_1'^2+p_{\mathrm{N1}}u_1'+p_{\mathrm{N0}}}{\left(u_1'^2+p_{\mathrm{D1}}u_1'+p_{\mathrm{D0}}+\left(z-z'\right)^2\right)^{\frac{3}{2}}}}_{I_{ZZ'U'1}}\mathrm{d}z\mathrm{d}z'\mathrm{d}u_1'\mathrm{d}u_2' \tag{3.145}$$

where are

$$p_{\mathrm{D0}}=\left|\boldsymbol{r}-\boldsymbol{C}_{\mathrm{A}}\right|^2-z^2=\left(x\left(u_1,u_2\right)-C_{\mathrm{AX'}}\left(u_2'\right)\right)^2+\left(y\left(u_1,u_2\right)-C_{\mathrm{AY'}}\left(u_2'\right)\right)^2, \tag{3.146}$$

$$p_{\mathrm{D1}}=2z_0\cdot\left(\frac{\boldsymbol{t}_{\mathrm{A}}}{\left|\boldsymbol{t}_{\mathrm{A}}\right|}\times\left(\boldsymbol{r}-\boldsymbol{C}_{\mathrm{A}}\right)\right)=-\frac{2\left(\left(x\left(u_1,u_2\right)-C_{\mathrm{AX'}}\left(u_2'\right)\right)\frac{\partial C_{\mathrm{AY'}}\left(u_2'\right)}{\partial u_2'}-\left(y\left(u_1,u_2\right)-C_{\mathrm{AY'}}\right)\frac{\partial C_{\mathrm{AX'}}\left(u_2'\right)}{\partial u_2'}\right)}{\sqrt{\left(\frac{\partial C_{\mathrm{AX'}}\left(u_2'\right)}{\partial u_2'}\right)^2+\left(\frac{\partial C_{\mathrm{AY'}}\left(u_2'\right)}{\partial u_2'}\right)^2}}, \tag{3.147}$$

$$p_{\mathrm{N0}} = \boldsymbol{z}_0 \cdot \left(\boldsymbol{t}_{\mathrm{A}} \times \left(\boldsymbol{r} - \boldsymbol{C}_{\mathrm{A}}\right)\right) = -\left(x\left(u_1, u_2\right) - C_{\mathrm{AX'}}\left(u_2'\right)\right)\frac{\partial C_{\mathrm{AY'}}\left(u_2'\right)}{\partial u_2'} + \left(y\left(u_1, u_2\right) - C_{\mathrm{AY'}}\left(u_2'\right)\right)\frac{\partial C_{\mathrm{AX'}}\left(u_2'\right)}{\partial u_2'}, \tag{3.148}$$

$$\begin{aligned} p_{\mathrm{N1}} &= \left|\boldsymbol{t}_{\mathrm{A}}\right| + \left(\boldsymbol{r} - \boldsymbol{C}_{\mathrm{A}}\right) \cdot \frac{\partial}{\partial u_2'}\left(\frac{\boldsymbol{t}_{\mathrm{A}}}{\left|\boldsymbol{t}_{\mathrm{A}}\right|}\right) = \\ &= \sqrt{\left(\frac{\partial C_{\mathrm{AX'}}\left(u_2'\right)}{\partial u_2'}\right)^2 + \left(\frac{\partial C_{\mathrm{AY'}}\left(u_2'\right)}{\partial u_2'}\right)^2} \\ &- \frac{\left(\left(x\left(u_1, u_2\right) - C_{\mathrm{AX'}}\left(u_2'\right)\right)\frac{\partial C_{\mathrm{AY'}}\left(u_2'\right)}{\partial u_2'} - \left(y\left(u_1, u_2\right) - C_{\mathrm{AY'}}\left(u_2'\right)\right)\frac{\partial C_{\mathrm{AX'}}\left(u_2'\right)}{\partial u_2'}\right)}{\left(\left(\frac{\partial C_{\mathrm{AX'}}\left(u_2'\right)}{\partial u_2'}\right)^2 + \left(\frac{\partial C_{\mathrm{AY'}}\left(u_2'\right)}{\partial u_2'}\right)^2\right)^{\frac{3}{2}}} \\ &\cdot \left(\frac{\partial C_{\mathrm{AX'}}\left(u_2'\right)}{\partial u_2'}\frac{\partial^2 C_{\mathrm{AY'}}\left(u_2'\right)}{\partial u_2'^2} - \frac{\partial C_{\mathrm{AY'}}\left(u_2'\right)}{\partial u_2'}\frac{\partial^2 C_{\mathrm{AX'}}\left(u_2'\right)}{\partial u_2'^2}\right), \end{aligned} \tag{3.149}$$

$$p_{\mathrm{N2}} = \boldsymbol{z}_0' \cdot \left(\frac{\boldsymbol{t}_{\mathrm{A}}}{\left|\boldsymbol{t}_{\mathrm{A}}\right|} \times \frac{\partial}{\partial u_2'}\left(\frac{\boldsymbol{t}_{\mathrm{A}}}{\left|\boldsymbol{t}_{\mathrm{A}}\right|}\right)\right) = \frac{\frac{\partial C_{\mathrm{AX'}}\left(u_2'\right)}{\partial u_2'}\frac{\partial^2 C_{\mathrm{AY'}}\left(u_2'\right)}{\partial u_2'^2} - \frac{\partial C_{\mathrm{AY'}}\left(u_2'\right)}{\partial u_2'}\frac{\partial^2 C_{\mathrm{AX'}}\left(u_2'\right)}{\partial u_2'^2}}{\left(\frac{\partial C_{\mathrm{AX'}}\left(u_2'\right)}{\partial u_2'}\right)^2 + \left(\frac{\partial C_{\mathrm{AY'}}\left(u_2'\right)}{\partial u_2'}\right)^2}. \tag{3.150}$$

The expression in (3.145) which is denoted $I_{\mathrm{ZZ'U'1}}$ is integral with respect to coordinates z, z', u'_1. This integral can be expressed analytically as follows:

$$I_{\mathrm{ZZ'U'1}} = \psi_{\mathrm{ZZ'U'1}}\left(w_{\mathrm{A}}, \frac{h_{\mathrm{A}}}{2}\right) - \psi_{\mathrm{ZZ'U'1}}\left(w_{\mathrm{A}}, -\frac{h_{\mathrm{A}}}{2}\right) - \psi_{\mathrm{ZZ'U'1}}\left(0, \frac{h_{\mathrm{A}}}{2}\right) + \psi_{\mathrm{ZZ'U'1}}\left(0, -\frac{h_{\mathrm{A}}}{2}\right) \tag{3.151}$$

where are

$$\begin{aligned} \psi_{\mathrm{ZZ'U'1}}\left(u_1', z'\right) &= \left(\left(-\frac{u_1'}{2} + \frac{3}{4}p_{\mathrm{D1}}\right)p_{\mathrm{N2}} - p_{\mathrm{N1}}\right)\sqrt{u_1'^2 + p_{\mathrm{D1}}u_1' + p_{\mathrm{D0}} + \left(z - z'\right)^2} \\ &+ \left(\left(-\frac{3}{8}p_{\mathrm{D1}}^2 + \frac{1}{2}p_{\mathrm{D0}} - \frac{1}{2}\left(z - z'\right)^2\right)p_{\mathrm{N2}} + \frac{1}{2}p_{\mathrm{D1}}p_{\mathrm{N1}} - p_{\mathrm{N0}}\right)\ln\left(u_1' + \frac{1}{2}p_{\mathrm{D1}} + \sqrt{u_1'^2 + p_{\mathrm{D1}}u_1' + p_{\mathrm{D0}} + \left(z - z'\right)^2}\right) \\ &+ \left|z - z'\right|\left(-\left(p_{\mathrm{D1}}p_{\mathrm{N2}} - p_{\mathrm{N1}}\right)\ln\left(\left|p_{\mathrm{R}}\left(u_1', z'\right)\right|\right) - \frac{\left(p_{\mathrm{D1}}^2 - 2p_{\mathrm{D0}}\right)p_{\mathrm{N2}} - p_{\mathrm{D1}}p_{\mathrm{N1}} + 2p_{\mathrm{N0}}}{\sqrt{4p_{\mathrm{D0}} - p_{\mathrm{D1}}^2}}\arg\left(p_{\mathrm{R}}\left(u_1', z'\right)\right)\right), \end{aligned} \tag{3.152}$$

$$p_{\mathrm{R}}\left(u_1', z'\right) = \frac{4\left(\left|z - z'\right| + \sqrt{u_1'^2 + p_{\mathrm{D1}}u_1' + p_{\mathrm{D0}} + \left(z - z'\right)^2}\right)^2 - \left(2u_1' + p_{\mathrm{D1}} + \sqrt{p_{\mathrm{D1}}^2 - 4p_{\mathrm{D0}}}\right)^2}{2\left(2u_1' + p_{\mathrm{D1}} + \sqrt{p_{\mathrm{D1}}^2 - 4p_{\mathrm{D0}}}\right)}. \tag{3.153}$$

The part of potential φ_{M} which is denoted φ_{C} in (3.142) can be then written using (3.145), (3.151)-(3.153)

$$\varphi_{\mathrm{C}} = \frac{M_{\mathrm{A}}N_{\mathrm{A}}I_{\mathrm{A}}}{4\pi h_{\mathrm{A}}w_{\mathrm{A}}}\mathrm{sgn}\left(z\right)\oint_{C_{\mathrm{A}}} h_{\mathrm{A}}w_{\mathrm{A}}p_{\mathrm{N2}} + h_{\mathrm{A}}\left(\left(p_{\mathrm{D1}}p_{\mathrm{N2}} - p_{\mathrm{N1}}\right)\ln\left(\left|p_{\mathrm{C}}\right|\right) + \frac{\left(p_{\mathrm{D1}}^2 - 2p_{\mathrm{D0}}\right)p_{\mathrm{N2}} - p_{\mathrm{D1}}p_{\mathrm{N1}} + 2p_{\mathrm{N0}}}{\sqrt{4p_{\mathrm{D0}} - p_{\mathrm{D1}}^2}}\arg\left(p_{\mathrm{C}}\right)\right)\mathrm{d}u_2' \tag{3.154}$$

where is

$$p_{\mathrm{C}} = \frac{p_{\mathrm{D1}} + \sqrt{p_{\mathrm{D1}}^2 - 4p_{\mathrm{D0}}}}{2w_{\mathrm{A}} + p_{\mathrm{D1}} + \sqrt{p_{\mathrm{D1}}^2 - 4p_{\mathrm{D0}}}}. \tag{3.155}$$

It is useful to consider two special cases of the coil when width w_{A} of the winding or height h_{A} of the coil can be assumed as zero respectively. If height h_{A} is zero the coil from Fig. 3.10. becomes thin-wall coil in Fig. 3.14. In this case, the individual turns of conductor with current I_{A}, see Fig. 3.14. a), are approximated by a continuous

current layer of thickness $h_A \to 0$, see Fig. 3.14. b). Thus, current of the layer is surface current with surface current density $\boldsymbol{K}_A$ given by relation

$$\boldsymbol{K}_A = \underbrace{\frac{M_A N_A I_A}{w_A}}_{K_A} \boldsymbol{u}'_{20} = K_A \boldsymbol{u}'_{20} . \tag{3.156}$$

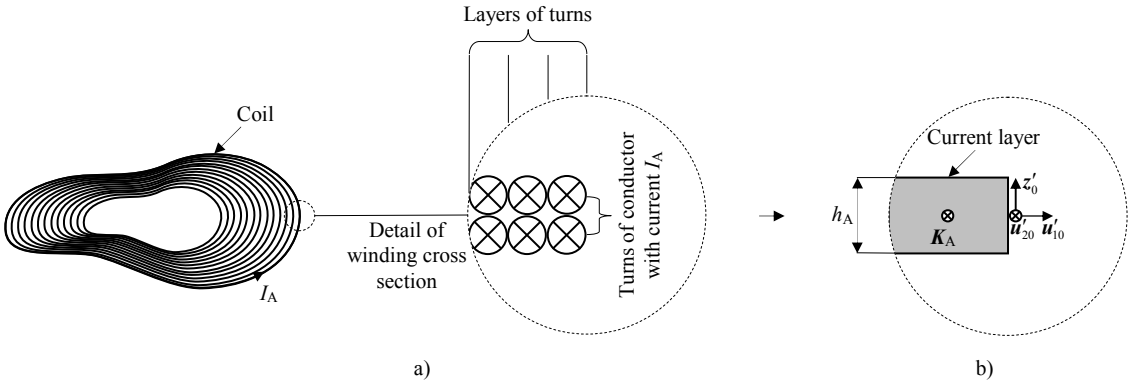

Fig. 3.14. a) Thin-wall coil with air core of arbitrary cross section with zero height, b) approximation of turns of conductor by current layer.

The relations (3.144) and (3.145) are then reduced using (3.156) and considering $h_A \to 0$ to

$$\begin{aligned}\varphi_M &= -\frac{K_A}{4\pi} \oint_{C_A} \int_0^{w_A} \int z_0 \cdot \left(\frac{\boldsymbol{r} - \boldsymbol{r}'}{|\boldsymbol{r} - \boldsymbol{r}'|^3} \times \frac{\partial(\boldsymbol{r} - \boldsymbol{r}')}{\partial u'_2} \right) \mathrm{d}z \mathrm{d}u'_1 \mathrm{d}u'_2 \\ &= -\frac{M_A N_A I_A}{4\pi w_A} \oint_{C_A} \int_0^{w_A} \int \underbrace{\frac{p_{N2} u'^2_1 + p_{N1} u'_1 + p_{N0}}{\left(u'^2_1 + p_{D1} u'_1 + p_{D0} + z^2 \right)^{\frac{3}{2}}}}_{I_{ZU'1}} \mathrm{d}z \mathrm{d}u'_1 \mathrm{d}u'_2 .\end{aligned} \tag{3.157}$$

The expression in (3.157) which is denoted $I_{ZU'1}$ is integral with respect to coordinates z, u'_1. This integral can be expressed analytically as follows:

$$I_{ZU'1} = \psi_{ZU'1}(w_A) - \psi_{ZU'1}(0) \tag{3.158}$$

where is

$$\begin{aligned}\psi_{ZU'1}(u'_1) &= z p_{N2} \ln\left(u'_1 + \frac{1}{2} p_{D1} + \sqrt{u'^2_1 + p_{D1} u'_1 + p_{D0} + z^2} \right) \\ &+ \operatorname{sgn}(z) \left((p_{D1} p_{N2} - p_{N1}) \ln\left(\left| p_R(u'_1, 0) \right| \right) + \frac{\left(p^2_{D1} - 2p_{D0} \right) p_{N2} - p_{D1} p_{N1} + 2p_{N0}}{\sqrt{4p_{D0} - p^2_{D1}}} \arg\left(p_R(u'_1, 0) \right) \right).\end{aligned} \tag{3.159}$$

The part of potential φ_M which is denoted φ_C in (3.142) can be then written using (3.157)-(3.159)

$$\varphi_C = -\frac{M_A N_A I_A}{4\pi w_A} \operatorname{sgn}(z) \oint_{C_A} w_A p_{N2} + \left((p_{D1} p_{N2} - p_{N1}) \ln\left(|p_C| \right) + \frac{\left(p^2_{D1} - 2p_{D0} \right) p_{N2} - p_{D1} p_{N1} + 2p_{N0}}{\sqrt{4p_{D0} - p^2_{D1}}} \arg(p_C) \right) \mathrm{d}u'_2 . \tag{3.160}$$

If width w_A is zero the coil from Fig. 3.10. becomes thin-wall coil in Fig. 3.15. In this case, the individual turns of conductor with current I_A, see Fig. 3.15. a), are approximated by a continuous current layer of thickness $w_A \to 0$, see Fig. 3.15. b). Thus, the current of the layer is surface current with surface current density $\boldsymbol{K}_A$ given by relation

$$\boldsymbol{K}_A = \underbrace{\frac{M_A N_A I_A}{h_A}}_{K_A} \boldsymbol{u}'_{20} = K_A \boldsymbol{u}'_{20} . \tag{3.161}$$

The relations (3.144) and (3.145) are then reduced using (3.161) and considering $w_A \to 0$ to

$$\varphi_{\mathrm{M}} = -\frac{K_{\mathrm{A}}}{4\pi}\oint_{C_{\mathrm{A}}}\int_{-\frac{h_{\mathrm{A}}}{2}}^{\frac{h_{\mathrm{A}}}{2}}\int z_0\cdot\left(\frac{\boldsymbol{r}-\boldsymbol{r}'}{\left|\boldsymbol{r}-\boldsymbol{r}'\right|^3}\times\frac{\partial\left(\boldsymbol{r}-\boldsymbol{r}'\right)}{\partial u_2'}\right)\mathrm{d}z\mathrm{d}z'\mathrm{d}u_2'$$
$$= -\frac{M_{\mathrm{A}}N_{\mathrm{A}}I_{\mathrm{A}}}{4\pi h_{\mathrm{A}}}\oint_{C_{\mathrm{A}}}\int_{-\frac{h_{\mathrm{A}}}{2}}^{\frac{h_{\mathrm{A}}}{2}}\int\frac{p_{\mathrm{N0}}}{\left(p_{\mathrm{D0}}+\left(z-z'\right)^2\right)^{\frac{3}{2}}}\mathrm{d}z\mathrm{d}z'\mathrm{d}u_2'. \tag{3.162}$$
$$I_{ZZ'}$$

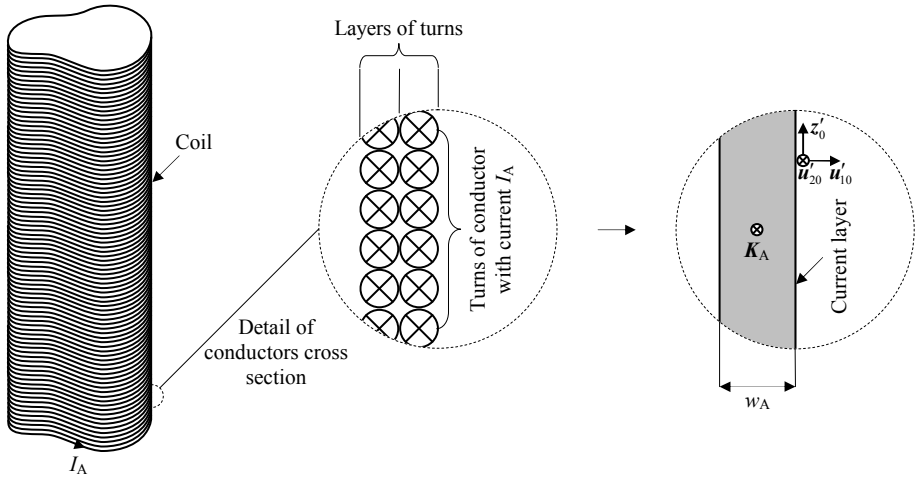

Fig. 3.15. a) Thin-wall coil with air core of arbitrary cross section with zero width of winding, b) approximation of turns of conductor by current layer.

The expression in (3.162) which is denoted $I_{ZZ'}$ is integral with respect to coordinates z, z'. This integral can be expressed analytically as follows:

$$I_{ZZ'} = \psi_{ZZ'}\left(\frac{h_{\mathrm{A}}}{2}\right) - \psi_{ZZ'}\left(-\frac{h_{\mathrm{A}}}{2}\right) \tag{3.163}$$

where is

$$\psi_{ZZ'}\left(z'\right) = -\frac{p_{\mathrm{N0}}\sqrt{p_{\mathrm{D0}}+\left(z-z'\right)^2}}{p_{\mathrm{D0}}}. \tag{3.164}$$

The part of potential φ_{M} which is denoted φ_{C} in (3.142) can be then written using (3.162)-(3.164)

$$\varphi_{\mathrm{C}} = -\frac{M_{\mathrm{A}}N_{\mathrm{A}}I_{\mathrm{A}}}{4\pi h_{\mathrm{A}}}\mathrm{sgn}\left(z\right)\oint_{C_{\mathrm{A}}}\frac{h_{\mathrm{A}}p_{\mathrm{N0}}}{p_{\mathrm{D0}}}\mathrm{d}u_2'. \tag{3.165}$$

The integrations in (3.145), (3.157), (3.162) with respect to coordinate u'_2 are necessary to perform numerically since it is not possible to find primitive function for $I_{ZZ'U'1}$, $I_{ZU'1}$, I_{ZZ} for general curve C_{A}. The order of integration with respect to coordinate u'_2 and derivations with respect to coordinates u_1, u_2, z in combination of (3.143) with (3.145), (3.154) or (3.157), (3.160) or (3.162), (3.165) can be interchanged and the derivatives can be performed analytically. However, derivatives can be quite complex. Thus, it is easier to perform derivatives numerically after numerical integration with respect to coordinate u'_2.

The magnetic flux density $\boldsymbol{B}_{\mathrm{A}}$ of the coil in Fig. 3.10. is continuous since for an arbitrary imaginary boundary can be written according to boundary conditions [33]

$$\boldsymbol{n}\times\left(\boldsymbol{B}_{\mathrm{A},1}-\boldsymbol{B}_{\mathrm{A},2}\right)=0, \tag{3.166}$$

$$\boldsymbol{n}\cdot\left(\boldsymbol{B}_{\mathrm{A},1}-\boldsymbol{B}_{\mathrm{A},2}\right)=0 \tag{3.167}$$

where

$\boldsymbol{n}$ is normal vector to boundary,

indices 1 and 2 denote one and other sides of boundary.

The right hand side of (3.166) is zero since no surface current is considered in this case. For components B_{U1}, B_{U2}, B_Z of vector of magnetic flux density $\boldsymbol{B}_A$ at the boundary, it can be then written using (3.143), (3.166), (3.167)

$$B_{U1} = B_{U1,1} = B_{U1,2} = -\mu_0 \frac{\partial \varphi_{M,1}}{h_1 \partial u_1} = -\mu_0 \frac{\partial \varphi_{M,2}}{h_1 \partial u_1}, \tag{3.168}$$

$$B_{U2} = B_{U2,1} = B_{U2,2} = -\mu_0 \frac{\partial \varphi_{M,1}}{h_2 \partial u_2} = -\mu_0 \frac{\partial \varphi_{M,2}}{h_2 \partial u_2}, \tag{3.169}$$

$$B_Z = B_{Z,1} = B_{Z,2} = -\mu_0 \frac{\partial \varphi_{M,1}}{\partial z} = -\mu_0 \frac{\partial \varphi_{M,2}}{\partial z}. \tag{3.170}$$

The conditions (3.168)-(3.170) admit discontinuous potential φ_M at any boundary, however, its derivatives with respect to coordinates u_1, u_2, z are continuous and magnetic flux density $\boldsymbol{B}_A$ can be fully determined with the help of potential φ_M out of the winding of the coil. The presented construction of potential φ_M leads to function which is continuous in space $S_{IN+} \cup S_{W+} \cup S_{OUT+}$ and space $S_{IN-} \cup S_{W-} \cup S_{OUT-}$ with discontinuity at boundaries between spaces S_{IN+}, S_{IN-} and S_{OUT+}, S_{OUT-} respectively. This discontinuity is caused by a choice of vector of integration constants $\boldsymbol{C}_B$ (3.140) which is different for space $S_{IN+} \cup S_{W+} \cup S_{OUT+}$ (it corresponds to $z \to \infty$ in (3.140)) and space $S_{IN-} \cup S_{W-} \cup S_{OUT-}$ (it corresponds to $z \to -\infty$ in (3.140)).

In the special cases of the coil, when height h_A of the coil or width w_A of the winding can be assumed as zero, see Fig. 3.14. or Fig. 3.15., the volume of the winding vanishes and a boundary between spaces S_{W+} and S_{W-} or spaces $S_{IN+} \cup S_{IN-}$ and $S_{OUT+} \cup S_{OUT-}$ appears. This boundary contains the layer with surface current density $\boldsymbol{K}_A$ which approximates the individual turns of conductor with current I_A. Surface current density $\boldsymbol{K}_A$ causes discontinuity of magnetic flux density $\boldsymbol{B}_A$ at a part of the boundary corresponding to the layer. If height h_A is zero, see Fig. 3.14., the condition (3.166) has to be changed for the layer in the form

$$\boldsymbol{z}_0 \times \left(\boldsymbol{B}_{A,W+} - \boldsymbol{B}_{A,W-} \right) = \mu_0 \boldsymbol{K}_A \tag{3.171}$$

where indices W+ and W− denote sides of the boundary corresponding to the spaces S_{W+} and S_{W-}. The condition (3.168) for component B_{U1} is then changed using (3.143), (3.156), (3.171) in the form

$$\mu_0 K_A = B_{U1,W+} - B_{U1,W-} = -\mu_0 \frac{\partial \varphi_{M,W+}}{h_1' \partial u_1'} + \mu_0 \frac{\partial \varphi_{M,W-}}{h_1' \partial u_1'}. \tag{3.172}$$

It has to be noted that coordinates (u'_1, u'_2, z') are used in (3.172) in place of coordinates (u_1, u_2, z) for decomposition of vector of magnetic flux density $\boldsymbol{B}_A$ at the layer since coordinates (u'_1, u'_2, z') are related to current density $\boldsymbol{K}_A$ by (3.156). If width w_A is zero, see Fig. 3.15., the condition (3.166) has to be changed for the layer in the form

$$\boldsymbol{u}'_{10} \times \left(\boldsymbol{B}_{A,OUT} - \boldsymbol{B}_{A,IN} \right) = \mu_0 \boldsymbol{K}_A \tag{3.173}$$

where indices IN and OUT denote sides of the boundary corresponding to the spaces $S_{IN+} \cup S_{IN-}$ and $S_{OUT+} \cup S_{OUT-}$. The condition (3.170) for component B_Z is then changed using (3.143), (3.161), (3.173) in the form

$$\mu_0 K_A = B_{Z,IN} - B_{Z,OUT} = -\mu_0 \frac{\partial \varphi_{M,IN}}{\partial z} + \mu_0 \frac{\partial \varphi_{M,OUT}}{\partial z}. \tag{3.174}$$

3.3.3. Examples

Examples of two different cross sections (circular and rectangular) of air core are described in Fig. 3.16. and Tab. 3.5. Tab. 3.5. specifies the parts of relations (3.143), (3.146)-(3.150) which differ for circular and rectangular cross section as well. Circular and rectangular cross sections are characterized by dimensions r_C, and a_R, b_R, r_R respectively. Corner radius r_R for rectangular cross section is necessary for continuous derivative of vector $\boldsymbol{C}_A$ with respect to coordinate u'_2, however, it can be considered as negligible with respect to dimensions a_R, b_R.

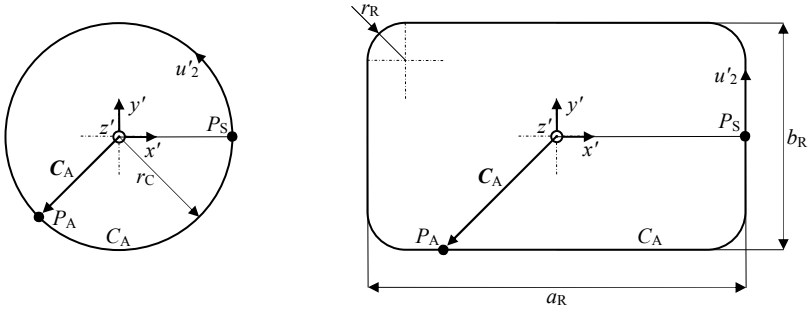

a) b)

Fig. 3.16. a) Circular and b) rectangular cross section of air core.

Name	Circular cross section	Rectangular cross section
Inner parameters of analysis		$p_1 = \frac{b_R}{2} - r_R$, $p_2 = \frac{b_R}{2} + r_R\left(\frac{\pi}{2} - 1\right)$, $p_3 = \frac{b_R}{2} + a_R + r_R\left(\frac{\pi}{2} - 3\right)$, $p_4 = \frac{b_R}{2} + a_R + r_R(\pi - 3)$, $p_5 = \frac{3b_R}{2} + a_R + r_R(\pi - 5)$, $p_6 = \frac{3b_R}{2} + a_R + r_R\left(\frac{3\pi}{2} - 5\right)$, $p_7 = \frac{3b_R}{2} + 2a_R + r_R\left(\frac{3\pi}{2} - 7\right)$, $p_8 = \frac{3b_R}{2} + 2a_R + r_R(2\pi - 7)$, $p_9 = 2b_R + 2a_R + r_R(2\pi - 8)$
(u_1, u_2)	(ρ, φ)	(x, y)
h_1	1	1
h_2	u_1	1
(x, y)	$(u_1\cos(u_2), u_1\sin(u_2))$	(u_1, u_2)
$(C_{AX'}, C_{AY'})$	$\left(r_C\cos\left(\frac{u'_2}{r_C}\right), r_C\sin\left(\frac{u'_2}{r_C}\right)\right), u'_2 \in \langle 0, 2\pi r_C)$	$\left(\frac{a_R}{2}, u'_2\right), u'_2 \in \langle 0, p_1)$ $\left(\frac{a_R}{2} + r_R\left(-1 + \cos\left(\frac{u'_2 - p_1}{r_R}\right)\right), \frac{b_R}{2} + r_R\left(-1 + \sin\left(\frac{u'_2 - p_1}{r_R}\right)\right)\right), u'_2 \in \langle p_1, p_2)$ $\left(\frac{a_R}{2} - r_R - u'_2 + p_2, \frac{b_R}{2}\right), u'_2 \in \langle p_2, p_3)$ $\left(-\frac{a_R}{2} + r_R\left(1 - \sin\left(\frac{u'_2 - p_3}{r_R}\right)\right), \frac{b_R}{2} + r_R\left(-1 + \cos\left(\frac{u'_2 - p_3}{r_R}\right)\right)\right), u'_2 \in \langle p_3, p_4)$ $\left(-\frac{a_R}{2}, \frac{b_R}{2} - r_R - u'_2 + p_4\right), u'_2 \in \langle p_4, p_5)$ $\left(-\frac{a_R}{2} + r_R\left(1 - \cos\left(\frac{u'_2 - p_5}{r_R}\right)\right), -\frac{b_R}{2} + r_R\left(1 - \sin\left(\frac{u'_2 - p_5}{r_R}\right)\right)\right), u'_2 \in \langle p_5, p_6)$ $\left(-\frac{a_R}{2} + r_R + u'_2 - p_6, -\frac{b_R}{2}\right), u'_2 \in \langle p_6, p_7)$ $\left(\frac{a_R}{2} + r_R\left(-1 + \sin\left(\frac{u'_2 - p_7}{r_R}\right)\right), -\frac{b_R}{2} + r_R\left(1 - \cos\left(\frac{u'_2 - p_7}{r_R}\right)\right)\right), u'_2 \in \langle p_7, p_8)$ $\left(\frac{a_R}{2}, -\frac{b_R}{2} + r_R + u'_2 - p_8\right), u'_2 \in \langle p_8, p_9)$

Tab. 3.5. Specification of parts of relations (3.143), (3.146)-(3.150) which depend on cross section of air core.

The above described analysis of magnetic field is verified using four examples of the coil. The magnetic flux density $\boldsymbol{B}_A$ calculated by the presented method is compared with other approaches for all examples.

The first example is a thin-wall coil (height of the coil $h_A \to 0$) with air core of circular cross section (multilayer circular coil). The multilayer circular coil has number of turns N_A, width w_A of the winding, radius r_C of the air core and current I_A, see Fig. 3.17. a). Its magnetic field is described in cylindrical coordinates (ρ, φ, z). Magnetic flux density $\boldsymbol{B}_A$ calculated by the presented method is compared with the method of finite integration technique.

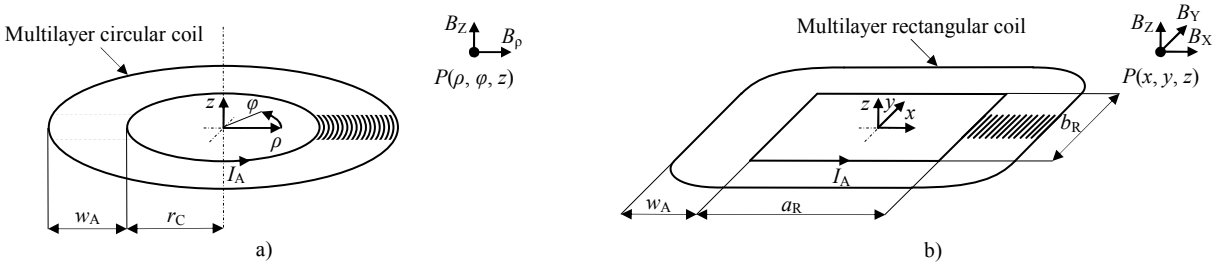

Fig. 3.17. Arrangement for analysis of magnetic field of a) multilayer circular coil, b) multilayer rectangular coil.

The second example is a thin-wall coil (height of the coil $h_A \to 0$) with air core of rectangular cross section (multilayer rectangular coil). The multilayer rectangular coil has number of turns N_A, width w_A of the winding, dimensions a_R, b_R of the air core and current I_A, see Fig. 3.17. b). Its magnetic field is described in Cartesian coordinates (x, y, z). Magnetic flux density $\boldsymbol{B}_A$ calculated by the presented method is compared with the method of finite integration technique.

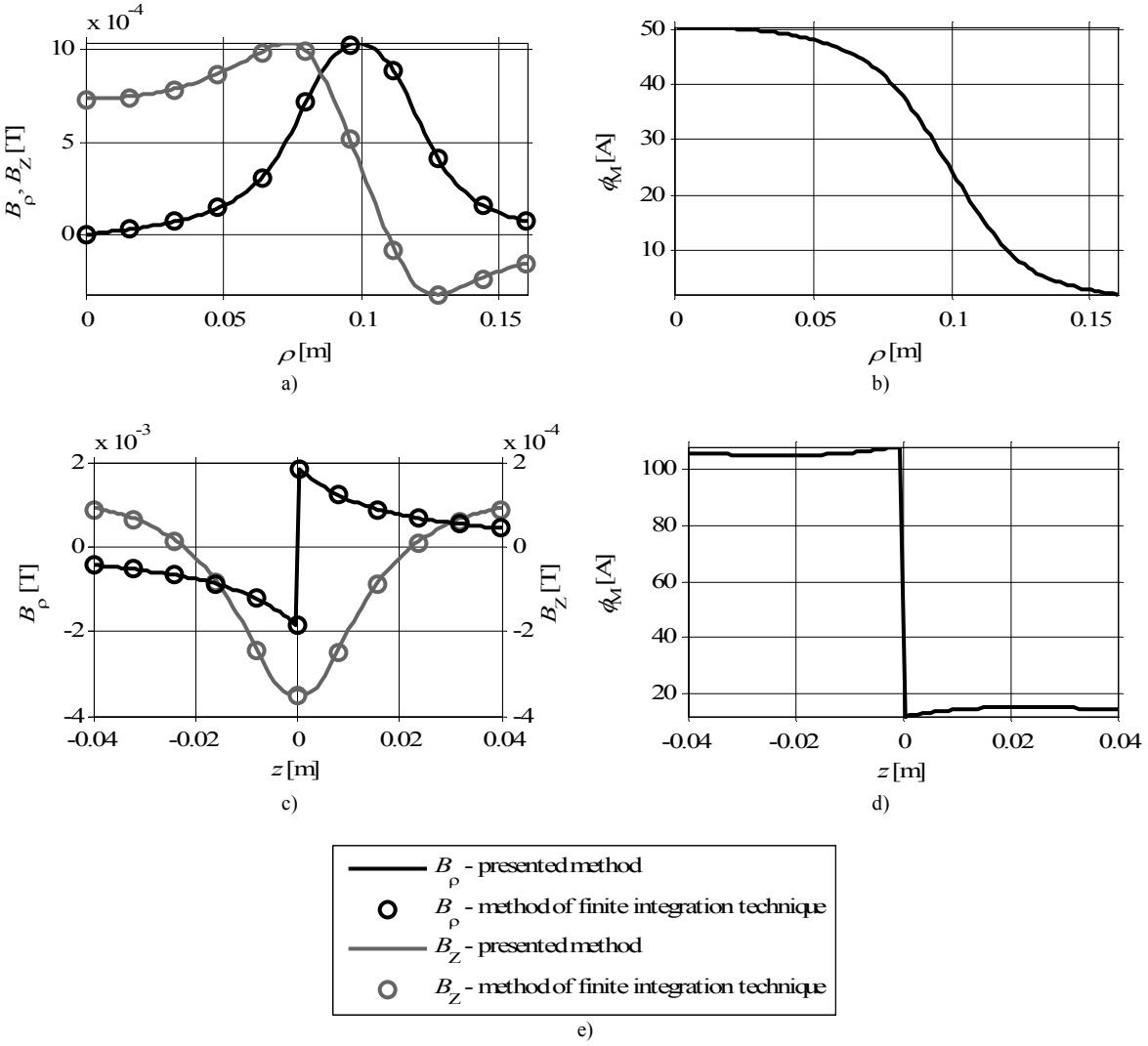

Fig. 3.18. Components B_ρ, B_Z of vector of magnetic flux density $\boldsymbol{B}_A$ (comparison of presented method and method of finite integration technique) and scalar magnetic potential φ_M of multilayer circular coil along chosen lines a), b) ρ, $z = 0.4w_A$, c), d) $\rho = r_C + 0.8w_A$, z, e) legend for graphs of components of magnetic flux density.

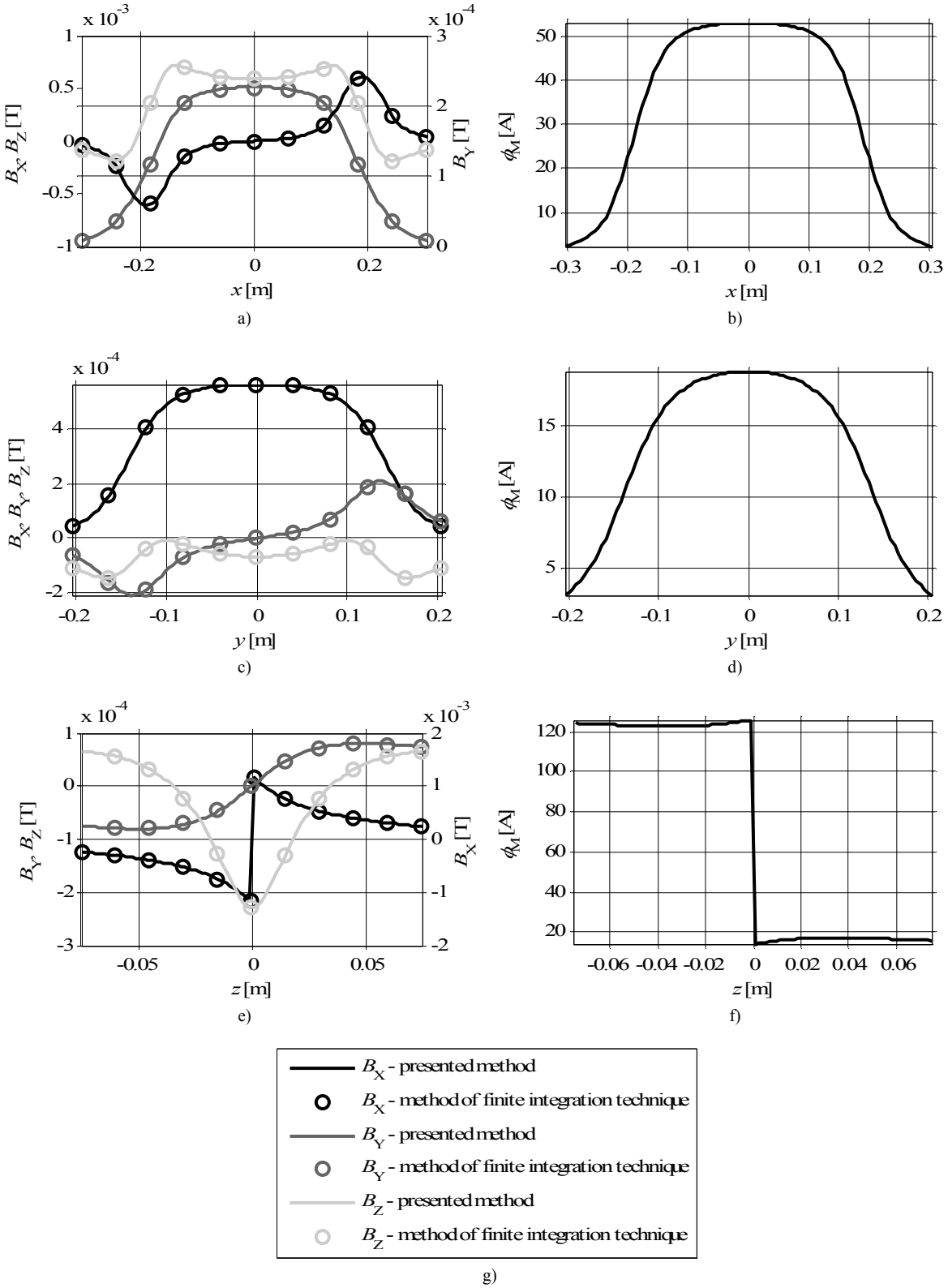

Fig. 3.19. Components B_X, B_Y, B_Z of vector of magnetic flux density $\boldsymbol{B}_A$ (comparison of presented method and method of finite integration technique) and scalar magnetic potential φ_M of multilayer rectangular coil along chosen lines a), b) x, $y = 0.4b_R$, $z = 0.4w_A$, c), d) $x = 0.5a_R + 0.8\ w_A$, y, $z = 0.4w_A$, e), f) $x = 0.5a_R + 0.8\ w_A$, $y = 0.4b_R$, z, g) legend for graphs of components of magnetic flux density.

Name	Multilayer circular coil	Multilayer rectangular coil
w_A [m]	0.04	0.075
N_A [-]	120	140
r_C [m]	0.08	-
a_R [m]	-	0.305
b_R [m]	-	0.205
I_A [A]	1	1

Tab. 3.6. Input parameters of analysis of multilayer circular and rectangular coils.

Method	Line			
	$\rho, z = 0.4h_A$ Fig. 3.18. a)		$\rho = r_C + 0.8w_A, z$ Fig. 3.18. c)	
	B_ρ	B_Z	B_ρ	B_Z
Presented	0.053	0.045	0.063	0.061
Finite integration technique	904	904	904	904

The CPU time is in seconds.

Tab. 3.7. CPU time required for evaluation of magnetic flux density $\boldsymbol{B}_A$ using different methods for multilayer circular coil.

Method	Line								
	$x, y = 0.4b_R, z = 0.4h_A$ Fig. 3.19. a)			$x = 0.5a_R + 0.8w_A, y, z = 0.4h_A$ Fig. 3.19. c)			$x = 0.5a_R + 0.8w_A, y = 0.4b_R, z$ Fig. 3.19. e)		
	B_X	B_Y	B_Z	B_X	B_Y	B_Z	B_X	B_Y	B_Z
Presented	0.399	0.384	0.381	0.384	0.382	0.383	0.384	0.381	0.382
Finite integration technique	549	549	549	549	549	549	549	549	549

The CPU time is in seconds.

Tab. 3.8. CPU time required for evaluation of magnetic flux density $\boldsymbol{B}_A$ using different methods for multilayer rectangular coil.

The third and fourth examples are thin-wall coils (width of the winding $w_A \to 0$) with air core of circular (circular coil) and rectangular (rectangular coil) cross section which are described in section 3.2.5. and depicted in Fig. 3.7. a) and b) respectively. Magnetic flux density $\boldsymbol{B}_A$ calculated by the presented method is compared with the methods described in section 3.2.5.

Fig. 3.18. and Fig. 3.19. show comparison of magnetic flux density $\boldsymbol{B}_A$ calculated by the presented method with the method of finite integration technique for the multilayer circular and rectangular coils respectively. The magnetic flux density $\boldsymbol{B}_A$ is evaluated along chosen lines for input analysis parameters given in Tab. 3.6. The evaluation is performed for 100 equidistant points (all points are not plotted for clarity) along every line for every component of magnetic flux density $\boldsymbol{B}_A$ by both methods. The required CPU time of evaluation for both methods is summarized in Tab. 3.7. and Tab. 3.8. for multilayer circular and rectangular coils respectively.

Magnetic flux density $\boldsymbol{B}_A$ calculated by the presented method for the circular and rectangular coils is not plotted for simplicity since the results are very similar to the results plotted in Fig. 3.8. and Fig. 3.9. Magnetic flux density $\boldsymbol{B}_A$ is evaluated along chosen lines for input analysis parameters given in Tab. 3.2. The evaluation is performed for 100 equidistant points along every line for every component of magnetic flux density $\boldsymbol{B}_A$. The required CPU time of evaluation for the presented method can be found in Tab. 3.3. and Tab. 3.4. for circular and rectangular coil respectively.

The CPU time of the presented method is very similar for all components evaluated along the given line since the character of evaluation through scalar magnetic potential φ_M is identical for all components. In the case of finite integration technique, the CPU time is equal for all components due to simultaneous evaluation of all components along all lines. The maximal deviation of results of the presented method with respect to the results of other considered methods is 0.6 %.

Numerical integrations in the presented method are evaluated using adaptive quadrature method implemented by function integral in Matlab [39]. All derivatives contained in gradient in (3.143) are evaluated numerically using central difference approximation.

3.4. Discussion on Maximal Power Transmission Efficiency

From (3.23), (3.27) and Fig. 1.12. a), it is apparent that maximal power transmission efficiency η_M depends on the term $k_M\sqrt{Q_A Q_S}$ only and increases with increase of this term. Thus it is desirable to maximize this term to maximize efficiency η_M.

Coupling coefficient k_M of the transceiving and receiving coils can achieve maximal value 1 in the ideal case. In the case of coils with air core which are used for WPT, this value can occur only if the coils are identical and occupy identical position since self and mutual energy of magnetic field of the receiving and transceiving coils are then equal which leads to equal self and mutual inductances L_A, L_S and M_{AS}, thus, coefficient k_M is equal to 1 according to (3.3), (3.12). In the real case, this value can be only approached when the coils occupy positions as identical as it is possible due to approaching of their windings. Nonidentical coils and positions can achieve lower value of coefficient k_M only.

The same considerations are valid for quality factors Q_A and Q_S of the receiving and transceiving coils, thus, in the following text the factor is identified by indices A only. From (3.3), (3.12), factor Q_A is given by relation

$$Q_A = \frac{\omega L_A}{R_A}. \tag{3.175}$$

It means inductance L_A and resistance R_A of the coil has to be found during the analysis of factor Q_A. Factor Q_A depends on dimensions of the coil, conductivity of the material of the conductor and frequency f through inductance L_A, resistance R_A and angular frequency ω. The dependence on frequency f is given not only by angular frequency ω ($\omega = 2\pi f$) but also by inductance L_A and resistance R_A as a result of eddy currents which occur in a coil carrying current of nonzero frequency. However, the dependence of inductance L_A on frequency f is weak, it is neglected in the further considerations and inductance L_A is found with the help of a stationary approach.

The parametrical analysis of factor Q_A for three type of coils is performed further. The chosen types of coils are coils whose turns of conductor are wound homogeneously close together around air core of a shape of finite cylinder of circular cross section, see Fig. 3.20. The first one is a single layer coil with N_A turns in the layer (single layer coil), see Fig. 3.20. a). The second one is a multilayer coil with 1 turn in every layer (multilayer coil), see Fig. 3.20. b). The third one is a multilayer coil with 1 turn in every layer (multilayer coil) and negligible radius of the air core with respect to width of the winding (full coil), see Fig. 3.20. b). The coils are considered to be wound by a conductor of rectangular cross section and a special case of square cross section is considered for the single and multilayer coil. The conductor of rectangular cross section can be considered as raw estimation of a conductor of circular cross section as well.

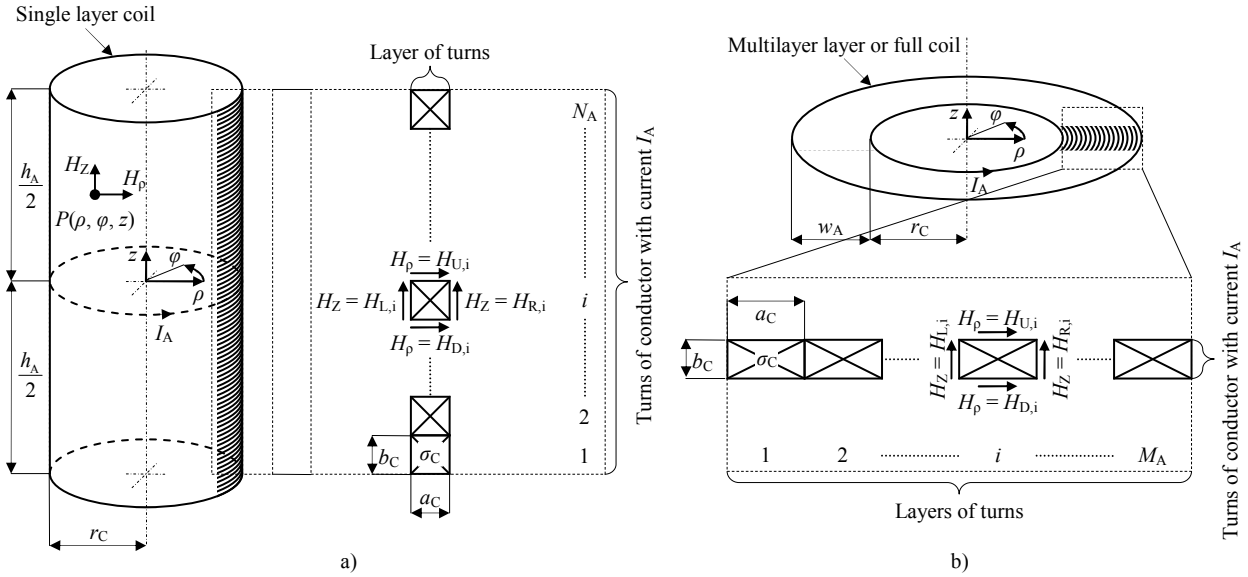

Fig. 3.20. Coils for parametrical analysis: a) Single layer coil, b) multilayer coil ($a_C = b_C$) or full coil ($r_C << w_A$).

The symbols in Fig. 3.20. mean:

h_A height of coil,

w_A width of winding of coil,

N_A number of turns of conductor in one layer of winding,

M_A number of layers,

r_C radius of air core,

a_C width of conductor cross section,

b_C height of conductor cross section,

σ_C conductivity of conductor.

The special relations considered for quantities which describe the coils are summarized in Tab. 3.9.

Quantity	Single layer coil	Multilayer coil	Full coil
h_A		b_C	b_C
w_A	a_C		
r_C			$0.001 w_A$
b_C	a_C	a_C	
M_A	$\frac{w_A}{a_C}=1$	$\frac{w_A}{a_C}$	$\frac{w_A}{a_C}$
N_A	$\frac{h_A}{b_C}$	$\frac{h_A}{b_C}=1$	$\frac{h_A}{b_C}=1$

Tab. 3.9. Special relations of quantities describing coils for parametrical analysis.

The analysis of factor Q_A is discussed in the sections 3.4.1.-3.4.4. Firstly, the organisation of the analysis is described in section 3.4.1. Secondly, the principles of calculation of inductance L_A and resistance R_A are explained in sections 3.4.2. and 3.4.3. respectively. Finally, the results of the analysis are presented and examined in section 3.4.4. The chosen types of coils allow a synoptic parametrical analysis of factor Q_A due to favourable low number of quantities which describe the problem. However, the described approaches can be used for analysis or estimation in the case of other types of coils as well.

3.4.1. Buckingham Theorem

The problem of analysis of factor Q_A is stated above. The first step of the analysis is the assessment of necessary parameters for description of this problem in order to provide a complete parametrical analysis for all allowable and realistic combinations of quantities which describe the chosen types of coils. The number of parameters can be equal or lower than the number of quantities since a parameter can be given by a product of powers of these quantities as it is explained further.

The Buckingham theorem solves the problem of number of necessary parameters for description of any physical phenomenon [42], [43]. The essential terms for formulation of the theorem are defined further and the theorem is stated subsequently. The theorem is applied to analysis of factor Q_A.

The Buckingham theorem is based on dimensional analysis of physical quantities (variables and constants) which describe any physical phenomenon. If the phenomenon is described by n quantities q_j, $j \in \{1, 2, \cdots, n\}$ j^{th} quantity q_j can be expressed as

$$q_j = (q_j)[q_j], \; j \in \{1,2, \quad ,n\} \tag{3.176}$$

where are

(q_j) value of quantity q_j,

$[q_j]$ unit of quantity q_j.

The unit $[q_j]$ can be written with the help of any consistent system of units e.g. SI units as

$$[q_j] = \prod_i^m u_i^{\alpha_{ij}} \tag{3.177}$$

where are

u_i i^{th} base unit of system of units,

α_{ij} power of unit u_i for expression of unit $[q_j]$,

m number of necessary base units for description of phenomenon.

Dimension vector $\boldsymbol{v}_j$ of unit $[q_j]$ can be constructed as

$$\boldsymbol{v}_j = \left(\alpha_{1j}, \alpha_{2j}, \quad , \alpha_{mj}\right) \tag{3.178}$$

and dimension matrix of the phenomenon can be defined then as

$$\boldsymbol{M}_{\text{D}} = \left(\boldsymbol{v}_1^{\text{T}} \quad \boldsymbol{v}_2^{\text{T}} \quad \boldsymbol{v}_n^{\text{T}}\right) = \begin{pmatrix} \alpha_{11} & \alpha_{1n} \\ & \\ \alpha_{m1} & \alpha_{mn} \end{pmatrix}. \tag{3.179}$$

Thus, the j^{th} column of the matrix $\boldsymbol{M}_{\text{D}}$ represents unit $[q_j]$ in the terms of powers α_{ij}, $i \in \{1, 2, \cdots, m\}$ according to (3.177). Rank r of matrix $\boldsymbol{M}_{\text{D}}$

$$r = \text{rank}\left(\boldsymbol{M}_{\text{D}}\right) \tag{3.180}$$

indicates number of quantities with independent unit in the set of all quantities in the sense of number of linear independent dimension vectors in the set of all dimension vectors. If first r quantities $q_j, j \in \{1, 2, \cdots, r\}$ are marked as quantities with independent unit then units $[q_{k+r}]$ of remaining $n - r$ quantities q_{k+r}, $k \in \{1, 2, \cdots, n - r\}$, which can be marked as quantities with dependant unit, can be expressed as

$$\left[q_{k+r}\right]^{-\beta_{k+r}} = \prod_{j=1}^{r} \left[q_j\right]^{\beta_j}, \; k \in \left\{1,2, \quad , n-r\right\} \tag{3.181}$$

where powers $\beta_j, j \in \{1, 2, \cdots, r\}$ and β_{k+r} fulfil condition

$$\beta_1 \boldsymbol{v}_1 + \beta_2 \boldsymbol{v}_2 + \quad + \beta_r \boldsymbol{v}_r = -\beta_{k+r} \boldsymbol{v}_{k+r}\,. \tag{3.182}$$

The Buckingham theorem states in the implicit form: If any physical phenomenon described by n quantities $q_j, j \in \{1, 2, \cdots, n\}$ can be expressed as

$$f_{\text{Q,I}}\left(q_1, q_2, \quad , q_n\right) = 0 \tag{3.183}$$

where $f_{\text{Q,I}}$ is function relating quantities then the relation (3.183) is equivalent to relation

$$f_{\text{D,I}}\left(d_1, d_2, \quad , d_{n-r}\right) = 0 \tag{3.184}$$

where are

d_k, $k \in \{1, 2, \cdots, n - r\}$ set of $n - r$ dimensionless parameters,

$f_{\text{D,I}}$ function relating parameters.

Additionally, dimensionless parameter d_k can be found as

$$d_k = q_{k+r}^{\beta_{k+r}} \prod_{j=1}^{r} q_j^{\beta_j}, \; k \in \left\{1,2, \quad , n-r\right\} \tag{3.185}$$

where powers $\beta_j, j \in \{1, 2, \cdots, r\}$ and β_{k+r} fulfil condition (3.182).

Alternatively to (3.183) and (3.184), the theorem can be written in the explicit form in the case when one of quantities is expected to be expressed as function of remaining quantities. Let it be without lose of generality quantity q_n with dependent unit. The theorem can be then stated: If any physical phenomenon can be expressed as

$$f_{\text{Q,E}}\left(q_1, q_2, \quad , q_{n-1}\right) = q_n \tag{3.186}$$

where $f_{\text{Q,E}}$ is function relating quantities then the relation (3.186) is equivalent to relation

$$f_{\text{D,E}}\left(d_1, d_2, \quad , d_{n-r-1}\right) = d_{n-r} \tag{3.187}$$

where $f_{\text{D,E}}$ is function relating parameters.

The theorem reduces a problem of n quantities to a problem of $n - r$ dimensionless parameters. All quantities which describe the phenomenon have to be known for proper use of the theorem. On the other hand, functions $f_{Q,I}, f_{D,I}$ or $f_{Q,E}, f_{D,E}$ can be unknown and the theorem does not provide any information about them.

Further the theorem is applied to analysis of factor Q_A. Inductance L_A and resistance R_A are analysed separately as well in order to observe their values for given value of factor Q_A. The dimensional properties of the analysis are summarized in Tab. 3.10. The chosen system of units is SI units. Every quantity q_j used for the analysis is written down and marked by indices j. Unit $[q_j]$ of every quantity q_j is expressed in terms product of powers of base SI units u_1 = A, u_2 = kg, u_3 = m, u_4 = s according to (3.177), elements α_{1j}, α_{2j}, α_{3j}, α_{4j} of dimension vector $\boldsymbol{v}_j$ (3.178) are extracted and matrix $\boldsymbol{M}_D$ (3.179) is constructed. The number $n - r$ of dimensionless parameters is determined with the help of number of quantities n and rank r of matrix $\boldsymbol{M}_D$. r quantities with independent unit are chosen. Every dimensionless parameter d_k which is found according to (3.182), (3.185) with the help of Tab. 3.10. is written down in Tab. 3.11. Parameters $L_A/(a_C\mu_0)$, $a_C\sigma_C R_A$, Q_A can be considered as parameters which are to be calculated since they contain quantities L_A, R_A, Q_A and are functions of remaining parameters in the sense of (3.187)

$$f_{LA}\left(\frac{b_C}{a_C}, \frac{h_A}{a_C}, \frac{w_A}{a_C}, \frac{r_C}{a_C}\right) = \frac{L_A}{a_C\mu_0}, \tag{3.188}$$

$$f_{RA}\left(\frac{b_C}{a_C}, \frac{h_A}{a_C}, \frac{w_A}{a_C}, \frac{r_C}{a_C}, a_C\sqrt{\pi f\mu_0\sigma_C}\right) = a_C\sigma_C R_A, \tag{3.189}$$

$$f_{QA}\left(\frac{b_C}{a_C}, \frac{h_A}{a_C}, \frac{w_A}{a_C}, \frac{r_C}{a_C}, a_C\sqrt{\pi f\mu_0\sigma_C}\right) = Q_A \tag{3.190}$$

where f_{LA}, f_{RA}, f_{QA} are functions relating parameters. It is apparent from comparison of (3.175), (3.188)-(3.190) that functions f_{LA}, f_{RA}, f_{QA} are related by formula

$$\begin{aligned} Q_A &= \frac{\omega L_A}{R_A} = 2\left(a_C\sqrt{\pi f\mu_0\sigma_C}\right)^2 \underbrace{\frac{L_A}{a_C\mu_0}}_{f_{LA}} \underbrace{\frac{1}{a_C\sigma_C R_A}}_{\frac{1}{f_{RA}}} \\ &= 2\left(a_C\sqrt{\pi f\mu_0\sigma_C}\right)^2 \frac{f_{LA}\left(\frac{b_C}{a_C}, \frac{h_A}{a_C}, \frac{w_A}{a_C}, \frac{r_C}{a_C}\right)}{\underbrace{f_{RA}\left(\frac{b_C}{a_C}, \frac{h_A}{a_C}, \frac{w_A}{a_C}, \frac{r_C}{a_C}, a_C\sqrt{\pi f\mu_0\sigma_C}\right)}_{f_{QA}}} = f_{QA}\left(\frac{b_C}{a_C}, \frac{h_A}{a_C}, \frac{w_A}{a_C}, \frac{r_C}{a_C}, a_C\sqrt{\pi f\mu_0\sigma_C}\right). \end{aligned} \tag{3.191}$$

Additionally, quantities L_A, R_A, Q_A are contained only in these parameters as a result of (3.185) since quantities L_A, R_A, Q_A are not chosen as quantities with independent unit, see Tab. 3.10. Parameters $L_A/(a_C\mu_0)$, $a_C\sigma_C R_A$ represent normalized dimensionless inductance and resistance. Some parameters have special value (b_C/a_C, w_A/a_C for single layer coil; b_C/a_C, h_A/a_C for multilayer coil; h_A/a_C, r_C/a_C for full coil) which is predetermined by a chosen type of the coil and special relations of their quantities according to Tab. 3.9. Parameters without special value (h_A/a_C, r_C/a_C, $a_C\sqrt{\pi f\mu_0\sigma_C}$ for single layer coil; w_A/a_C, r_C/a_C, $a_C\sqrt{\pi f\mu_0\sigma_C}$ for multilayer coil; b_C/a_C, w_A/a_C, $a_C\sqrt{\pi f\mu_0\sigma_C}$ for full coil) are consider in the wide ranges for calculations of parameters $L_A/(a_C\mu_0)$, $a_C\sigma_C R_A$, Q_A in the following parametrical analysis. It has to be noted that parameter w_A/a_C corresponds to number M_A of the layers of turns of the conductor. and, in the case of the single layer coil, parameter h_A/a_C corresponds to number N_A of turns of the conductor in the layer since $a_C = b_C$. Parameter $a_C\sqrt{\pi f\mu_0\sigma_C}$ contains multiplicative dimensionless constant π which does not change the dimensional properties of this parameter and enable to interpret parameter as

$$\underbrace{a_C\sqrt{\pi f\mu_0\sigma_C}}_{\frac{1}{\delta_C}} = \frac{a_C}{\delta_C} \tag{3.192}$$

where δ_C is commonly used quantity of skin depth [33].

Quantity q_j	Indices j of q_j for analysis of			Unit $[q_j]=\prod_{i=1}^{m=4} u_i^{\alpha_{ij}} =$ $\mathrm{A}^{\alpha_{1j}}\mathrm{kg}^{\alpha_{2j}}\mathrm{m}^{\alpha_{3j}}\mathrm{s}^{\alpha_{4j}}$	Elements α_{ij} of dimension vector $\boldsymbol{v}_j$ – powers of base SI units				Columns of dimension matrix $\boldsymbol{M}_\mathrm{D}$ – quantities describing analysis of			Quantity with independent unit for analysis of		
	L_A	R_A	Q_A		α_{1j}	α_{2j}	α_{3j}	α_{4j}	L_A	R_A	Q_A	L_A	R_A	Q_A
f		1	1	s^{-1}	0	0	0	−1		×	×		×	×
μ_0	1	2	2	$\mathrm{A}^{-2}\mathrm{kg\,m\,s}^{-2}$	−2	1	1	−2	×	×	×	×	×	×
a_C	2	3	3	m	0	0	1	0	×	×	×	×	×	×
b_C	3	4	4	m	0	0	1	0	×	×	×			
h_A	4	5	5	m	0	0	1	0	×	×	×			
w_A	5	6	6	m	0	0	1	0	×	×	×			
r_C	6	7	7	m	0	0	1	0	×	×	×			
σ_C		8	8	$\mathrm{A}^2\mathrm{kg}^{-1}\mathrm{m}^{-3}\mathrm{s}^3$	2	−1	−3	3		×	×			
L_A	7			$\mathrm{A}^{-2}\mathrm{kg\,m}^2\mathrm{s}^{-2}$	−2	1	2	−2	×					
R_A		9		$\mathrm{A}^{-2}\mathrm{kg\,m}^2\mathrm{s}^{-3}$	−2	1	2	−3		×				
Q_A			9	1	0	0	0	0			×			
Number of quantities $n = \max(j)$									7	9	9			
$r = \mathrm{rank}(M_\mathrm{D})$									2	3	3			
Number of dimensionless parameters $n - r$									5	6	6			

Symbol × marks that given quantity has property indicated in heading of column.

Tab. 3.10. Dimensional properties of parametrical analysis of coils.

Dimensionless parameter d_k for calculation of			Indices k of d_k for calculation of			Special value of dimensionless parameter d_k according to Tab. 3.9.		
L_A	R_A	Q_A	L_A	R_A	Q_A	Single layer coil	Multilayer coil	Full coil
$\frac{b_\mathrm{C}}{a_\mathrm{C}}$	$\frac{b_\mathrm{C}}{a_\mathrm{C}}$	$\frac{b_\mathrm{C}}{a_\mathrm{C}}$	1	1	1	1	1	
$\frac{h_\mathrm{A}}{a_\mathrm{C}}$	$\frac{h_\mathrm{A}}{a_\mathrm{C}}$	$\frac{h_\mathrm{A}}{a_\mathrm{C}}$	2	2	2		1	1
$\frac{w_\mathrm{A}}{a_\mathrm{C}}$	$\frac{w_\mathrm{A}}{a_\mathrm{C}}$	$\frac{w_\mathrm{A}}{a_\mathrm{C}}$	3	3	3	1		
$\frac{r_\mathrm{C}}{a_\mathrm{C}}$	$\frac{r_\mathrm{C}}{a_\mathrm{C}}$	$\frac{r_\mathrm{C}}{a_\mathrm{C}}$	4	4	4			$0.001\frac{w_\mathrm{A}}{a_\mathrm{C}} = 0.001 d_3$
$\frac{L_\mathrm{A}}{a_\mathrm{C}\mu_0}$	$a_\mathrm{C}\sqrt{\pi f \mu_0 \sigma_\mathrm{C}}$	$a_\mathrm{C}\sqrt{\pi f \mu_0 \sigma_\mathrm{C}}$	5	5	5			
	$a_\mathrm{C}\sigma_\mathrm{C}R_\mathrm{A}$	Q_A		6	6			
Number of parameters $n - r = \max(k)$			5	6	6			
Number of parameters with special value			2	2	2			

Tab. 3.11. Dimensionless parameters of parametrical analysis of coils.

3.4.2. Self Inductance of Induction Coil

Self inductance L_A of induction coil carrying direct current can be defined by relation

$$L_\mathrm{A} = \frac{2W_\mathrm{M}}{I_\mathrm{A}^2} \tag{3.193}$$

where are

I_A current flowing through conductor of coil,

W_M energy of magnetic field of coil excited by current I_A.

Energy W_M can be written as [28]

$$W_\mathrm{M} = \frac{\mu_0}{8\pi}\iiint_{V_\mathrm{C}} \boldsymbol{J}_\mathrm{A}(\boldsymbol{r}) \cdot \iiint_{V'_\mathrm{C}} \frac{\boldsymbol{J}_\mathrm{A}(\boldsymbol{r}')}{|\boldsymbol{r}-\boldsymbol{r}'|}\,\mathrm{d}V'_\mathrm{C}\,\mathrm{d}V_\mathrm{C} \tag{3.194}$$

where are

V_C, V'_C volume of conductor,

$\mathrm{d}V_\mathrm{C}$, $\mathrm{d}V'_\mathrm{C}$ element of V_C, V'_C,

$\boldsymbol{J}_\mathrm{A}$ current density in conductor corresponding to current I_A.

$\boldsymbol{r}$, $\boldsymbol{r}'$ position vector of element $\mathrm{d}V_\mathrm{C}$, $\mathrm{d}V'_\mathrm{C}$.

Insertion of (3.194) to (3.193) leads to expression of inductance L_A as

$$L_\mathrm{A} = \frac{\mu_0}{4\pi I_\mathrm{A}^2} \iiint_{V_\mathrm{C}} \boldsymbol{J}_\mathrm{A}(\boldsymbol{r}) \cdot \iiint_{V'_\mathrm{C}} \frac{\boldsymbol{J}_\mathrm{A}(\boldsymbol{r}')}{|\boldsymbol{r}-\boldsymbol{r}'|} \mathrm{d}V'_\mathrm{C} \mathrm{d}V_\mathrm{C} \,. \tag{3.195}$$

For calculation of inductance L_A, the following approximation is used for the winding of the coil. The individual turns of conductor are replaced by a slab with homogenous current density $\boldsymbol{J}_\mathrm{A}$, see Fig. 3.10., given by (3.129). The relation (3.195) can be manipulated using (3.129) for the chosen types of coils in the form [32]

$$L_\mathrm{A} = \frac{2}{3}\mu_0 \frac{M_\mathrm{A}^2 N_\mathrm{A}^2}{h_\mathrm{A}^2} \int_{r_\mathrm{C}}^{r_\mathrm{C}+w_\mathrm{A}} \int_{r_\mathrm{C}}^{r_\mathrm{C}+w_\mathrm{A}} (\rho\rho')^{\frac{3}{2}} \left(\psi_\mathrm{L}\left(\frac{\rho^2+\rho'^2}{2\rho\rho'}, \frac{2h_\mathrm{A}^2}{\rho\rho'} \right) - \psi_\mathrm{L}\left(\frac{\rho^2+\rho'^2}{2\rho\rho'}, 0 \right) \right) \mathrm{d}\rho \mathrm{d}\rho' \tag{3.196}$$

where is

$$\psi_\mathrm{L}(\beta_\mathrm{A},\gamma_\mathrm{A}) = \begin{cases} 1, & \beta_\mathrm{A}=1, \gamma_\mathrm{A}=0, \\ \mathrm{cel}\left(\sqrt{1-\kappa_\mathrm{A}^2}, 1, \frac{1}{\kappa_\mathrm{A}}, 2\frac{1-\kappa_\mathrm{A}^2}{\kappa_\mathrm{A}} \right), & \kappa_\mathrm{A} = \sqrt{\frac{2}{2+\gamma_\mathrm{A}}}, \beta_\mathrm{A}=1, \gamma_\mathrm{A}>0, \\ \mathrm{cel}\left(\sqrt{1-\kappa_\mathrm{A}^2}, 1, \frac{1}{\kappa_\mathrm{A}}\left(1-\frac{3\gamma_\mathrm{A}\kappa_\mathrm{A}^2}{4}\right), \frac{1}{\kappa_\mathrm{A}}\left(\kappa_\mathrm{A}^2-1+\frac{3\gamma_\mathrm{A}\kappa_\mathrm{A}^2}{4}\right) \right) & \\ + \mathrm{cel}\left(\sqrt{1-\kappa_\mathrm{A}^2}, \frac{\beta_\mathrm{A}+1}{\beta_\mathrm{A}-1}\left(1-\kappa_\mathrm{A}^2\right), -\frac{3\gamma_\mathrm{A}\kappa_\mathrm{A}}{4}, \frac{3\gamma_\mathrm{A}\kappa_\mathrm{A}}{4}\frac{\beta_\mathrm{A}+1}{\beta_\mathrm{A}-1}\left(1-\kappa_\mathrm{A}^2\right) \right), & \kappa_\mathrm{A} = \sqrt{\frac{2}{1+\beta_\mathrm{A}+\gamma_\mathrm{A}}}, \beta_\mathrm{A}>1, \gamma_\mathrm{A}\geq 0 \end{cases} \tag{3.197}$$

and function cel represents general complete elliptic integral given by (3.95). Integral given by function cel and integrations with respect to ρ, ρ' in (3.196) have to be performed numerically.

3.4.3. Frequency-Dependent Resistance of Induction Coil

The frequency-dependent resistance R_A of induction coil carrying harmonic current can be defined by relation

$$R_\mathrm{A} = \frac{P_\mathrm{A}}{|\mathrm{I}_\mathrm{A}|^2} \tag{3.198}$$

where are

I_A phasor (in rms scale) of current flowing through conductor of coil,

P_A active power dissipated in volume of conductor.

Power P_A can be written as [33]

$$P_\mathrm{A} = \frac{1}{\sigma_\mathrm{C}} \iiint_{V_\mathrm{C}} |\mathbf{J}_\mathrm{A}|^2 \mathrm{d}V_\mathrm{C} \tag{3.199}$$

where are

σ_C conductivity of conductor,

V_C volume of conductor,

$\mathrm{d}V_\mathrm{C}$ element of V_C,

$\mathbf{J}_\mathrm{A}$ phasor (in rms scale) of current density in conductor corresponding to phasor I_A.

The frequency dependence of resistance R_A is a consequence of inhomogeneous frequency-dependant distribution of current density in a conductor of the coil caused by eddy currents. Eddy currents arise in a conductor exposed to time-varying electromagnetic field. Impact of time-varying electromagnetic field can be divided into skin and proximity effects. The skin effect is retroaction of electromagnetic field of the conductor on its current density which excited the electromagnetic field. The proximity effect is influence of distribution of current density of the

given conductor by a time-varying electromagnetic field of other conductors. Action of these effects is frequency-dependent.

Resistance R_A is usually expressed in comparison to a direct current resistance R_D of the coil by relation [41]

$$R_A = c_F R_D \tag{3.200}$$

where c_F is coefficient taking into account frequency dependence of resistance R_A. Comparison of (3.198), (3.200) and insertion of (3.199) lead to expression of coefficient c_F as

$$c_F = \frac{P_A}{R_D |I_A|^2} = \frac{\frac{1}{\sigma_C} \iiint_{V_C} |\mathbf{J}_A|^2 \, dV_C}{R_D |I_A|^2} . \tag{3.201}$$

One continuous conductor can create a complex spatial structure which can be divided into section connected in series for purpose of analysis. Influence of one section by others sections is then considered as proximity effect whereas skin effect is considered only for a single section. Total frequency-dependent resistance R_A of the coil can be expressed as sum of frequency-dependent resistances of all sections in this case

$$R_A = \sum_{i}^{n_C} R_{A,i} \tag{3.202}$$

where are

n_C number of sections,

$R_{A,i}$ frequency-dependent resistance of i^{th} section.

Quantities R_A, R_D, P_A, V_C, c_F, $\mathbf{J}_A$, in relations (3.198)-(3.201) are assigned to i^{th} section and become $R_{A,i}$, $R_{D,i}$, $P_{A,i}$, $V_{C,i}$, $c_{F,i}$, $\mathbf{J}_{A,i}$. Current I_A and conductivity σ_C are assumed identical for all sections since these sections belong to one continuous conductor. The equation (3.202) can be then written considering (3.200), (3.201) as

$$R_A = \sum_{i=1}^{n_C} c_{F,i} R_{D,i} = \sum_{i=1}^{n_C} \underbrace{\frac{P_{A,i}}{R_{D,i} |I_A|^2}}_{c_{F,i}} R_{D,i} = \sum_{i=1}^{n_C} \underbrace{\frac{\frac{1}{\sigma_C} \iiint_{V_{C,i}} |\mathbf{J}_{A,i}|^2 \, dV_{C,i}}{R_{D,i} |I_A|^2}}_{c_{F,i}} R_{D,i} . \tag{3.203}$$

For calculation of resistance R_A the winding of the chosen types of coils is divided in sections which correspond to the individual turns of conductor, see Fig. 3.20. The individual turn of conductor representing i^{th} section with resistance $R_{A,i}$ is then treated as a part of a straight infinitely long conductor of rectangular cross section i.e. curvature of the turn of conductor is neglected [44], see Fig. 3.21. The length $l_{C,i}$ of this part is assumed to be equal to average length of the given turn of the conductor. Direct current resistance $R_{D,i}$ of the i^{th} section can be then written as

$$R_{D,i} = \frac{l_{C,i}}{\sigma_C a_C b_C} . \tag{3.204}$$

Additionally, the following assumptions are taken into account, see Fig. 3.21.: Components of electromagnetic field are constant with respect to coordinate y_C which corresponds to independence on coordinate φ for a rotational symmetrical coil. Current density $\boldsymbol{J}_C$ and electric field strength $\boldsymbol{E}_C$ have only component perpendicular to cross section of the conductor i.e. component in y_C-axis direction. Magnetic field strength $\boldsymbol{H}_C$ has only components in plane of cross section of the conductor i.e. components perpendicular to y_C-axis direction. Tangential components of magnetic field strength $H_{D,i}$, $H_{U,i}$, $H_{L,i}$, $H_{R,i}$ at the surface of the conductor are constant. Components $H_{D,i}$, $H_{U,i}$ and $H_{L,i}$, $H_{R,i}$ are found with the help of the stationary approach described in the section 3.3. and they are calculated as components H_ρ, and H_Z of magnetic field strength $\boldsymbol{H}_A$ of the coil in the place of surface of the conductor of turn which represents the i^{th} section, see Fig. 3.20. and Fig. 3.21. Components $H_{D,i}$, $H_{U,i}$ and $H_{L,i}$, $H_{R,i}$ are evaluated in the center of edges of lenghts a_C and b_C as average value for the i^{th} section since they are considered to be constant as it is mentioned above.

The coefficient $c_{F,i}$ can be then expressed as [44]

$$c_{F,i} = 1 + \frac{1}{I_A^2} \left(a_C^2 \left(\left(H_{U,i} - H_{D,i} \right)^2 \left(\psi_S(\xi_B) - 1 \right) + H_{U,i} H_{D,i} \psi_P(\xi_B) \right) + b_C^2 \left(\left(H_{R,i} - H_{L,i} \right)^2 \left(\psi_S(\xi_A) - 1 \right) + H_{R,i} H_{L,i} \psi_P(\xi_A) \right) \right) \tag{3.205}$$

where are

$$\xi_{\mathrm{A}} = a_{\mathrm{C}}\sqrt{\pi f \sigma_{\mathrm{C}} \mu_0}\ , \tag{3.206}$$

$$\xi_{\mathrm{B}} = b_{\mathrm{C}}\sqrt{\pi f \sigma_{\mathrm{C}} \mu_0}\ , \tag{3.207}$$

$$\psi_{\mathrm{S}}(\xi) = \xi \frac{\sinh(2\xi) + \sin(2\xi)}{\cosh(2\xi) - \cos(2\xi)}, \tag{3.208}$$

$$\psi_{\mathrm{P}}(\xi) = 2\xi \frac{\sinh(\xi) - \sin(\xi)}{\cosh(\xi) + \cos(\xi)}. \tag{3.209}$$

and I_{A} is direct current of the coil which excites components of magnetic field strength $H_{\mathrm{D},i}$, $H_{\mathrm{U},i}$, $H_{\mathrm{L},i}$, $H_{\mathrm{R},i}$. The expressions of length $l_{\mathrm{C},i}$ and components $H_{\mathrm{D},i}$, $H_{\mathrm{U},i}$, $H_{\mathrm{L},i}$, $H_{\mathrm{R},i}$ for chosen types of coils are specified in Tab. 3.12. Resistance R_{A} of the coil is then given by (3.203) using (3.204)-(3.209) and Tab. 3.12.

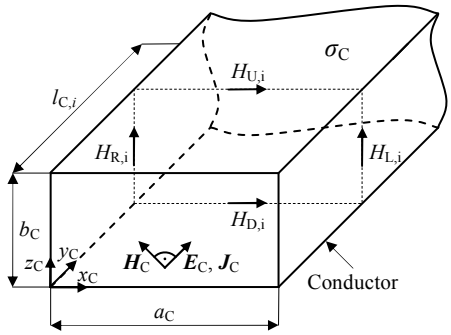

Fig. 3.21. Arrangement for calculation of frequency-dependent resistance of straight infinitely long conductor of rectangular cross section.

Name	Single layer coil	Multilayer coil	Full coil
i	$\{1, 2, \cdots, N_{\mathrm{A}}\}$	$\{1, 2, \cdots, M_{\mathrm{A}}\}$	$\{1, 2, \cdots, M_{\mathrm{A}}\}$
$l_{\mathrm{C},i}$	$2\pi\left(r_{\mathrm{C}} + \frac{1}{2}a_{\mathrm{C}}\right)$	$2\pi\left(r_{\mathrm{C}} + \left(i - \frac{1}{2}\right)a_{\mathrm{C}}\right)$	$2\pi\left(r_{\mathrm{C}} + \left(i - \frac{1}{2}\right)a_{\mathrm{C}}\right)$
$H_{\mathrm{D},i}$	$H_{\rho}\left(\rho = r_{\mathrm{C}} + \frac{1}{2}a_{\mathrm{C}}, z = -\frac{h_{\mathrm{A}}}{2} + (i-1)b_{\mathrm{C}}\right)$	$H_{\rho}\left(\rho = r_{\mathrm{C}} + \left(i - \frac{1}{2}\right)a_{\mathrm{C}}, z = -\frac{h_{\mathrm{A}}}{2}\right)$	$H_{\rho}\left(\rho = r_{\mathrm{C}} + \left(i - \frac{1}{2}\right)a_{\mathrm{C}}, z = -\frac{h_{\mathrm{A}}}{2}\right)$
$H_{\mathrm{U},i}$	$H_{\rho}\left(\rho = r_{\mathrm{C}} + \frac{1}{2}a_{\mathrm{C}}, z = -\frac{h_{\mathrm{A}}}{2} + ib_{\mathrm{C}}\right)$	$H_{\rho}\left(\rho = r_{\mathrm{C}} + \left(i - \frac{1}{2}\right)a_{\mathrm{C}}, z = \frac{h_{\mathrm{A}}}{2}\right)$	$H_{\rho}\left(\rho = r_{\mathrm{C}} + \left(i - \frac{1}{2}\right)a_{\mathrm{C}}, z = \frac{h_{\mathrm{A}}}{2}\right)$
$H_{\mathrm{L},i}$	$H_{\mathrm{Z}}\left(\rho = r_{\mathrm{C}}, z = -\frac{h_{\mathrm{A}}}{2} + \left(i - \frac{1}{2}\right)b_{\mathrm{C}}\right)$	$H_{\mathrm{Z}}(\rho = r_{\mathrm{C}} + (i-1)a_{\mathrm{C}}, z = 0)$	$H_{\mathrm{Z}}(\rho = r_{\mathrm{C}} + (i-1)a_{\mathrm{C}}, z = 0)$
$H_{\mathrm{R},i}$	$H_{\mathrm{Z}}\left(\rho = r_{\mathrm{C}} + w_{\mathrm{A}}, z = -\frac{h_{\mathrm{A}}}{2} + \left(i - \frac{1}{2}\right)b_{\mathrm{C}}\right)$	$H_{\mathrm{Z}}(\rho = r_{\mathrm{C}} + ia_{\mathrm{C}}, z = 0)$	$H_{\mathrm{Z}}(\rho = r_{\mathrm{C}} + ia_{\mathrm{C}}, z = 0)$

Tab. 3.12. Specification of parts of relations (3.204) and (3.205).

3.4.4. Results of Analysis of Quality Factor for Chosen Types of Induction Coils

This section presents and discusses the result of analysis of quality factor Q_A of chosen types of coils. Inductance L_A is found using (3.196), (3.197). The resistance R_A is determined with the help of (3.203), (3.204)-(3.209) and Tab. 3.12. Factor Q_A is then calculated according to (3.175). The results are presented graphically in the form of dimensionless parameters summarized in Tab. 3.11. Inductance L_A and resistance R_A are evaluated in absolute values by insertion of certain values of quantities from Tab. 3.10. in the mentioned relations which lead to desired values of dimensionless parameters from Tab. 3.11. Inductance L_A and resistance R_A are then normalized to parameters $L_A/(a_C\mu_0)$ and $a_C\sigma_C R_A$ for separate graphical representation. It has to be noted that, in the case, when close form relations are known, they can be usually manipulated to express functional dependence of dimensionless parameters directly and to proof the number of necessary parameters for description of a problem. However, the former approach of determination of necessary dimensionless parameters without knowledge or before derivation of close form relations governing the problem and adjusting dimensional quantities to desired values of dimensionless parameters can be used e.g. for numerical simulators which use dimensional quantities usually. Fig. 3.22.-Fig. 3.30. depict normalized inductance $L_A/(a_C\mu_0)$, normalized resistance $a_C\sigma_C R_A$ and quality factor Q_A of the single layer, multilayer and full coils.

In the case of the single layer coil, see Fig. 3.22.-Fig. 3.24., normalized inductance $L_A/(a_C\mu_0)$, normalized resistance $a_C\sigma_C R_A$ and factor Q_A increase with increasing parameters h_A/a_C, r_C/a_C monotonically. Normalized resistance $a_C\sigma_C R_A$ and factor Q_A depend on parameter $a_C\sqrt{\pi f\mu_0\sigma_C}$ additionally and increase with this parameter monotonically as well. Normalized inductance $L_A/(a_C\mu_0)$, normalized resistance $a_C\sigma_C R_A$, factor Q_A, inductance L_A and resistance R_A are related by (3.191). Thus, the increase of factor Q_A with increasing parameters h_A/a_C, r_C/a_C, $a_C\sqrt{\pi f\mu_0\sigma_C}$ can be interpreted as a more rapid increase of reactance ωL_A than increase of resistance R_A with increase of these parameters.

In the case of the multilayer coil, see Fig. 3.25.-Fig. 3.27., normalized inductance $L_A/(a_C\mu_0)$, normalized resistance $a_C\sigma_C R_A$ and factor Q_A increase with increasing parameters w_A/a_C, r_C/a_C monotonically. The normalized resistance $a_C\sigma_C R_A$ and factor Q_A depend on parameter $a_C\sqrt{\pi f\mu_0\sigma_C}$ additionally and increase with this parameter monotonically as well. Normalized inductance $L_A/(a_C\mu_0)$, normalized resistance $a_C\sigma_C R_A$, factor Q_A, inductance L_A and resistance R_A are related by (3.191). Thus, the increase of factor Q_A of the multilayer coil with increasing parameters w_A/a_C, r_C/a_C, $a_C\sqrt{\pi f\mu_0\sigma_C}$ can be interpreted as a more rapid increase of reactance of the coil ωL_A than increase of resistance R_A with increase of these parameters, similarly as in the case of the single layer coil.

In the case of the full coil, see Fig. 3.28.-Fig. 3.30., normalized inductance $L_A/(a_C\mu_0)$, normalized resistance $a_C\sigma_C R_A$ and factor Q_A increase with increasing parameters w_A/a_C monotonically. Normalized resistance $a_C\sigma_C R_A$ and factor Q_A depend on parameter $a_C\sqrt{\pi f\mu_0\sigma_C}$ additionally and increase with this parameter monotonically as well. The dependence of normalized inductance $L_A/(a_C\mu_0)$, normalized resistance $a_C\sigma_C R_A$ and factor Q_A on parameter b_C/a_C is different. Normalized inductance $L_A/(a_C\mu_0)$ increases with increasing parameter b_C/a_C. However, this dependence is almost negligible. On the other hand normalized resistance $a_C\sigma_C R_A$ exhibits minimum with respect to parameter b_C/a_C and factor Q_A exhibits maximum as a result of (3.191).

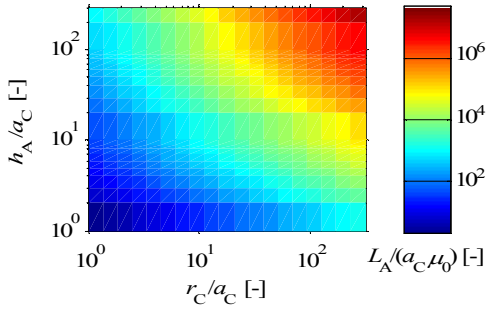

Fig. 3.22. Normalized inductance $L_A/(a_C\mu_0)$ of single layer coil.

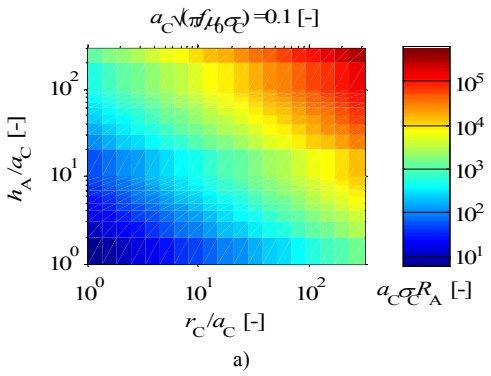

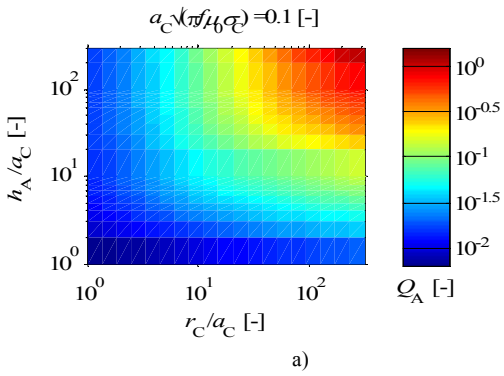

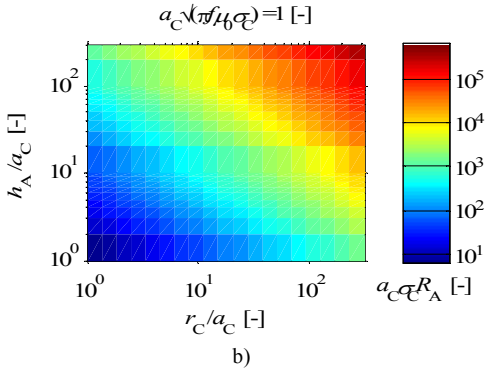

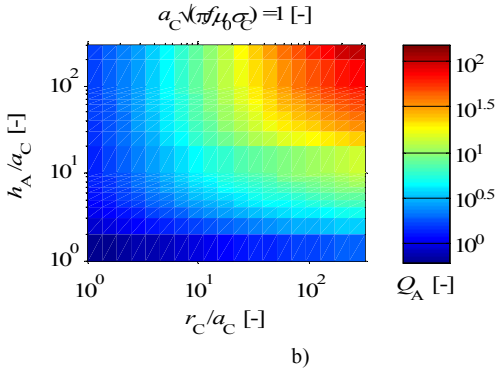

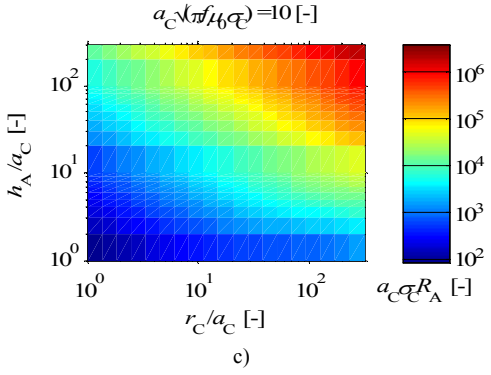

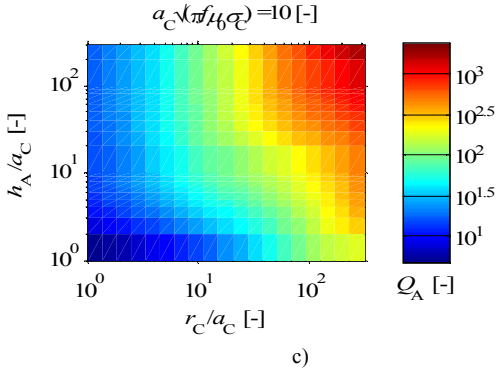

Fig. 3.23. Normalized resistance $a_C\sigma_C R_A$ of single layer coil for

a) $a_C\sqrt{\pi f\mu_0\sigma_C} = 0.1$,

b) $a_C\sqrt{\pi f\mu_0\sigma_C} = 1$,

c) $a_C\sqrt{\pi f\mu_0\sigma_C} = 10$.

Fig. 3.24. Quality factor Q_A of single layer coil for a) $a_C\sqrt{\pi f\mu_0\sigma_C} = 0.1$,

b) $a_C\sqrt{\pi f\mu_0\sigma_C} = 1$,

c) $a_C\sqrt{\pi f\mu_0\sigma_C} = 10$.

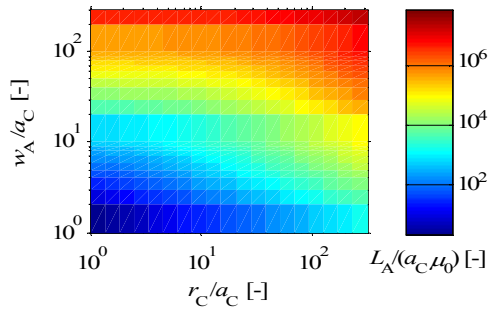

Fig. 3.25. Normalized inductance $L_A/(a_C\mu_0)$ of multilayer coil.

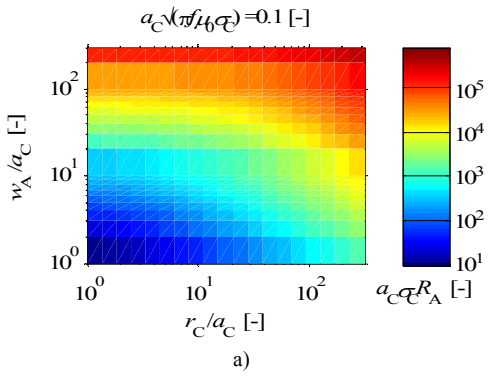

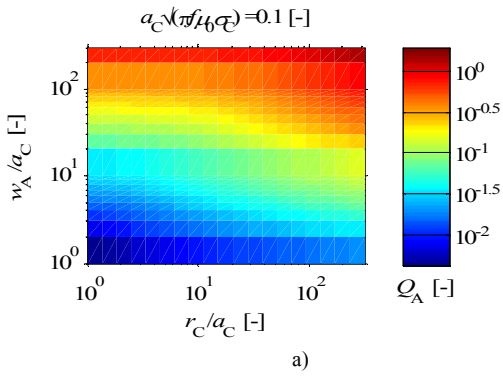

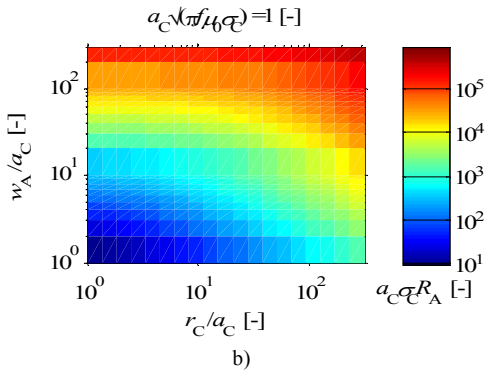

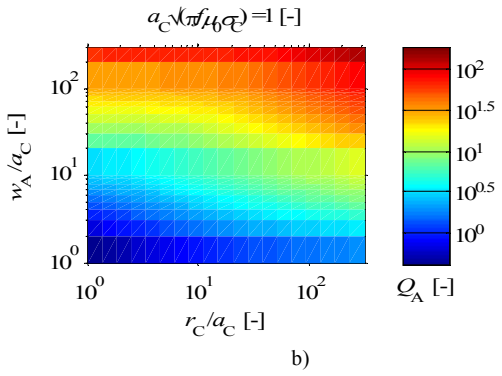

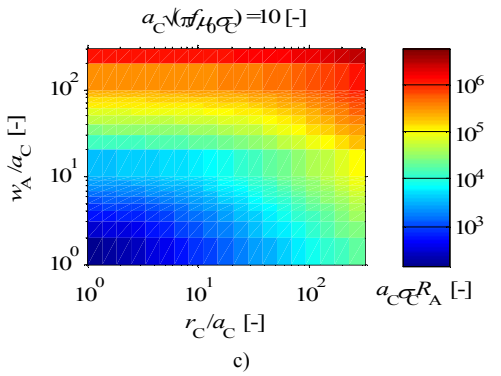

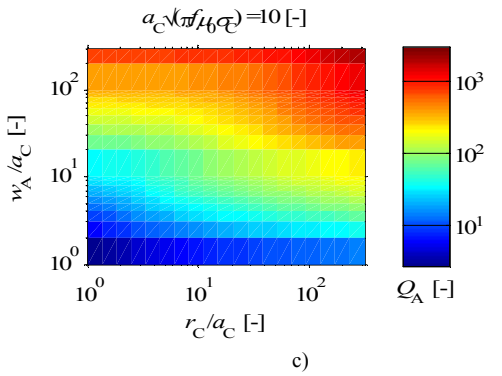

Fig. 3.26. Normalized resistance $a_C\sigma_C R_A$ of multilayer coil for

a) $a_C\sqrt{\pi f\mu_0\sigma_C} = 0.1$,

b) $a_C\sqrt{\pi f\mu_0\sigma_C} = 1$,

c) $a_C\sqrt{\pi f\mu_0\sigma_C} = 10$.

Fig. 3.27. Quality factor Q_A of multilayer coil for a) $a_C\sqrt{\pi f\mu_0\sigma_C} = 0.1$,

b) $a_C\sqrt{\pi f\mu_0\sigma_C} = 1$,

c) $a_C\sqrt{\pi f\mu_0\sigma_C} = 10$.

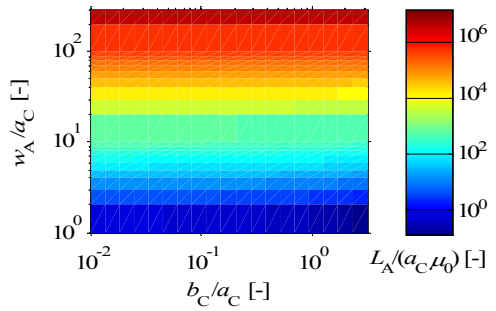

Fig. 3.28. Normalized inductance $L_A/(a_C\mu_0)$ of full coil.

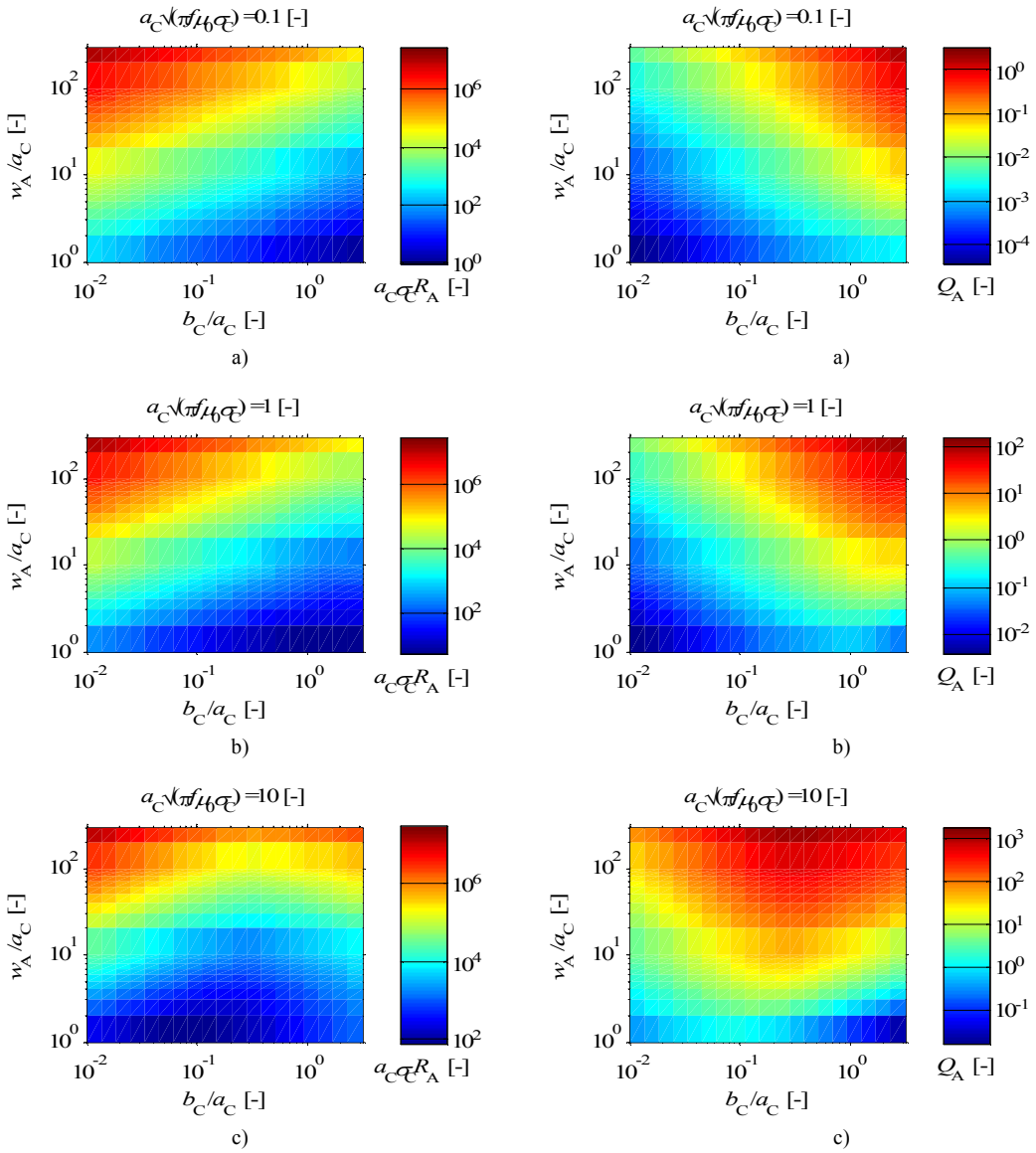

Fig. 3.29. Normalized resistance $a_C\sigma_C R_A$ of full coil for a) $a_C\sqrt{\pi f\mu_0\sigma_C}=0.1$,
b) $a_C\sqrt{\pi f\mu_0\sigma_C}=1$,
c) $a_C\sqrt{\pi f\mu_0\sigma_C}=10$.

Fig. 3.30. Quality factor Q_A of full coil for
a) $a_C\sqrt{\pi f\mu_0\sigma_C}=0.1$,
b) $a_C\sqrt{\pi f\mu_0\sigma_C}=1$,
c) $a_C\sqrt{\pi f\mu_0\sigma_C}=10$.

4. 2D Concept with Transmission by Electromagnetic Wave

This section deals with 2D concept with TEW. A basic principle of power extraction from a dielectric slab waveguide based on this concept is studied. The section is structured as follows. In sections 4.1. and 4.2., the introduction and formulation of the problem is made respectively. In section 4.3., electromagnetic field in the structure of the waveguide is analyzed and its characteristics are expressed as functions of the structure parameters. In section 4.4., the link of electromagnetic field approach for power extraction with circuit approach is proposed. In section 4.5., the design of the structure is discussed and the theory is verified by full-wave numerical analysis.

4.1. Introduction

An example of 2D concept with TEW is depicted in Fig. 4.1. The waveguide represented by a dielectric slab (a table top) is used as a transmission medium between a source and an appliance (a laptop). The power of electromagnetic wave is launched at the edge of the slab and propagates through it. A portion of the power is extracted using a suitable coupling element positioned under the appliance and delivered to the appliance. Analytical description of basic principle of power extraction from the dielectric slab waveguide is discussed further.

In this system, the power transmission efficiency depends on the capability of creating a good matching between the power source and the slab waveguide and between the slab waveguide and the appliance using coupling elements. In [5], the dielectric slab waveguide is covered by a mesh conductor to create an evanescent field upon the slab which enables the power extraction through interaction with a suitable coupling element. In a further discussed case, the necessity of mesh conductor for power extraction is considered under the appliance as a part of its coupling element only. The mesh conductor positioned on the slab can be actually replaced by a generic "metasurface" and characterized through an equivalent admittance layer. Metasurfaces, which are the two-dimensional realization of metamaterials, consist of a periodical arrangement of electrically small elements [45]-[47]. In a WPT system, the absorbing metasurface can represent a network of wireless sensors or a network for collection of power.

The interaction of these periodic structures with an impinging plane wave can be rigorously studied by expanding the field in terms of Floquet Waves centred around the wavenumber imposed by the excitation [48]. For electrically small periodicities, however, higher order Floquet Waves rapidly decay away from the periodic surface, and the metasurface can be characterized through an equivalent admittance layer [49]. A simple and intuitive way to design a metasurface resorts to equivalent discrete reactive circuits based on quasi-static concepts. A more rigorous approach consists in extracting from the full-wave analysis the minimum number of wavenumber-dependent parameters for an analytical synthesis of the surface impedance [50].

Starting from the modelling of the periodic surface trough an equivalent admittance layer, a simple model for the dielectric slab waveguide is provided, where the presence of an appliance is accounted for by adding a real part to the equivalent admittance associated with the metasurface. This model is used to identify the conditions providing optimal performance.

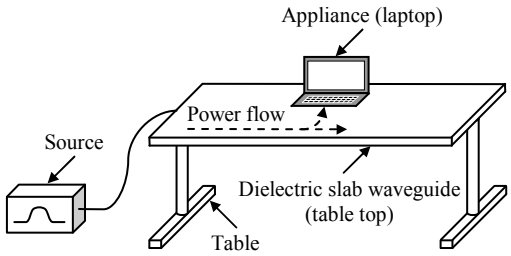

Fig. 4.1. Example of 2D concept with TEW.

4.2. Problem Formulation

Qualitative and quantitative description of a basic principle of power extraction from the dielectric slab waveguide based on 2D concept with TEW using an admittance layer is discussed further. The arrangement of the problem is depicted in Fig. 4.2.

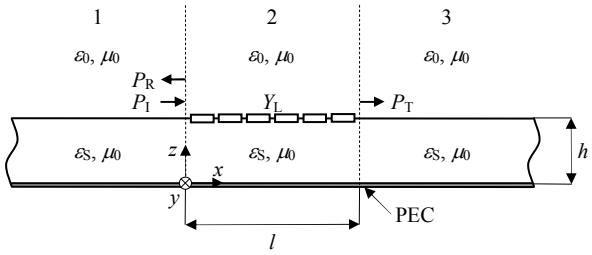

Fig. 4.2. Arrangement of dielectric slab waveguide for power extraction.

The waveguide consists of a dielectric slab with permittivity ε_S and thickness h. A bottom wall is represented by metal which is approximated by perfect electric conductor (PEC) and a top wall is represented by boundary between the slab and free space. The sections 1 and 3 are the same and serve for power transmission only. The section 2 with length l has additionally an admittance layer with surface admittance Y_L on the top boundary. The section 2 serves for power transmission and extraction. The admittance Y_L consists of conductance G_L and susceptance B_L

$$Y_L = G_L + \mathrm{j}B_L . \tag{4.1}$$

The primary purpose of the admittance layer is to represent the phenomenon of power extraction by conductance G_L. Susceptance B_L is added secondarily for better matching of section 2 with sections 1 and 3. The structure is considered to be infinite in the direction of y-axis. The symbols ε_0 and μ_0 mean permittivity and permeability of vacuum.

From the electromagnetic field point of view, the following situation is considered in the structure: The incident wave with power P_I which propagates in the positive direction of x-axis in the section 1 is partially reflected at the boundary between the sections 1 and 2 and partially enters the section 2 because the properties of the section 2 slightly differ from the properties of sections 1 and 3 due to the admittance layer. A part of wave which entered the section 2 propagates in the positive direction of x-axis in the section 2 and is partially extracted by the admittance layer, partially reflected at the boundary between the sections 2 and 3, and partially enters the section 3. A part of wave which entered the section 3 propagates in the positive direction of x-axis in the section 3. A part of wave which is reflected at this boundary propagates in the negative direction of x-axis in the section 2 and is partially extracted by the admittance layer, partially reflected at boundary between sections 1 and 2, and partially enters the section 1, etc. In the consequence of these phenomena, the reflected wave with total power P_R which propagates in the negative direction of x-axis occurs in the section 1 and the transmitted wave with total power P_T which propagates in the positive direction of x-axis occurs in the section 3. Thus, the relation between the total power P_L extracted by the admittance layer and powers P_I, P_R, P_T is

$$P_L = P_I - P_R - P_T . \tag{4.2}$$

In other words, power flow in the direction of x-axis exists in the sections 1, 2, 3, however, power flow in the direction of z-axis, which represents power extraction, exists in the section 2 additionally. Since the structure is passive the following relations between powers P_I, P_L, P_R, P_T are valid

$$P_I > P_R , P_I > P_T , P_I > P_L . \tag{4.3}$$

Thus, in the steady state, the wave propagating in the positive direction of x-axis exists in the sections 1, 2, 3 and the standing waves exists in the sections 1, 2 additionally, both as a consequence of superposition of the partial waves propagating in the positive and negative directions of x-axis. In the direction of z-axis, the standing wave is assumed in the slab and the evanescent wave in the free space in the sections 1, 2, 3 as it is usual for this type of waveguide [51]. Additionally, in the section 2, the propagating wave is assumed in the positive direction of z-axis in the slab and in the negative direction of z-axis in the free space, both as a consequence of power extraction.

The optimal performance of power extraction can be expressed by condition

$$P_{\mathrm{I}} \to P_{\mathrm{L}} , \tag{4.4}$$

This condition can be expressed equivalently as two conditions

$$P_{\mathrm{R}} \to 0 , \tag{4.5}$$

$$P_{\mathrm{T}} \to 0 . \tag{4.6}$$

Ideally, all incident power P_{I} should be extracted in the section 2 and power P_{R} reflected back to the section 1 and power P_{T} transmitted to the section 3 should then be zero. These conditions can be met only approximately. Only in the limit cases when the admittance $Y_{\mathrm{L}} \to 0$ (section 2 is the same as sections 1 and 3) or the length $l \to 0$ (section 2 is missing), power P_{R} is zero. Only in the limit case when the length $l \to \infty$ (all power which entered the section 2 is extracted), power P_{T} is zero.

For analysis, it is more convenient to reformulate conditions (4.5) and (4.6) and express them by power reflection coefficient R and power transmission coefficient T which are given by formulas

$$R = \frac{P_{\mathrm{R}}}{P_{\mathrm{I}}} \to 0 , \tag{4.7}$$

$$T = \frac{P_{\mathrm{T}}}{P_{\mathrm{I}}} \to 0 . \tag{4.8}$$

4.3. Analysis of Structure

In order to analyze the power balance of the structure, to approach conditions (4.7), (4.8), and to find out how parameters of the structure are related to these conditions, the electromagnetic field in the structure is analyzed in section 4.3.1. The goal of analysis is to express admittance Y_{L} and coefficients R and T as functions of structure parameters. The admittance Y_{L} and dispersion equations of the structure are treated in section 4.3.2. Power balance of the structure is expressed in terms of coefficients R and T in section 4.3.3.

4.3.1. Electromagnetic Field

The further derivation is performed for the fundamental mode of the structure which is TM mode [51]. Vectors of electromagnetic field are expressed for harmonic steady state in the form of phasors (in rms scale). The electromagnetic field in the sections 1, 2, 3 is constructed from the electric Hertz's vector $\mathbf{\Pi}^{\mathrm{e}}$ [52]. The vector $\mathbf{E}$ of electric field strength and vector $\mathbf{H}$ of magnetic field strength are consequently expressed from the vector $\mathbf{\Pi}^{\mathrm{e}}$ by relations

$$\mathbf{E} = k^2 \mathbf{\Pi}^{\mathrm{e}} + \nabla\nabla \cdot \mathbf{\Pi}^{\mathrm{e}} , \tag{4.9}$$

$$\mathbf{H} = \mathrm{j}\omega\varepsilon \nabla \times \mathbf{\Pi}^{\mathrm{e}} \tag{4.10}$$

where μ is permeability of medium, ε is permittivity of medium, ω is angular frequency, and k is wave number given by formula

$$k = \omega\sqrt{\mu\varepsilon} . \tag{4.11}$$

The wave number k is related by the x-, y-, z-components k_{X}, k_{Y}, k_{Z} of the wave vector by a formula

$$k = \sqrt{k_{\mathrm{X}}^2 + k_{\mathrm{Y}}^2 + k_{\mathrm{Z}}^2} . \tag{4.12}$$

The vector $\mathbf{\Pi}^{\mathrm{e}}$ for the different sections of the structure has forms

$$\mathbf{\Pi}^{\mathrm{e}}_{\mathrm{S1}} = \left(C_{1\mathrm{S1}} \mathrm{e}^{-\mathrm{j}k_{\mathrm{XS1}}x} + C_{2\mathrm{S1}} \mathrm{e}^{\mathrm{j}k_{\mathrm{XS1}}x}\right) \cos\left(k_{\mathrm{ZS1}} z\right) \boldsymbol{z}_0 , \tag{4.13}$$

$$\mathbf{\Pi}^{\mathrm{e}}_{\mathrm{S2}} = \left(C_{1\mathrm{S2}} \mathrm{e}^{-\mathrm{j}k_{\mathrm{XS2}}x} + C_{2\mathrm{S2}} \mathrm{e}^{\mathrm{j}k_{\mathrm{XS2}}x}\right) \cos\left(k_{\mathrm{ZS2}} z\right) \boldsymbol{z}_0 , \tag{4.14}$$

$$\mathbf{\Pi}^{\mathrm{e}}_{\mathrm{S3}} = C_{1\mathrm{S3}}\mathrm{e}^{-\mathrm{j}k_{\mathrm{XS3}}x}\cos\left(k_{\mathrm{ZS3}}z\right)\boldsymbol{z}_0\,, \tag{4.15}$$

$$\mathbf{\Pi}^{\mathrm{e}}_{\mathrm{F1}} = \left(C_{1\mathrm{F1}}\mathrm{e}^{-\mathrm{j}k_{\mathrm{XF1}}x} + C_{2\mathrm{F1}}\mathrm{e}^{\mathrm{j}k_{\mathrm{XF1}}x}\right)\mathrm{e}^{\mathrm{j}k_{\mathrm{ZF1}}z}\boldsymbol{z}_0\,, \tag{4.16}$$

$$\mathbf{\Pi}^{\mathrm{e}}_{\mathrm{F2}} = \left(C_{1\mathrm{F2}}\mathrm{e}^{-\mathrm{j}k_{\mathrm{XF2}}x} + C_{2\mathrm{F2}}\mathrm{e}^{\mathrm{j}k_{\mathrm{XF2}}x}\right)\mathrm{e}^{\mathrm{j}k_{\mathrm{ZF2}}z}\boldsymbol{z}_0\,, \tag{4.17}$$

$$\mathbf{\Pi}^{\mathrm{e}}_{\mathrm{F3}} = C_{1\mathrm{F3}}\mathrm{e}^{-\mathrm{j}k_{\mathrm{XF3}}x}\mathrm{e}^{\mathrm{j}k_{\mathrm{ZF3}}z}\boldsymbol{z}_0 \tag{4.18}$$

where C_1, C_2 are constants. For $\mathbf{\Pi}^{\mathrm{e}}$, C_1, C_2, and k, k_{X}, k_{Z}, the indices 1, 2, 3 denote the sections 1, 2, 3 and indices S and F denote the slab and free space. The properties of wave number and wave vector components in the different sections of the structure are described in Tab. 4.1.

Section	Slab	Free space
1, 2, 3	$k_{\mathrm{S}} = \omega\sqrt{\mu_0\varepsilon_{\mathrm{S}}}$	$k_{\mathrm{F}} = \omega\sqrt{\mu_0\varepsilon_0}$
1	$k_{\mathrm{XS1}} = \beta_{\mathrm{XS1}}$, $\beta_{\mathrm{XS1}} > 0$ $k_{\mathrm{ZS1}} = \beta_{\mathrm{ZS1}}$, $\beta_{\mathrm{ZS1}} > 0$	$k_{\mathrm{XF1}} = \beta_{\mathrm{XF1}}$, $\beta_{\mathrm{XF1}} > 0$ $k_{\mathrm{ZF1}} = -\mathrm{j}\alpha_{\mathrm{ZF1}}$, $\alpha_{\mathrm{ZF1}} < 0$
2	$k_{\mathrm{XS2}} = \beta_{\mathrm{XS2}} - \mathrm{j}\alpha_{\mathrm{XS2}}$ $\beta_{\mathrm{XS2}} > 0$, $\alpha_{\mathrm{XS2}} > 0$ $k_{\mathrm{ZS2}} = \beta_{\mathrm{ZS2}} - \mathrm{j}\alpha_{\mathrm{ZS2}}$ $\beta_{\mathrm{ZS2}} > 0$, $\alpha_{\mathrm{ZS2}} < 0$	$k_{\mathrm{XF2}} = \beta_{\mathrm{XF2}} - \mathrm{j}\alpha_{\mathrm{XF2}}$ $\beta_{\mathrm{XF2}} > 0$, $\alpha_{\mathrm{XF2}} > 0$ $k_{\mathrm{ZF2}} = \beta_{\mathrm{ZF2}} - \mathrm{j}\alpha_{\mathrm{ZF2}}$ $\beta_{\mathrm{ZF2}} > 0$, $\alpha_{\mathrm{ZF2}} < 0$
3	$k_{\mathrm{XS3}} = k_{\mathrm{XS1}}$, $k_{\mathrm{ZS3}} = k_{\mathrm{ZS1}}$ *	$k_{\mathrm{XF3}} = k_{\mathrm{XF1}}$, $k_{\mathrm{ZF3}} = k_{\mathrm{ZF1}}$ *

* The sections 1 and 3 have the same properties.

Tab. 4.1. Properties of wave number and wave vector components in different sections of structure.

This construction of electromagnetic field describes behaviour of the wave in the direction of x-axis and z-axis for the different sections as it is mentioned above. In the direction of z-axis for all sections, the construction fulfils the condition for PEC in $z = 0$. The construction is constant in the direction of y-axis since the structure is assumed to be infinite in this direction. The vectors **E** and **H** for the different sections of the structure which are expressed from (4.13)-(4.18) by using (4.9), (4.10), (4.12) have form

$$\mathbf{E}_{\mathrm{S1}} = \mathrm{j}k_{\mathrm{XS1}}k_{\mathrm{ZS1}}\left(C_{1\mathrm{S1}}\mathrm{e}^{-\mathrm{j}k_{\mathrm{XS1}}x} - C_{2\mathrm{S1}}\mathrm{e}^{\mathrm{j}k_{\mathrm{XS1}}x}\right)\sin\left(k_{\mathrm{ZS1}}z\right)\boldsymbol{x}_0 + k^2_{\mathrm{XS1}}\left(C_{1\mathrm{S1}}\mathrm{e}^{-\mathrm{j}k_{\mathrm{XS1}}x} + C_{2\mathrm{S1}}\mathrm{e}^{\mathrm{j}k_{\mathrm{XS1}}x}\right)\cos\left(k_{\mathrm{ZS1}}z\right)\boldsymbol{z}_0\,, \tag{4.19}$$

$$\mathbf{H}_{\mathrm{S1}} = -\omega\varepsilon_{\mathrm{S}}k_{\mathrm{XS1}}\left(C_{1\mathrm{S1}}\mathrm{e}^{-\mathrm{j}k_{\mathrm{XS1}}x} - C_{2\mathrm{S1}}\mathrm{e}^{\mathrm{j}k_{\mathrm{XS1}}x}\right)\cos\left(k_{\mathrm{ZS1}}z\right)\boldsymbol{y}_0\,, \tag{4.20}$$

$$\mathbf{E}_{\mathrm{S2}} = \mathrm{j}k_{\mathrm{XS2}}k_{\mathrm{ZS2}}\left(C_{1\mathrm{S2}}\mathrm{e}^{-\mathrm{j}k_{\mathrm{XS2}}x} - C_{2\mathrm{S2}}\mathrm{e}^{\mathrm{j}k_{\mathrm{XS2}}x}\right)\sin\left(k_{\mathrm{ZS2}}z\right)\boldsymbol{x}_0 + k^2_{\mathrm{XS2}}\left(C_{1\mathrm{S2}}\mathrm{e}^{-\mathrm{j}k_{\mathrm{XS2}}x} + C_{2\mathrm{S2}}\mathrm{e}^{\mathrm{j}k_{\mathrm{XS2}}x}\right)\cos\left(k_{\mathrm{ZS2}}z\right)\boldsymbol{z}_0\,, \tag{4.21}$$

$$\mathbf{H}_{\mathrm{S2}} = -\omega\varepsilon_{\mathrm{S}}k_{\mathrm{XS2}}\left(C_{1\mathrm{S2}}\mathrm{e}^{-\mathrm{j}k_{\mathrm{XS2}}x} - C_{2\mathrm{S2}}\mathrm{e}^{\mathrm{j}k_{\mathrm{XS2}}x}\right)\cos\left(k_{\mathrm{ZS2}}z\right)\boldsymbol{y}_0\,, \tag{4.22}$$

$$\mathbf{E}_{\mathrm{S3}} = \mathrm{j}k_{\mathrm{XS3}}k_{\mathrm{ZS3}}C_{1\mathrm{S3}}\mathrm{e}^{-\mathrm{j}k_{\mathrm{XS3}}x}\sin\left(k_{\mathrm{ZS3}}z\right)\boldsymbol{x}_0 + k^2_{\mathrm{XS3}}C_{1\mathrm{S3}}\mathrm{e}^{-\mathrm{j}k_{\mathrm{XS3}}x}\cos\left(k_{\mathrm{ZS3}}z\right)\boldsymbol{z}_0\,, \tag{4.23}$$

$$\mathbf{H}_{\mathrm{S3}} = -\omega\varepsilon_{\mathrm{S}}k_{\mathrm{XS3}}C_{1\mathrm{S3}}\mathrm{e}^{-\mathrm{j}k_{\mathrm{XS3}}x}\cos\left(k_{\mathrm{ZS3}}z\right)\boldsymbol{y}_0\,, \tag{4.24}$$

$$\mathbf{E}_{\mathrm{F1}} = k_{\mathrm{XF1}}k_{\mathrm{ZF1}}\left(C_{1\mathrm{F1}}\mathrm{e}^{-\mathrm{j}k_{\mathrm{XF1}}x} - C_{2\mathrm{F1}}\mathrm{e}^{\mathrm{j}k_{\mathrm{XF1}}x}\right)\mathrm{e}^{\mathrm{j}k_{\mathrm{ZF1}}z}\boldsymbol{x}_0 + k^2_{\mathrm{XF1}}\left(C_{1\mathrm{F1}}\mathrm{e}^{-\mathrm{j}k_{\mathrm{XF1}}x} + C_{2\mathrm{F1}}\mathrm{e}^{\mathrm{j}k_{\mathrm{XF1}}x}\right)\mathrm{e}^{\mathrm{j}k_{\mathrm{ZF1}}z}\boldsymbol{z}_0\,, \tag{4.25}$$

$$\mathbf{H}_{\mathrm{F1}} = -\omega\varepsilon_0 k_{\mathrm{XF1}}\left(C_{1\mathrm{F1}}\mathrm{e}^{-\mathrm{j}k_{\mathrm{XF1}}x} - C_{2\mathrm{F1}}\mathrm{e}^{\mathrm{j}k_{\mathrm{XF1}}x}\right)\mathrm{e}^{\mathrm{j}k_{\mathrm{ZF1}}z}\boldsymbol{y}_0\,, \tag{4.26}$$

$$\mathbf{E}_{\mathrm{F2}} = k_{\mathrm{XF2}}k_{\mathrm{ZF2}}\left(C_{1\mathrm{F2}}\mathrm{e}^{-\mathrm{j}k_{\mathrm{XF2}}x} - C_{2\mathrm{F2}}\mathrm{e}^{\mathrm{j}k_{\mathrm{XF2}}x}\right)\mathrm{e}^{\mathrm{j}k_{\mathrm{ZF2}}z}\boldsymbol{x}_0 + k^2_{\mathrm{XF2}}\left(C_{1\mathrm{F2}}\mathrm{e}^{-\mathrm{j}k_{\mathrm{XF2}}x} + C_{2\mathrm{F2}}\mathrm{e}^{\mathrm{j}k_{\mathrm{XF2}}x}\right)\mathrm{e}^{\mathrm{j}k_{\mathrm{ZF2}}z}\boldsymbol{z}_0\,, \tag{4.27}$$

$$\mathbf{H}_{\mathrm{F2}} = -\omega\varepsilon_0 k_{\mathrm{XF2}}\left(C_{1\mathrm{F2}}\mathrm{e}^{-\mathrm{j}k_{\mathrm{XF2}}x} - C_{2\mathrm{F2}}\mathrm{e}^{\mathrm{j}k_{\mathrm{XF2}}x}\right)\mathrm{e}^{\mathrm{j}k_{\mathrm{ZF2}}z}\boldsymbol{y}_0\,, \tag{4.28}$$

$$\mathbf{E}_{\mathrm{F3}} = k_{\mathrm{XF3}}k_{\mathrm{ZF3}}C_{1\mathrm{F3}}\mathrm{e}^{-\mathrm{j}k_{\mathrm{XF3}}x}\mathrm{e}^{\mathrm{j}k_{\mathrm{ZF3}}z}\boldsymbol{x}_0 + k^2_{\mathrm{XF3}}C_{1\mathrm{F3}}\mathrm{e}^{-\mathrm{j}k_{\mathrm{XF3}}x}\mathrm{e}^{\mathrm{j}k_{\mathrm{ZF3}}z}\boldsymbol{z}_0\,, \tag{4.29}$$

$$\mathbf{H}_{\mathrm{F3}} = -\omega\varepsilon_0 k_{\mathrm{XF3}}C_{1\mathrm{F3}}\mathrm{e}^{-\mathrm{j}k_{\mathrm{XF3}}x}\mathrm{e}^{\mathrm{j}k_{\mathrm{ZF3}}z}\boldsymbol{y}_0\,. \tag{4.30}$$

With respect to indices, the same formalism is valid for the vectors **E** and **H** as for the vector $\mathbf{\Pi}^{\mathrm{e}}$.

The tangential components of the electromagnetic field $\mathrm{E_Z}$, $\mathrm{H_Y}$ have to be continuous at the boundaries between the sections 1, 2 ($x = 0$) and the sections 2, 3 ($x = l$). The two approximations are made for matching of electromagnetic field at these boundaries. The first approximation is matching of electromagnetic field at the cross-section of the slab only ($z \in \langle 0, h\rangle$) since it is assumed that the majority of the electromagnetic field energy is concentrated in the slab. The second approximation is integral averaging of tangential components in this cross-

section in the direction of z-axis since the fundamental mode is used only and this mode differs at the different sides of the boundary slightly (in the sections 1, 3, the components of the wave vector are real whereas, in the section 2, are complex). By these approximations, the matching of electromagnetic field at the boundaries forms the following system

$$\int_0^h \mathrm{E}_{\mathrm{ZS1}}\left(x=0\right)\mathrm{d}z = \int_0^h \mathrm{E}_{\mathrm{ZS2}}\left(x=0\right)\mathrm{d}z\,, \tag{4.31}$$

$$\int_0^h \mathrm{H}_{\mathrm{YS1}}\left(x=0\right)\mathrm{d}z = \int_0^h \mathrm{H}_{\mathrm{YS2}}\left(x=0\right)\mathrm{d}z\,, \tag{4.32}$$

$$\int_0^h \mathrm{E}_{\mathrm{ZS2}}\left(x=l\right)\mathrm{d}z = \int_0^h \mathrm{E}_{\mathrm{ZS3}}\left(x=l\right)\mathrm{d}z\,, \tag{4.33}$$

$$\int_0^h \mathrm{H}_{\mathrm{YS2}}\left(x=l\right)\mathrm{d}z = \int_0^h \mathrm{H}_{\mathrm{YS3}}\left(x=l\right)\mathrm{d}z\,. \tag{4.34}$$

The constants C_{1S1}, C_{2S1}, C_{1S2}, C_{2S2}, C_{1S3} can be related to one chosen from them solving this system and using (4.19)-(4.24) and Tab. 4.1. When the constant C_{1S1} is chosen the other ones are given by relations

$$C_{2S1} = \frac{2\mathrm{j}\left(k_{\mathrm{XS2}}^2 - k_{\mathrm{XS1}}^2\right)\sin\left(k_{\mathrm{XS2}}l\right)}{\left(k_{\mathrm{XS1}}+k_{\mathrm{XS2}}\right)^2 \mathrm{e}^{\mathrm{j}k_{\mathrm{XS2}}l} - \left(k_{\mathrm{XS1}}-k_{\mathrm{XS2}}\right)^2 \mathrm{e}^{-\mathrm{j}k_{\mathrm{XS2}}l}} C_{1S1}\,, \tag{4.35}$$

$$C_{1S2} = \frac{2k_{\mathrm{XS1}}^2 k_{\mathrm{ZS2}}\left(k_{\mathrm{XS1}}+k_{\mathrm{XS2}}\right)\sin\left(k_{\mathrm{ZS1}}h\right)\mathrm{e}^{\mathrm{j}k_{\mathrm{XS2}}l}}{k_{\mathrm{XS2}}k_{\mathrm{ZS1}}\sin\left(k_{\mathrm{ZS2}}h\right)\left(\left(k_{\mathrm{XS1}}+k_{\mathrm{XS2}}\right)^2 \mathrm{e}^{\mathrm{j}k_{\mathrm{XS2}}l} - \left(k_{\mathrm{XS1}}-k_{\mathrm{XS2}}\right)^2 \mathrm{e}^{-\mathrm{j}k_{\mathrm{XS2}}l}\right)} C_{1S1}\,, \tag{4.36}$$

$$C_{2S2} = \frac{2k_{\mathrm{XS1}}^2 k_{\mathrm{ZS2}}\left(k_{\mathrm{XS1}}-k_{\mathrm{XS2}}\right)\sin\left(k_{\mathrm{ZS1}}h\right)\mathrm{e}^{-\mathrm{j}k_{\mathrm{XS2}}l}}{k_{\mathrm{XS2}}k_{\mathrm{ZS1}}\sin\left(k_{\mathrm{ZS2}}h\right)\left(\left(k_{\mathrm{XS1}}+k_{\mathrm{XS2}}\right)^2 \mathrm{e}^{\mathrm{j}k_{\mathrm{XS2}}l} - \left(k_{\mathrm{XS1}}-k_{\mathrm{XS2}}\right)^2 \mathrm{e}^{-\mathrm{j}k_{\mathrm{XS2}}l}\right)} C_{1S1}\,, \tag{4.37}$$

$$C_{1S3} = \frac{4k_{\mathrm{XS1}}k_{\mathrm{XS2}}\mathrm{e}^{\mathrm{j}k_{\mathrm{XS1}}l}}{\left(k_{\mathrm{XS1}}+k_{\mathrm{XS2}}\right)^2 \mathrm{e}^{\mathrm{j}k_{\mathrm{XS2}}l} - \left(k_{\mathrm{XS1}}-k_{\mathrm{XS2}}\right)^2 \mathrm{e}^{-\mathrm{j}k_{\mathrm{XS2}}l}} C_{1S1}\,. \tag{4.38}$$

The tangential component of the electric field strength $\mathrm{E_X}$, has to be continuous at the boundaries between the slab and free space ($z = h$) for all sections

$$\mathrm{E}_{\mathrm{XS1}}\left(z=h\right) = \mathrm{E}_{\mathrm{XF1}}\left(z=h\right), \tag{4.39}$$

$$\mathrm{E}_{\mathrm{XS2}}\left(z=h\right) = \mathrm{E}_{\mathrm{XF2}}\left(z=h\right), \tag{4.40}$$

$$\mathrm{E}_{\mathrm{XS3}}\left(z=h\right) = \mathrm{E}_{\mathrm{XF3}}\left(z=h\right). \tag{4.41}$$

The electric field strength $\mathrm{E_{XS2}}$ ($z = h$) is electric strength on the admittance layer too. The tangential component of the magnetic field strength $\mathrm{H_Y}$, has to be continuous at the boundaries between the slab and free space ($z = h$) in the sections 1, 3 and it is discontinuous in the section 2 because of surface current density $\mathrm{K_L}$ which is flowing in the admittance layer

$$\mathrm{H}_{\mathrm{YS1}}\left(z=h\right) = \mathrm{H}_{\mathrm{YF1}}\left(z=h\right), \tag{4.42}$$

$$\mathrm{H}_{\mathrm{YS2}}\left(z=h\right) - \mathrm{H}_{\mathrm{YF2}}\left(z=h\right) = \mathrm{K}_{\mathrm{L}}\,, \tag{4.43}$$

$$\mathrm{H}_{\mathrm{YS3}}\left(z=h\right) = \mathrm{H}_{\mathrm{YF3}}\left(z=h\right). \tag{4.44}$$

Matching of electromagnetic field along all boundaries in the direction of x-axis is only possible if the component k_X of the wave vector is the same at the both sides of the boundary for all sections

$$k_{\mathrm{XS1}} = k_{\mathrm{XF1}}\,, \tag{4.45}$$

$$k_{\mathrm{XS2}} = k_{\mathrm{XF2}}\,, \tag{4.46}$$

$$k_{\mathrm{XS3}} = k_{\mathrm{XF3}}\,. \tag{4.47}$$

The component k_Z for both sides of the boundary and all sections can be expressed using Tab. 4.1.

$$k_{\mathrm{ZS1}} = \sqrt{k_{\mathrm{S}}^2 - k_{\mathrm{XS1}}^2} = \sqrt{\omega^2\mu_0\varepsilon_{\mathrm{S}} - k_{\mathrm{XS1}}^2}\,, \tag{4.48}$$

$$k_{\mathrm{ZS2}} = \sqrt{k_{\mathrm{S}}^2 - k_{\mathrm{XS2}}^2} = \sqrt{\omega^2 \mu_0 \varepsilon_{\mathrm{S}} - k_{\mathrm{XS2}}^2}\ , \tag{4.49}$$

$$k_{\mathrm{ZS3}} = \sqrt{k_{\mathrm{S}}^2 - k_{\mathrm{XS3}}^2} = \sqrt{\omega^2 \mu_0 \varepsilon_{\mathrm{S}} - k_{\mathrm{XS3}}^2}\ , \tag{4.50}$$

$$k_{\mathrm{ZF1}} = \sqrt{k_{\mathrm{F}}^2 - k_{\mathrm{XF1}}^2} = \sqrt{\omega^2 \mu_0 \varepsilon_0 - k_{\mathrm{XF1}}^2}\ , \tag{4.51}$$

$$k_{\mathrm{ZF2}} = \sqrt{k_{\mathrm{F}}^2 - k_{\mathrm{XF2}}^2} = \sqrt{\omega^2 \mu_0 \varepsilon_0 - k_{\mathrm{XF2}}^2}\ , \tag{4.52}$$

$$k_{\mathrm{ZF3}} = \sqrt{k_{\mathrm{F}}^2 - k_{\mathrm{XF3}}^2} = \sqrt{\omega^2 \mu_0 \varepsilon_0 - k_{\mathrm{XF3}}^2}\ . \tag{4.53}$$

For analysis of the electromagnetic field, it is useful to express constants $C_{1\mathrm{F1}}$, $C_{2\mathrm{F1}}$, $C_{1\mathrm{F2}}$, $C_{2\mathrm{F2}}$, $C_{1\mathrm{F3}}$ for the free space in the terms of their counterparts for the slab constants $C_{1\mathrm{S1}}$, $C_{2\mathrm{S1}}$, $C_{1\mathrm{S2}}$, $C_{2\mathrm{S2}}$, $C_{1\mathrm{S3}}$ whose relations are mentioned above. The constants for the free space are given using (4.19), (4.21), (4.23), (4.25), (4.27), (4.29), (4.39)-(4.41), and (4.45)-(4.47) by relations

$$C_{1\mathrm{F1}} = \frac{\mathrm{j}k_{\mathrm{ZS1}} \sin\left(k_{\mathrm{ZS1}} h\right) \mathrm{e}^{-\mathrm{j}k_{\mathrm{ZF1}} h}}{k_{\mathrm{ZF1}}} C_{1\mathrm{S1}}\ , \tag{4.54}$$

$$C_{2\mathrm{F1}} = \frac{\mathrm{j}k_{\mathrm{ZS1}} \sin\left(k_{\mathrm{ZS1}} h\right) \mathrm{e}^{-\mathrm{j}k_{\mathrm{ZF1}} h}}{k_{\mathrm{ZF1}}} C_{2\mathrm{S1}}\ , \tag{4.55}$$

$$C_{1\mathrm{F2}} = \frac{\mathrm{j}k_{\mathrm{ZS2}} \sin\left(k_{\mathrm{ZS2}} h\right) \mathrm{e}^{-\mathrm{j}k_{\mathrm{ZF2}} h}}{k_{\mathrm{ZF2}}} C_{1\mathrm{S2}}\ , \tag{4.56}$$

$$C_{2\mathrm{F2}} = \frac{\mathrm{j}k_{\mathrm{ZS2}} \sin\left(k_{\mathrm{ZS2}} h\right) \mathrm{e}^{-\mathrm{j}k_{\mathrm{ZF2}} h}}{k_{\mathrm{ZF2}}} C_{2\mathrm{S2}}\ , \tag{4.57}$$

$$C_{1\mathrm{F3}} = \frac{\mathrm{j}k_{\mathrm{ZS3}} \sin\left(k_{\mathrm{ZS3}} h\right) \mathrm{e}^{-\mathrm{j}k_{\mathrm{ZF3}} h}}{k_{\mathrm{ZF3}}} C_{1\mathrm{S3}}\ . \tag{4.58}$$

4.3.2. Admittance of Layer, Dispersion Equations

The relation for the admittance Y_{L} of the admittance layer can be found as ratio of electric field strength $\mathrm{E}_{\mathrm{XS2}}$ ($z = h$) on the admittance layer and surface current density K_{L} flowing throw

$$Y_{\mathrm{L}} = \frac{\mathrm{E}_{\mathrm{XS2}}\left(z = h\right)}{\mathrm{K}_{\mathrm{L}}}\ . \tag{4.59}$$

This relation can be manipulated using (4.21), (4.22), (4.28), (4.36), (4.37), (4.43), (4.46), (4.56), (4.57) in the form

$$Y_{\mathrm{L}} = \omega\left(\frac{\mathrm{j}\varepsilon_{\mathrm{S}}}{k_{\mathrm{ZS2}}} \cot\left(k_{\mathrm{ZS2}} h\right) + \frac{\varepsilon_0}{k_{\mathrm{ZF2}}}\right). \tag{4.60}$$

The next point of structure analysis are dispersion equations of grounded dielectric slab waveguide without the admittance layer (sections 1 and 3) and with the admittance layer (section 2) respectively. The dispersion equation for sections 1 and 3 can be written in the form [51]

$$\frac{\varepsilon_{\mathrm{S}}}{\sqrt{\omega^2 \mu_0 \varepsilon_{\mathrm{S}} - \beta_{\mathrm{XS1}}^2}} \cot\left(\sqrt{\omega^2 \mu_0 \varepsilon_{\mathrm{S}} - \beta_{\mathrm{XS1}}^2}\, h\right) - \frac{\varepsilon_0}{\sqrt{\beta_{\mathrm{XS1}}^2 - \omega^2 \mu_0 \varepsilon_0}} = 0\ . \tag{4.61}$$

It can be manipulated using (4.45), (4.48), (4.51), Tab. 4.1. in the form similar to (4.60)

$$\frac{\varepsilon_{\mathrm{S}}}{k_{\mathrm{ZS1}}} \cot\left(k_{\mathrm{ZS1}} h\right) - \frac{\mathrm{j}\varepsilon_0}{k_{\mathrm{ZF1}}} = 0\ . \tag{4.62}$$

On the other hand the dispersion equation for section 2 is expressed by (4.60) and can be manipulated using (4.46), (4.49), (4.52), Tab. 4.1. in the form similar to (4.61)

$$\frac{\mathrm{j}\varepsilon_{\mathrm{S}}}{\sqrt{\omega^2\mu_0\varepsilon_{\mathrm{S}}-k_{\mathrm{XS2}}^2}}\cot\left(\sqrt{\omega^2\mu_0\varepsilon_{\mathrm{S}}-k_{\mathrm{XS2}}^2}\,h\right)+\frac{\varepsilon_0}{\sqrt{\omega^2\mu_0\varepsilon_0-k_{\mathrm{XS2}}^2}}=\frac{Y_{\mathrm{L}}}{\omega}. \tag{4.63}$$

4.3.3. Power Balance

The powers P_{I}, P_{R}, P_{T} can be expressed with the help of electric and magnetic field strengths as [28]

$$P_{\mathrm{I}}=\lim_{v\to\infty}\mathrm{Re}\left(\int_{-v}^{v}\int_{0}^{h}\left(\mathbf{E}_{\mathrm{S1}}^{+}\times\mathbf{H}_{\mathrm{S1}}^{+*}\right)\cdot x_0\,\mathrm{d}z\mathrm{d}y\right)\Bigg|_{z=0}, \tag{4.64}$$

$$P_{\mathrm{R}}=\lim_{v\to\infty}\mathrm{Re}\left(\int_{-v}^{v}\int_{0}^{h}\left(\mathbf{E}_{\mathrm{S1}}^{-}\times\mathbf{H}_{\mathrm{S1}}^{-*}\right)\cdot\left(-x_0\right)\mathrm{d}z\mathrm{d}y\right)\Bigg|_{z=0}, \tag{4.65}$$

$$P_{\mathrm{T}}=\lim_{v\to\infty}\mathrm{Re}\left(\int_{-v}^{v}\int_{0}^{h}\left(\mathbf{E}_{\mathrm{S3}}^{+}\times\mathbf{H}_{\mathrm{S3}}^{+*}\right)\cdot x_0\,\mathrm{d}z\mathrm{d}y\right)\Bigg|_{z=l} \tag{4.66}$$

where + denotes the wave propagating in the positive direction of x-axis (a part of the solution (4.19)-(4.30) of the electromagnetic field which contains term $\exp(-\mathrm{j}k_{\mathrm{XS}}x)$), − denotes the wave propagating in the negative direction of x-axis (a part of the solution (4.19)-(4.30) of the electromagnetic field which contains term $\exp(\mathrm{j}k_{\mathrm{XS}}x)$) and $\boldsymbol{x}_0$ is unit vector in the direction of x-axis. The approximation that the majority of the electromagnetic field energy is concentrated in the slab is used here again since the integration in the direction of z-axis is performed for $z\in\langle 0,\,h\rangle$ only. The formulas (4.7), (4.8) for coefficients R, T can be rewritten using (4.64)-(4.66), (4.19)-(4.30), (4.35), (4.38), and Tab. 4.1. as

$$R=\frac{\left|C_{\mathrm{2S1}}\right|^2}{\left|C_{\mathrm{1S1}}\right|^2}=\frac{N_{\mathrm{R}}}{D_{\mathrm{RT}}}, \tag{4.67}$$

$$T=\frac{\left|C_{\mathrm{1S3}}\right|^2}{\left|C_{\mathrm{1S1}}\right|^2}=\frac{N_{\mathrm{T}}}{D_{\mathrm{RT}}} \tag{4.68}$$

where are

$$N_{\mathrm{R}}=\left(\cos\left(2\beta_{\mathrm{XS2}}l\right)-\cosh\left(2\alpha_{\mathrm{XS2}}l\right)\right)\left(\left(2\beta_{\mathrm{XS1}}\beta_{\mathrm{XS2}}\right)^2-\left(\alpha_{\mathrm{XS2}}^2+\beta_{\mathrm{XS1}}^2+\beta_{\mathrm{XS2}}^2\right)^2\right), \tag{4.69}$$

$$N_{\mathrm{T}}=8\beta_{\mathrm{XS1}}^2\left(\alpha_{\mathrm{XS2}}^2+\beta_{\mathrm{XS2}}^2\right), \tag{4.70}$$

$$\begin{aligned}D_{\mathrm{RT}}=&\left(\left(2\beta_{\mathrm{XS1}}\beta_{\mathrm{XS2}}\right)^2+\left(\alpha_{\mathrm{XS2}}^2+\beta_{\mathrm{XS1}}^2+\beta_{\mathrm{XS2}}^2\right)^2\right)\cosh\left(2\alpha_{\mathrm{XS2}}l\right)+4\beta_{\mathrm{XS1}}\beta_{\mathrm{XS2}}\left(\alpha_{\mathrm{XS2}}^2+\beta_{\mathrm{XS1}}^2+\beta_{\mathrm{XS2}}^2\right)\sinh\left(2\alpha_{\mathrm{XS2}}l\right)\\&+\left(\left(2\beta_{\mathrm{XS1}}\alpha_{\mathrm{XS2}}\right)^2-\left(\alpha_{\mathrm{XS2}}^2-\beta_{\mathrm{XS1}}^2+\beta_{\mathrm{XS2}}^2\right)^2\right)\cos\left(2\beta_{\mathrm{XS2}}l\right)+4\beta_{\mathrm{XS1}}\alpha_{\mathrm{XS2}}\left(\alpha_{\mathrm{XS2}}^2-\beta_{\mathrm{XS1}}^2+\beta_{\mathrm{XS2}}^2\right)\sin\left(2\beta_{\mathrm{XS2}}l\right).\end{aligned} \tag{4.71}$$

If it is denoted

$$p_1=\frac{\beta_{\mathrm{XS1}}}{\alpha_{\mathrm{XS2}}}, \tag{4.72}$$

$$p_2=\frac{\beta_{\mathrm{XS2}}}{\alpha_{\mathrm{XS2}}}, \tag{4.73}$$

$$p_3=l\alpha_{\mathrm{XS2}} \tag{4.74}$$

(4.69)-(4.71) can be rewritten as

$$N_{\mathrm{R}}=\left(\cos\left(2p_2p_3\right)-\cosh\left(2p_3\right)\right)\left(\left(2p_1p_2\right)^2-\left(1+p_1^2+p_2^2\right)^2\right), \tag{4.75}$$

$$N_{\mathrm{T}}=8p_1^2\left(1+p_2^2\right), \tag{4.76}$$

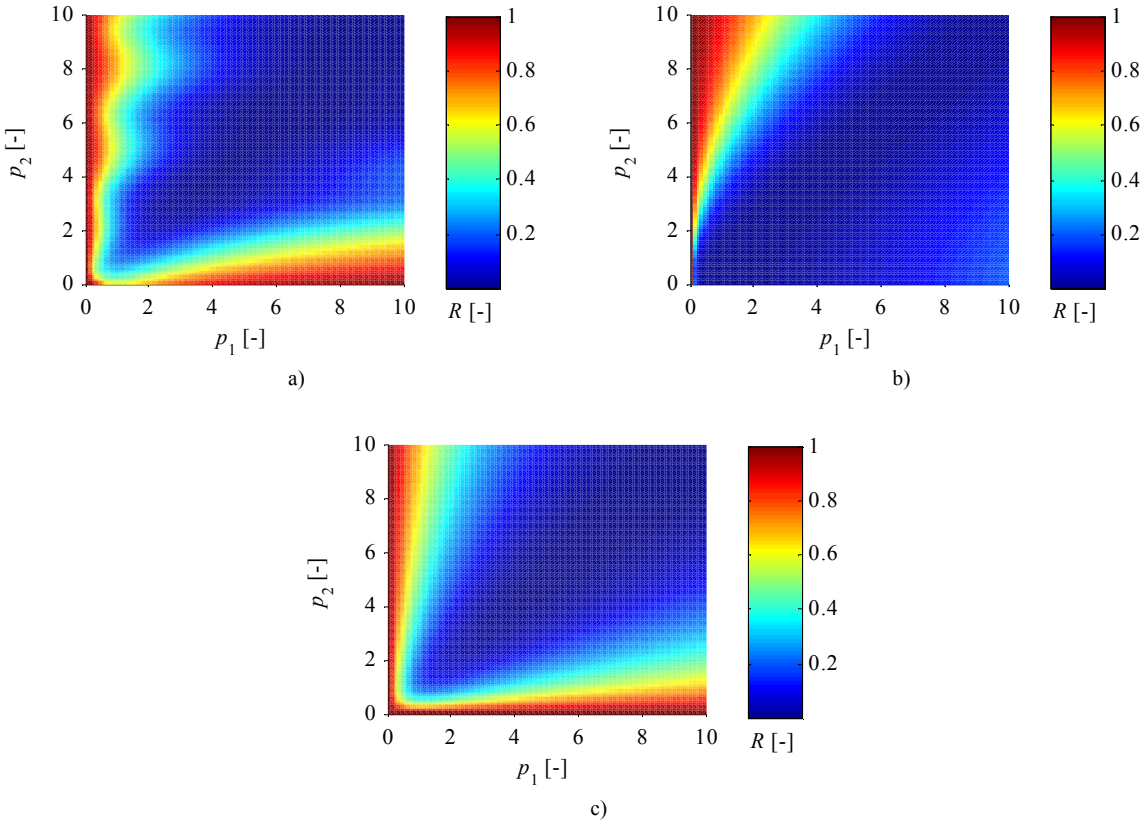

Fig. 4.3. Power reflection coefficient R: a) $p_3 = 0.1$, b) $p_3 = 1$, c) $p_3 = 10$.

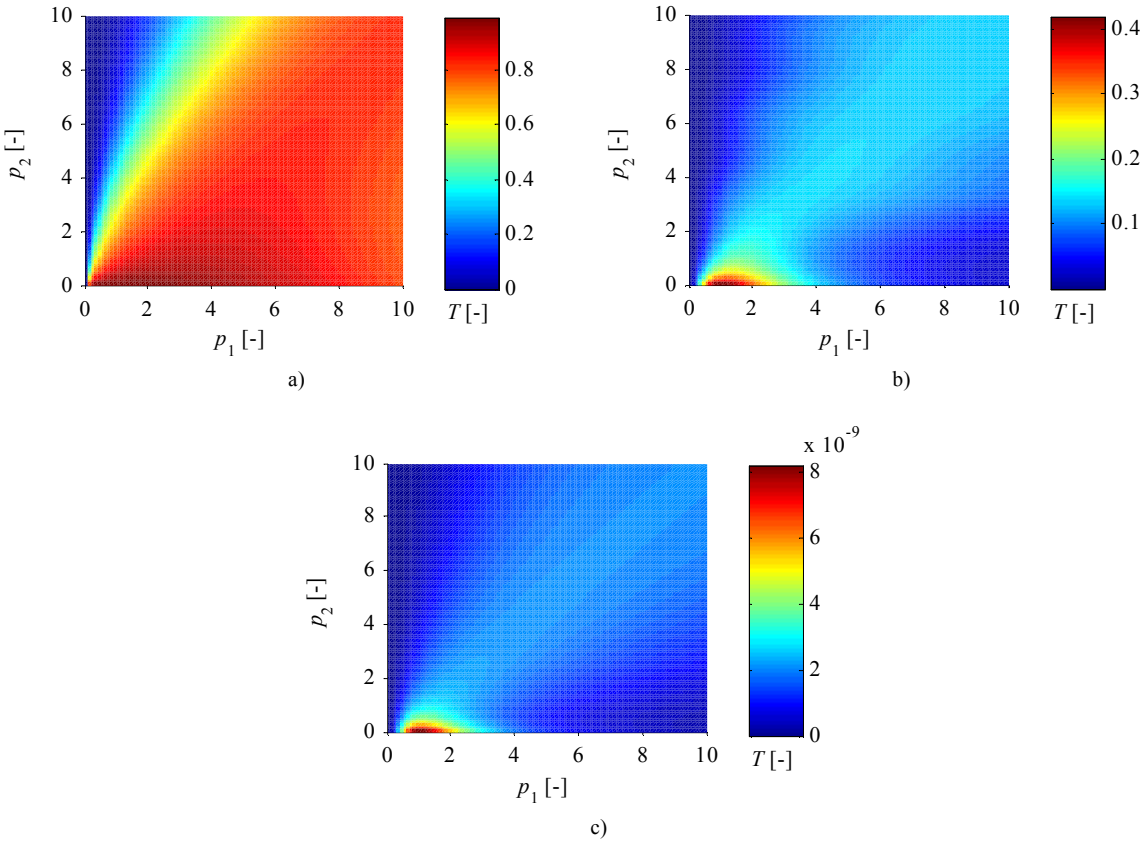

Fig. 4.4. Power transmission coefficient T: a) $p_3 = 0.1$, b) $p_3 = 1$, c) $p_3 = 10$.

$$D_{\mathrm{RT}} = \left((2p_1p_2)^2 + \left(1+p_1^2+p_2^2\right)^2\right)\cosh(2p_3) + 4p_1p_2\left(1+p_1^2+p_2^2\right)\sinh(2p_3) + \left((2p_1)^2 - \left(1-p_1^2+p_2^2\right)^2\right)\cos(2p_2p_3) + 4p_1\left(1-p_1^2+p_2^2\right)\sin(2p_2p_3). \tag{4.77}$$

Thus, the coefficients R, T are functions of three parameters p_1, p_2, p_3. The coefficients R and T based on (4.67), (4.68), (4.75)-(4.77) are plotted in Fig. 4.3. and Fig. 4.4. for three fixed value of the parameter p_3. It seems to be that the best approach to the conditions (4.7) and (4.8) of optimal performance occurs when the properties of the structure correspond to choice of parameters p_1, p_2

$$p_1 = p_2 \tag{4.78}$$

by all three values of parameter p_3. Substituting (4.72), (4.73) in (4.78) yields for this choice

$$\beta_{\mathrm{XS1}} = \beta_{\mathrm{XS2}}. \tag{4.79}$$

The relations (4.75)-(4.77) become using (4.78)

$$N_{\mathrm{R}} = \left(\cos(2p_1p_3) - \cosh(2p_3)\right)\left(\left(2p_1^2\right)^2 - \left(1+2p_1^2\right)^2\right), \tag{4.80}$$

$$N_{\mathrm{T}} = 8p_1^2\left(1+p_1^2\right), \tag{4.81}$$

$$D_{\mathrm{RT}} = \left(\left(2p_1^2\right)^2 + \left(1+2p_1^2\right)^2\right)\cosh(2p_3) + 4p_1^2\left(1+2p_1^2\right)\sinh(2p_3) + \left((2p_1)^2 - 1\right)\cos(2p_1p_3) + 4p_1\sin(2p_1p_3). \tag{4.82}$$

The coefficients R and T based on (4.67), (4.68) and manipulated relations (4.80)-(4.82) are plotted in Fig. 4.5.

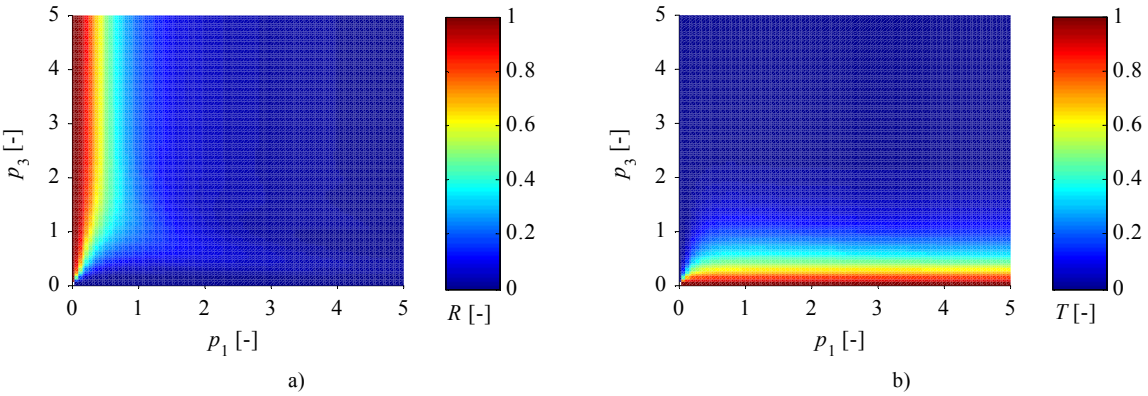

Fig. 4.5. a) Power reflection coefficient R, b) power transmission coefficient T for quasi-optimal performance.

4.4. Discretisation of Admittance Layer

It is difficult to realize a continuous admittance layer with given admittance Y_{L}, which is considered in the section 2 of the structure. Thus, the admittance layer can be approximated by a network of equidistantly placed discrete admittances where every element has the same admittance Y_{D}, see Fig. 4.6. For this approximation, the following condition has to be valid

$$l_{\mathrm{Y}} \qquad \lambda_{\mathrm{X}} = \frac{2\pi}{\beta_{\mathrm{XS2}}} \tag{4.83}$$

where λ_{X} is wavelength in the direction of x-axis and l_{Y} is length of the discrete admittance. The admittance Y_{D} can be use for considerations based on circuit approach e.g. for design of a real structure of the appliance coupling element.

The discrete admittance Y_{D} can be defined by its voltage $\mathrm{U_Y}$ and current $\mathrm{I_Y}$ if the condition (4.83) is valid by relation

$$Y_{\mathrm{D}} = \frac{\mathrm{U_Y}}{\mathrm{I_Y}} \tag{4.84}$$

where are

$$\mathrm{U_Y} = \int_{x_\mathrm{Y}}^{x_\mathrm{Y}+l_\mathrm{Y}} \mathrm{E_{XS2}}\left(z=h\right)\mathrm{d}x' , \tag{4.85}$$

$$\mathrm{I_Y} = \int_{y_\mathrm{Y}}^{y_\mathrm{Y}+w_\mathrm{Y}} \mathrm{K_L}\left(x = x_\mathrm{Y} + \frac{l_\mathrm{Y}}{2}, z=h\right)\mathrm{d}y' , \tag{4.86}$$

w_Y is width of area considered as belonging to one element of network of discrete admittances and x_Y and y_Y are x-coordinate and y-coordinate to which definitions of voltage $\mathrm{U_Y}$ and current $\mathrm{I_Y}$ are related. The voltage $\mathrm{U_Y}$ is chosen as voltage between points P_1 and P_2 and current $\mathrm{I_Y}$ is chosen as surface current flowing through the line given by points P_3 and P_4, see Fig. 4.6. The equation (4.84) can be manipulated using (4.21), (4.22), (4.28), (4.36), (4.37), (4.43), (4.46), (4.56), (4.57), (4.86), (4.85) in the form

$$Y_{\mathrm{D}} = Y_{\mathrm{L}} \frac{k_{\mathrm{XS2}} w_\mathrm{Y}}{2\sin\left(\frac{k_{\mathrm{XS2}}}{2} l_\mathrm{Y}\right)} . \tag{4.87}$$

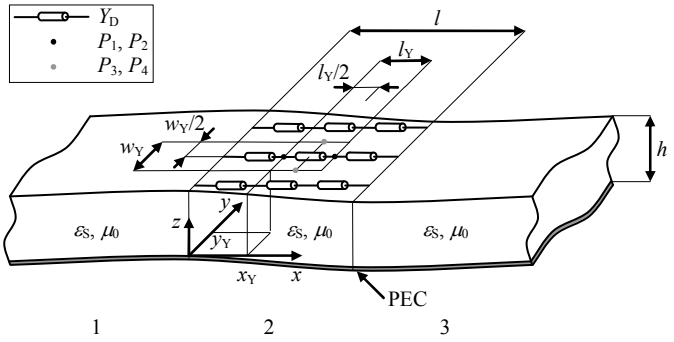

Fig. 4.6. Discretisation of continuous admittance layer.

4.5. Example

The design of the above described structure is discussed further. The input parameters for design are permittivity ε_S (or relative permittivity $\varepsilon_\mathrm{SR} = \varepsilon_\mathrm{S}/\varepsilon_0$) and thickness h of a slab, angular frequency ω (or frequency f), power reflection coefficient R and power transmission coefficient T. The output parameters of design are length l of the section 2 and admittance Y_L of the admittance layer. The procedure of calculation for structure design is shown in Tab. 4.2. The rows of Tab. 4.2. describe the steps of calculation from input design parameters to output design parameters. For evaluation of the calculation for selected values of input design parameters, see Tab. 4.3.

The analytical approach to analysis of the structure is verified by full-wave numerical analysis of the structure. Electromagnetic field in the structure is analyzed by both methods and results are compared. The input parameters for analysis are permittivity ε_S (or relative permittivity $\varepsilon_\mathrm{SR} = \varepsilon_\mathrm{S}/\varepsilon_0$) and thickness h of a slab, angular frequency ω (or frequency f), length l of the section 2 and admittance Y_L. The analytical description of electromagnetic field is given by expressions (4.19)-(4.30). The procedure of calculation of unknown parameters in expressions (4.19)-(4.30) is shown in Tab. 4.4. whose rows describe the steps of calculation. The numerical analysis is performed with the help of finite integration technique [53]. For the numerical analysis, the infinity of the structure in y-axis direction is realized by magnetic walls inserted in the planes $y = -w/2$ and $y = w/2$ and the admittance layer is represented by zero thickness transparent sheet with surface admittance Y_L inserted in the plane $z = h$. Fig. 4.7. and Fig. 4.8. show comparison of analytical an numerical analysis of the structure. The electromagnetic field is evaluated along chosen lines for input analysis parameters given in Tab. 4.5.

Direction of calculation ↓	Output variable	Input variable	Equation *
	p_1	R, T	(4.67), (4.68), (4.80), (4.81), (4.82)
	p_3		
	ε_S	ε_0, ε_{SR}	$\varepsilon_{SR}\varepsilon_0$
	ω	f	$2\pi f$
	k_F	μ_0, ε_0, ω	Tab. 4.1.
	k_S	μ_0, ε_S, ω	Tab. 4.1.
	β_{XS1}	μ_0, ε_0, ε_S, ω, h	(4.61)
	α_{XS2}	β_{XS1}, p_1	(4.72)
	l	α_{XS2}, p_3	(4.74)
	β_{XS2}	β_{XS1}	(4.79)
	k_{XS2}	α_{XS2}, β_{XS2}	Tab. 4.1.
	k_{ZS2}	k_S, k_{XS2}	(4.49)
	k_{XF2}	k_{XS2}	(4.46)
	k_{ZF2}	k_F, k_{XF2}	(4.52)
	Y_L	ε_0, ε_S, h, k_{ZS2}, k_{ZF2}	(4.60)

* The mentioned equations express the output variable implicitly in terms of input variables or have to be solved for output variable.

Tab. 4.2. Procedure of calculation for design of structure of dielectric slab waveguide.

	Name	Value
Input parameters	ε_{SR} [-]	5
	f [Hz]	$2.45 \cdot 10^9$
	h [m]	0.015
	R [-]	0.0025
	T [-]	0.000045
Output parameters	Name	Value
	l [m]	0.652
	Y_L [S]	0.00146 − j0.000117

Tab. 4.3. Evaluation of calculation for design of structure of dielectric slab waveguide.

Direction of calculation ↓	Output variable	Input variable	Equation *
	ε_S	ε_0, ε_{SR}	$\varepsilon_{SR}\varepsilon_0$
	ω	f	$2\pi f$
	k_F	μ_0, ε_0, ω	Tab. 4.1.
	k_S	μ_0, ε_S, ω	Tab. 4.1.
	β_{XS1}	μ_0, ε_0, ε_S, ω, h	(4.61)
	k_{XS1}	β_{XS1}	Tab. 4.1.
	k_{ZS1}	k_S, k_{XS1}	(4.48)
	k_{XF1}	k_{XS1}	(4.45)
	k_{ZF1}	k_F, k_{XF1}	(4.51)
	k_{XS2}	μ_0, ε_0, ε_S, ω, h, Y_L,	(4.63)
	k_{ZS2}	k_S, k_{XS2}	(4.49)
	k_{XF2}	k_{XS2}	(4.46)
	k_{ZF2}	k_F, k_{XF2}	(4.52)
	k_{XS3}	k_{XS1}	Tab. 4.1.
	k_{ZS3}	k_{ZS1}	Tab. 4.1.
	k_{XF3}	k_{XF1}	Tab. 4.1.
	k_{ZF3}	k_{ZF1}	Tab. 4.1.
	C_{2S1}	k_{XS1}, k_{XS2}, l, C_{1S1}	(4.35)
	C_{1S2}	k_{XS1}, k_{ZS1}, k_{XS2}, k_{ZS2}, l, h, C_{1S1}	(4.36)
	C_{2S2}	k_{XS1}, k_{ZS1}, k_{XS2}, k_{ZS2}, l, h, C_{1S1}	(4.37)
	C_{1S3}	k_{XS1}, k_{XS2}, l, C_{1S1}	(4.38)
	C_{1F1}	k_{ZS1}, k_{ZF1}, h, C_{1S1}	(4.54)
	C_{2F1}	k_{ZS1}, k_{ZF1}, h, C_{2S1}	(4.55)
	C_{1F2}	k_{ZS2}, k_{ZF2}, h, C_{1S2}	(4.56)
	C_{2F2}	k_{ZS2}, k_{ZF2}, h, C_{2S2}	(4.57)
	C_{1F3}	k_{ZS3}, k_{ZF3}, h, C_{1S3}	(4.58)

* The mentioned equations express output variable implicitly in terms of input variables or have to be solved for output variable.

Tab. 4.4. Procedure of calculation of electromagnetic field in structure of dielectric slab waveguide.

Name	Value
ε_{SR} [-]	5
f [Hz]	$2.45 \cdot 10^9$
h [m]	0.015
l [m]	0.652
Y_L [S]	0.00146 − j0.000117
w [m]	0.020
C_{1S1} [Vm]	1

Tab. 4.5. Input parameters for analysis of structure of dielectric slab waveguide.

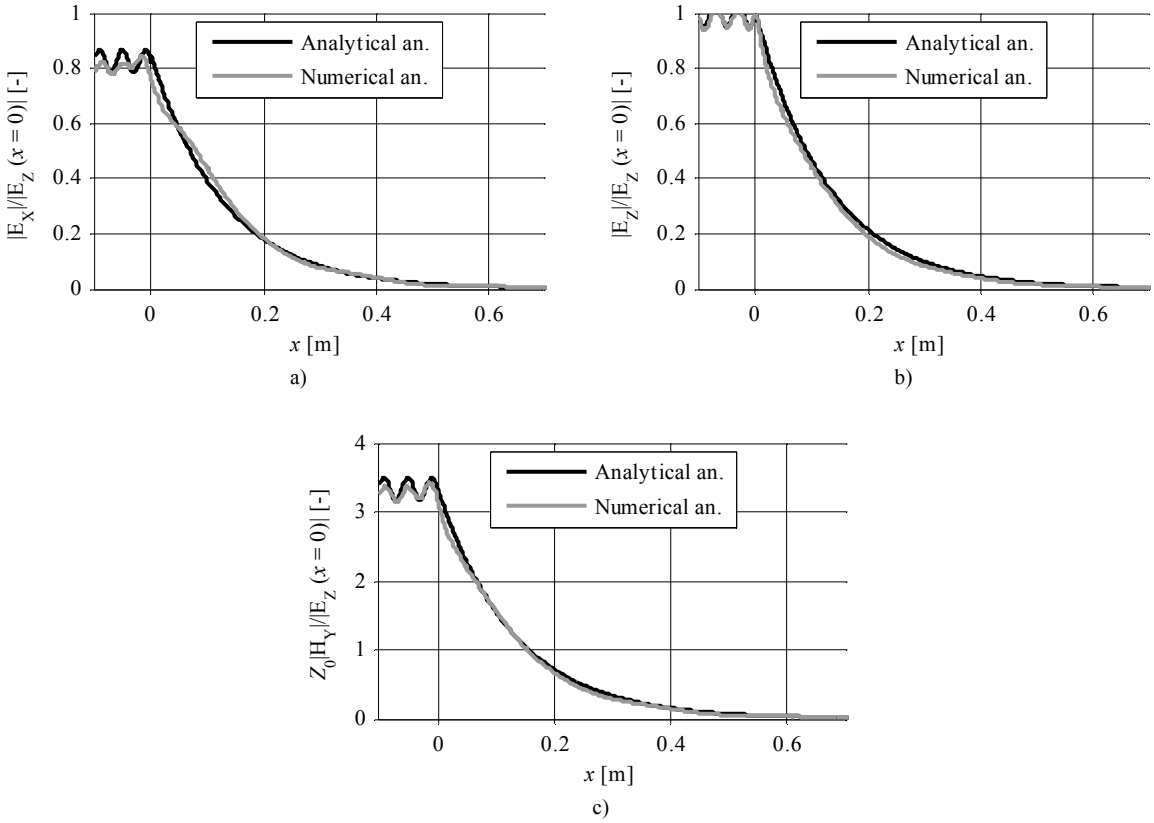

Fig. 4.7. a) Magnitude of component E_X of electric field strength vector **E** (normalized value), b) magnitude of component E_Z of electric field strength vector **E** (normalized value), c) magnitude of component H_Y of magnetic field strength vector **H** (normalized value, Z_0 is free space impedance, $Z_0 = 120\pi$) along line x, $z = h/2$.

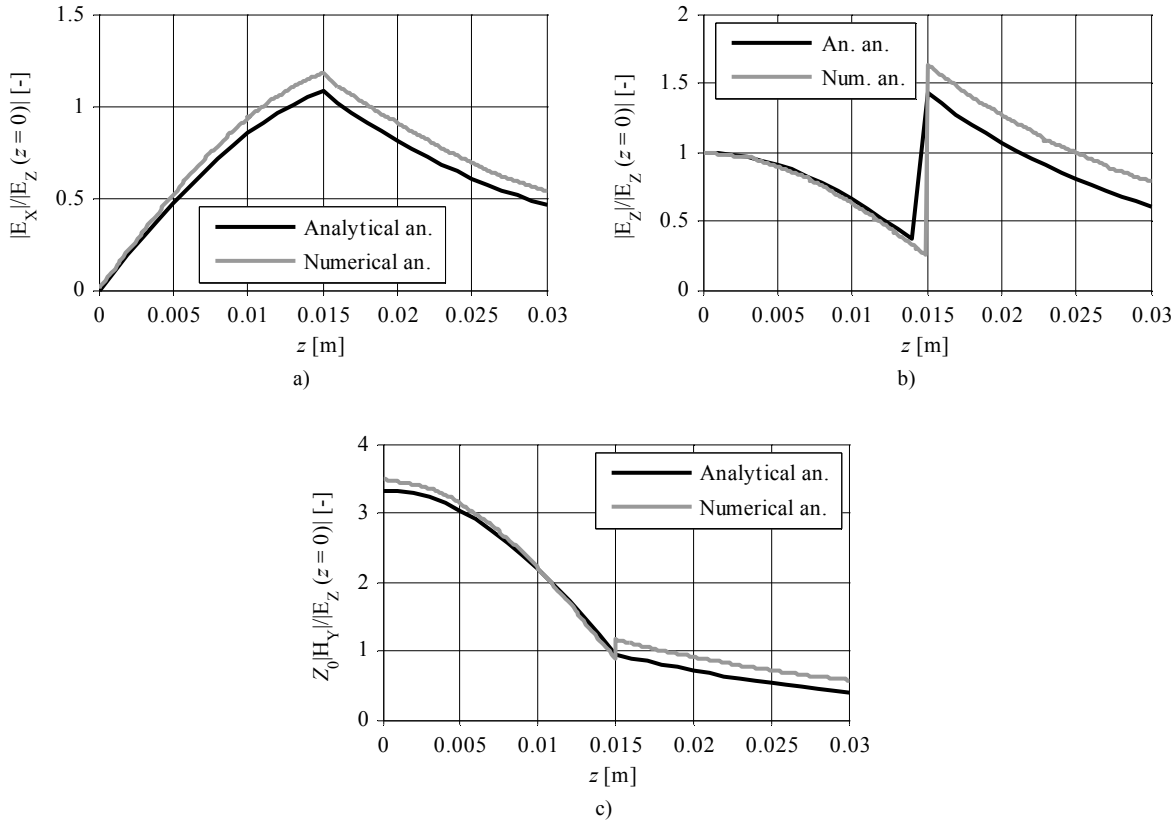

Fig. 4.8. a) Magnitude of component E_X of electric field strength vector **E** (normalized value), b) magnitude of component E_Z of electric field strength vector **E** (normalized value), c) magnitude of component H_Y of magnetic field strength vector **H** (normalized value, Z_0 is free space impedance, $Z_0 = 120\pi$) along line $x = l/2$, z.

5. Conclusion

5.1. Work Done in Thesis

This thesis dealt with wireless power transmission (WPT). A concept with transmission by magnetic field (TMF) and a two dimensional (2D) concept with transmission by electromagnetic wave (TEW) were chosen for more detail study after review of different concepts of WPT.

5.1.1. Concept with Transmission by Magnetic Field

A general circuit model of a transmission chain for concept with TMF was developed. The nature of this type of transmission was described by self and mutual inductances of transceiving and receiving coils which represent coupling elements. The end parts of the transmission chain connected to coupling elements on the sides of source and appliance were taken into account as an equivalent source and an equivalent load. This circuit model enables to define suitable characteristics of transmission, power transmission efficiency and normalized active powers, in a general way and to examine conditions of their optimum. It was shown that these conditions can be adapted for different arrangement of the circuit represented by the equivalent load. The characteristic of normalized active power delivered to the appliance can be interpreted as a demand on implementation of the equivalent source which follows from desired absolute active power delivered to the appliance and a given arrangement of the coupling elements and equivalent load.

The circuit model of the transmission chain of concept with TMF demonstrated that the characteristics, power transmission efficiency and normalized active powers, are functions of coupling coefficient and quality factors of the transceiving and receiving coils. The maximal value of coupling coefficient equal to 1 occurs for coils with air core which are used for WPT in the unreal ideal case when the coils are identical and occupy identical position. Nonidentical coils and positions can achieve lower value of coupling coefficient only. The behaviour of quality factor of induction coil is not so obvious with respect to quantities which describe geometrical and material properties of the coil. The three types of coils were chosen to illustrate this behaviour. The combination of approach from electromagnetic point of view and method for determination of necessary number of parameters governing the problem was used for calculation of quality factor of the coil. This method relates the geometrical and material properties of the given types of coils with quality factor and enables complete parametrical analysis presented in the form of dimensionless parameters.

The analysis of magnetic field of a thin-wall induction coil whose turns of conductor are wound homogeneously close together around air core of a shape of finite cylinder of arbitrary cross section was described. The result of the analysis was method for finding of scalar magnetic potential of the coil with the help of mutual inductance of the coil and elementary loop. The properties of scalar magnetic potential were discussed. The magnetic flux density of the coil was found as gradient of scalar magnetic potential. The mutual inductance can be found by an arbitrary method which leads to expression of mutual inductance as a function of mutual position of the coil and elementary loop. The method for calculation of mutual inductance of the thin-wall coil with air core of arbitrary cross section and thin-wall coil with air core of circular cross section was used in this case where the elementary loop was considered as a limit case of the coil of circular cross section. The air core of arbitrary cross section was specified in this method by shape function which has to be found for given cross section. Due to this approach, one numerical integration was necessary for calculation of magnetic flux density only.

The other method generalized the use of scalar magnetic potential for description of magnetic field out of the winding of the multilayer coil whose turns of conductor are wound homogeneously close together around air core of a shape of finite cylinder of arbitrary cross section. The characterization of cross section of the air core by shape function whose determination can be complex and time consuming was replaced by description of circumference of cross section by a curve expressed parametrically. The special coordinate system was defined for description of the winding which led to use of one numerical integration for calculation of magnetic flux density only. The relations for special cases of thin-wall coil with zero width of winding and thin-wall coil with zero height were presented additionally.

5.1.2. 2D Concept with Transmission by Electromagnetic Wave

The basic principle of power extraction from a dielectric slab based on 2D concept with TEW was studied. The model representing the principle was developed using approach from electromagnetic point of view. The process of power extraction was described by an equivalent dissipative admittance layer (metasurface) which covers the dielectric slab in the region of power extraction. The suitable characteristics were found using power balance of the structure, in particular, the power reflection and transmission coefficients were used to quantify the efficiency of the process of power extraction and to formulate the optimal performance. The coefficients were expressed as functions of three parameters through the analysis of the electromagnetic field in the structure and the condition of quasi-optimal performance was found. The discretisation of the continuous admittance layer was proposed.

5.2. Future Suggestions

The concept of WPT based on transmission by electric field (TEF) can be introduced as a dual concept to TMF. It means capacitive electrodes are used as coupling elements instead of induction coils in this case. The description of this concept can lead to similar characteristics of power transmission efficiency and active normalized powers as for concept with TMF. Eventually, combination of concepts with TMF and TEF can be considered.

The circuit model of transmission chain of concept with TMF takes into account the circuit connected to the coupling element on the side of appliance as an equivalent load. This description can be extended in order to involve effects caused by frequency converter (rectifier).

The parametrical analysis of quality factor, which enables to present the results in the form of dimensionless parameters describing geometrical and material properties of the induction coils, can be performed for other types of coils. However, the results can be less synoptic for other types of coils which need more quantities for their description. The analysis of quality factor for other types of coils is limited by availability of effective algorithms for calculations of inductance and resistance of coil which enable to evaluate them for many combinations of dimensionless parameters in the real time. The usability of the results of analysis of quality factor, which is based on a model of the coil consisting of serial connection of inductance and resistance, is restricted to the cases when a self capacitance of the coil can be considered as negligible. The phenomenon of the self capacitance desires to be treated in a similar form of parametrical analysis as inductance and resistance were.

An appliance coupling element for power extraction from the dielectric slab waveguide can be designed. The coupling element can be represented by a network for collection of power from the waveguide. The synthesis can be based on realization of a network of admittances which represent an absorbing layer on the surface of the waveguide.

References

[1] BALANIS, C. A. *Antenna Theory – Analysis and Designs*. 3th ed. New Jersey: John Wiley & Sons, 2005.

[2] BALANIS, C. A. *Advanced Engineering Electromagnetics*. New York: John Wiley & Sons, 1989.

[3] KVASIL, B. *Vybrané kapitoly z radioelektroniky*. Praha: Academia, 1969.

[4] HUI, S. Y. R., HO, W. W. C. A new generation of universal contactless battery charging platform for portable consumer electronic equipment. *Power Electronics, IEEE Transactions on*, vol. 20, no. 3, p. 620-627, May 2005.

[5] SHINODA, H., MAKINO, Y., YAMAHIRA, N., ITAI, H. Surface sensor network using inductive signal transmission layer. *Networked Sensing Systems, 2007. INSS '07. Fourth International Conference on*, p. 201-206, 6-8 June 2007.

[6] ZHANG, B., LIM, A. O., KADO, Y., ITAI, H. SHINODA, H. An efficient power supply system using phase control in 2D communication. *Networked Sensing Systems (INSS), 2009 Sixth International Conference on*, p. 1-4, 17-19 Jun. 2009.

[7] KURS, A., KARALIS, A., MOFFATT, R., JOANNOPOULOS, J. D., FISHER, P., SOLJACIC, M. Wireless power transfer via strongly coupled magnetic resonances. *Science*, vol. 317, p. 83 – 86, 6 July 2007.

[8] SCHEIBLE, G., SCHUTZ, J., APNESETH, C. Novel wireless power supply system for wireless communication devices in industrial automation systems. *IECON 02 [Industrial Electronics Society, IEEE 2002 28th Annual Conference of the]*, vol. 2, p. 1358-1363, 5-8 Nov. 2002.

[9] ZHI WEI SIM, SHUTTLEWORTH, R., GRIEVE, B. Investigation of PCB microstrip patch receiving antenna for outdoor RF energy harvesting in wireless sensor networks. *Antennas & Propagation Conference, 2009. LAPC 2009. Loughborough*, p. 129-132, 16-17 Nov. 2009.

[10] www.powercastco.com

[11] MCSPADDEN, J.O., LU FAN, KAI CHANG. Design and experiments of a high-conversion-efficiency 5.8-GHz rectenna. *Microwave Theory and Techniques, IEEE Transactions on*, vol. 46, no. 12, p. 2053-2060, Dec. 1998.

[12] STRASSNER, B., KAI CHANG. 5.8 GHz circular polarized rectifying antenna for microwave power transmission. *Microwave Symposium Digest, 2001 IEEE MTT-S International*, vol. 3, p. 1859-1862, 2001.

[13] SHINOHARA, N., MITANI, T., MATSUMOTO, H. Study on ubiquitous power source with microwave power transmission. *Proc. of International Union of Radio Science (URSI) General Assembly 2005*, 2005.

[14] TESLA, N. System of Transmission of Electrical Energy, US Patent 645 576, 1900.

[15] SCHUDER, J. C., STEPHENSON JR., H. E., TOWNSEND, J.F. High level electromagnetic energy transfer through a closed chest wall. *IRE International Convention Record*, vol. 9, no. 9, p. 119-126, 1961.

[16] MOHAN, N., UNDELAND, T. M., ROBBINS, W. P. *Power Electronics: Converters, Applications, and Design*. New York: John Wiley & Sons, 2002.

[17] BROWN, W. C. A survey of the elements of power transmission by microwave beam. *IRE International Convention Record*, vol. 9, no. 3, p. 93-105, 1961.

[18] BROWN, W. C. Experiments involving a microwave beam to power and position a helicopter. *Aerospace and Electronic Systems, IEEE Transactions on*, vol. AES-5, no. 5, p. 692-702, Sept. 1969.

[19] BROWN, W. C. Microwave to DC converter, US Patent 3 434 678, 1969.

[20] WAFFENSCHMIDT, E., STARING, T. Limitation of inductive power transfer for consumer applications. *Power Electronics and Applications, 2009. EPE '09. 13th European Conference on*, p. 1-10, 8-10 Sept. 2009.

[21] KRAUS, J. D. *Antennas*. 2nd ed. New York: McGraw-Hill, 1988.

[22] INTERNATIONAL COMMISSION ON NON-IONIZING RADIATION PROTECTION. Guidelines for limiting exposure to time-varying electric, magnetic, and electromagnetic fields (up to 300 GHz). 29 pages. [Online] Cited 2010-05-08. Available at: http://www.icnirp.de/documents/emfgdl.pdf.

[23] STRATTON, J. A. *Electromagnetic Theory*. New York: McGraw-Hill, 1941.

[24] ISHIDA, K., ITAYA, T., TANAKA, A., TAKEHIRA, N. Magnetic field analysis of an arbitrary shaped coil using shape functions. *Magnetics, IEEE Transactions on*, vol. 45, no. 1, p. 104-112, Jan. 2009.

[25] HONG LEI, LIAN-ZE WANG, ZI-NIU WU. Integral analysis of a magnetic field for an arbitrary geometry coil with rectangular cross section. *Magnetics, IEEE Transactions on*, vol. 38, no. 6, p. 3589-3593, Nov. 2002.

[26] WEGGEL, C. F., SCHWARTZ, D. P. New analytical formulas for calculating magnetic field. *Magnetics, IEEE Transactions on*, vol. 24, no. 2, p. 1544-1547, Mar. 1988.

[27] JACKSON, J. D. *Classical Electrodynamics*. New York: John Wiley & Sons, Inc., 1962.

[28] BUENO DE ALMEIDA, M., ASSIS, A. K. T. Deriving force from inductance. *Magnetics, IEEE Transactions on*, vol. 34, no. 1, p. 317-319, Jan 1998.

[29] SPIEGEL, M. R. *Schaum's Outline of Theory and Problems of Vector Analysis and an Introducing to Tensor Analysis*. New York: McGraw-Hill, 1959.

[30] PANKRAC, V. Generalization of relations for calculating the mutual inductance of coaxial coils in terms of their applicability to non-coaxial coils. *Magnetics, IEEE Transactions on*, vol. 47, no. 11, p. 4552-4563, Nov. 2011.

[31] CONWAY, J. T. Noncoaxial inductance calculations without the vector potential for axisymmetric coils and planar coils. *Magnetics, IEEE Transactions on*, vol. 44, no. 4, p. 453-462, April 2008.

[32] HAAS, H. Contribution to calculation of mutual inductance of coaxial solenoids (Ein Beitrag zur Berechnung der Gegeninduktivität koaxialer Zylinderspülen). *Electrical Engineering (Archiv für Elektrotechnik)*, vol. 57, no. 1, p. 21–26, Jan. 1975.

[33] SADIKU, M. N. O. *Elements of Electromagnetics*. Philadelphia: Saunders College Publishing, 1989.

[34] BULIRSCH, R. Numerical calculation of elliptic integrals and elliptic functions. III. *Numerische Mathematik*, vol. 13, no. 4, p. 305-315, Aug. 1969.

[35] CLEMENS, M., WEILAND, T. Magnetic field simulation using conformal FIT formulations. *Magnetics, IEEE Transactions on*, vol. 38, no. 2, p. 389-392, Mar. 2002.

[36] PANKRAC, V., KRACEK, J. Simple algorithms for the calculation of the intensity of the magnetic field of current loops and thin-wall air coils of a general shape using magnetic dipoles. *Magnetics, IEEE Transactions on*, vol. 48, no. 12, p. 4767-4778, Dec. 2012.

[37] KENNEDY, J. The arc length parametrization of a curve. 10 pages. [Online] Cited 2015-02-01. Available at: https://sites.google.com/site/johnkennedyshome/home/class-downloads.

[38] MATHCAD, [Online] Cited 2012-10-25. Available at: http://www.ptc.com/product/mathcad.

[39] MATLAB, [Online] Cited 2013-08-24. Available at: http://www.mathworks.com/products/matlab.

[40] MAYER, D., POLÁK, J. *Metody řešení elektrických a magnetických polí*. Praha: SNTL, 1983.

[41] WALLMEIER, P. Generalization of orthogonality principle to model solenoidal wound multiwinding transformers. *(2001) Conference Record - IAS Annual Meeting (IEEE Industry Applications Society)*, vol. 4, p. 2195-2022.

[42] BUCKINGHAM, E. On physically similar systems; Illustrations of the use of dimensional equations. *Physical Review*, vol. 4, no. 4, p. 345-376, Oct. 1914.

[43] HANCHE-OLSEN, H. Buckingham's pi-theorem. 7 pages. [Online] Cited 2014-11-07. Available at: http://www.math.ntnu.no/~hanche/notes/buckingham/buckingham-a4.pdf

[44] DIETRICH, W. Calculation of active power losses of transformer windings taking into account the actual stray field pattern (Berechnung der Wirkverluste von Transformatorenwicklungen unter Berücksichtigung des tatsächlichen Streufeldverlaufes). *Electrical Engineering (Archiv für Elektrotechnik)*, vol. 46, no. 4, p. 209-222, 1961.

[45] HOLLOWAY, C. L., DIENSTFREY, A., KUESTER, E. F., O'HARA, J. F., AZAD, A. K., TAYLOR, A. J. A discussion on the interpretation and characterization of metafilms/metasurfaces: The two-dimensional equivalent of metamaterials. *Metamaterials*, vol. 3, no. 2, p. 100-112, 2009.

[46] HOLLOWAY, C. L., KUESTER, E. F., GORDON, J. A., O'HARA, J., BOOTH, J., SMITH, D. R. An overview of the theory and applications of metasurfaces: The two-dimensional equivalents of metamaterials. *Antennas and Propagation Magazine, IEEE*, vol. 54, no. 2, p. 10-35, April 2012.

[47] MACI, S., MINATTI, G., CASALETTI, M., BOSILJEVAC, M. Metasurfing: Addressing waves on impenetrable metasurfaces. *Antennas and Wireless Propagation Letters, IEEE*, vol. 10, p 1499-1502, 2011.

[48] VARDAXOGLOU, J. C. *Frequency Selective Surfaces: Analysis and Design*. New York: John Wiley & Sons, 1997).

[49] SINING ZHOU, ZHENGBIN WANG, YIJUN FENG. Optimal design of wideband microwave absorber consisting of resistive meta-surface layers. *Journal of Electromagnetic Analysis and Applications*, vol. 4, no. 5, p. 187-191, 2012.

[50] MACI, S., CAIAZZO, M., CUCINI, A., CASALETTI, M. A pole-zero matching method for EBG surfaces composed of a dipole FSS printed on a grounded dielectric slab. *Antennas and Propagation, IEEE Transactions on*, vol. 53, no. 1, p. 70-81, 2005.

[51] POZAR, D. M. *Microwave Engineering* (New York: John Wiley & Sons, Inc., 2nd ed., 1998).

[52] COLLIN, R. E. *Field Theory of Guided Waves*. New York: McGraw-Hill, 1960.

[53] CLEMENS, M., WEILAND, T. Discrete electromagnetism with the finite integration technique. *Progress in Electromagnetics Research*, vol. 32, p. 65-87, 2001.

Publications of Doctoral Candidate

A. Related to Doctoral Thesis

A.1. Impacted

KRACEK, J., MAZANEK, M. Wireless power transmission for power supply: State of art. *Radioengineering*, vol. 20, no. 2, p. 457-463, 2011.

Contribution: 50%

Citations: 1

PANKRAC, V., KRACEK, J. Simple algorithms for the calculation of the intensity of the magnetic field of current loops and thin-wall air coils of a general shape using magnetic dipoles. *IEEE Transactions on Magnetics*, vol. 48, no. 12, p. 4767-4778, 2012.

Contribution: 50%

Citations: 1

BORGES CARVALHO, N., GEORGIADIS, A., COSTANZO, A., ROGIER, H., COLLADO, A., GARCIA, J.A., LUCYSZYN, S., MEZZANOTTE, P., KRACEK, J., MASOTTI, D., BOAVENTURA, A. J. S., DE LAS NIEVES RUIZ LAVIN, M., PINUELA, M., YATES, D. C., MITCHESON, P. D., MAZANEK, M., PANKRAC, V. Wireless power transmission: R&D activities within Europe. *IEEE Transactions on Microwave Theory and Techniques*, vol. 62, no. 4, p. 1031-1045, 2014.

Contribution: 6%

Citations: 4

KRACEK, J., PANKRAC, V., MAZANEK, M. Analysis of magnetic field of thin-wall air induction coil of arbitrary cross section with the help of scalar magnetic potential. *IEEE Transactions on Magnetics*, accepted for publication.

Contribution: 33%

Citations: 0

A.2. Peer-reviewed

KRACEK, J., MAZANEK, M. Possibilities of wireless power supply. *International Journal of Microwave and Wireless Technologies*, vol. 2, no. 2, p. 153-157, 2010.

Contribution: 50%

Citations: 1

A.3. Other

KRACEK, J., MAZANEK, M. The wireless power supply with the use of coupling surface. *Proceedings of 4th European Conference on Antennas and Propagation, EuCAP 2010*, 2010.

Contribution: 50%

Citations: 0

KRACEK, J., MAZANEK, M. Power balance of inductive wireless power transmission. *Proceedings of the 5th European Conference on Antennas and Propagation, EuCAP 2011*, p. 3974-3978, 2011.

Contribution: 50%

Citations: 0

KRACEK, J., MAZANEK, M. Measurement of magnetic flux density vector. *Proceedings of 6th European Conference on Antennas and Propagation, EuCAP 2012*, p. 2173-2174, 2012.

Contribution: 50%

Citations: 0

KRACEK, J., MAZANEK, M., MARTINI, E., MACI, S. Study of sheet-like structures for wireless power transmission. *Workshop: Wireless Power Transmission – Techniques and Applications, 43rd European Microwave Conference*, 2013.

Contribution: 25%

KRACEK, J., MAZANEK, M., PANKRAC, V. Analysis of induction coils for inductive wireless power transmission. *Workshop: Wireless Power Transmission – Near and Far Field Approaches, 44th European Microwave Conference*, 2014.

Contribution: 33%

KRACEK, J., MAZANEK, M. Wireless power supply. *2nd Management Committee/Working Group Meeting and Workshop of ICT COST Action IC0803 – RF/Microwave Communication Subsystems for Emerging Wireless Technologies (RFCSET)*, 2009.

Contribution: 50%

Citations: 0

KRACEK, J., MAZANEK, M. Wireless power supply systems. *3rd Management Committee/Working Group Meeting and Workshop of ICT COST Action IC0803 – RF/Microwave Communication Subsystems for Emerging Wireless Technologies (RFCSET)*, 2009.

Contribution: 50%

Citations: 0

KRACEK, J., MAZANEK, M. Possibilities of microwave wireless power supply. *4th Management Committee/Working Group Meeting and Workshop of ICT COST Action IC0803 – RF/Microwave Communication Subsystems for Emerging Wireless Technologies (RFCSET)*, 2010.

Contribution: 50%

Citations: 0

KRACEK, J., MAZANEK, M. Isotropic receiving coil for wireless power transmission. *5th Management Committee/Working Group Meeting and Workshop of ICT COST Action IC0803 – RF/Microwave Communication Subsystems for Emerging Wireless Technologies (RFCSET)*, 2010.

Contribution: 50%

Citations: 0

KRACEK, J., MAZANEK, M. Efficiency of inductive power transmission. *6th Management Committee/Working Group Meeting and Workshop of ICT COST Action IC0803 – RF/Microwave Communication Subsystems for Emerging Wireless Technologies (RFCSET)*, 2011.

Contribution: 50%

Citations: 0

KRACEK, J., MAZANEK, M. Self and mutual inductance of thin-wall rectangular coils. *7th Management Committee/Working Group Meeting and Workshop of ICT COST Action IC0803 – RF/Microwave Communication Subsystems for Emerging Wireless Technologies (RFCSET)*, 2011.

Contribution: 50%

Citations: 0

KRACEK, J., MAZANEK, M., MARTINI, E., MACI, S. Research on wireless power transmission with the help of guided wave. *8th Management Committee/Working Group Meeting and Workshop of ICT COST Action IC0803 – RF/Microwave Communication Subsystems for Emerging Wireless Technologies (RFCSET)*, 2012.

Contribution: 25%

Citations: 0

KRACEK, J., MAZANEK, M. Research on wireless power transmission. *9th Management Committee/Working Group Meeting and Workshop of ICT COST Action IC0803 – RF/Microwave Communication Subsystems for Emerging Wireless Technologies (RFCSET)*, 2012.

Contribution: 50%

Citations: 0

B. Nonrelated to Doctoral Thesis

B.1. Other

HAZDRA, P., CAPEK, M., KRACEK, J. Optimization tool for fractal patches based on the IFS algorithm. *Proceedings of 3rd European Conference on Antennas and Propagation, EuCAP 2009*, p. 1837-1839, 2009.

Contribution: 33%

Citations: 1